MICROPARTICLES COMPOSED OF NANOPARTICLES

FOR PULMONARY APPLICATION OF ANTIBIOTICS

IN CYSTIC FIBROSIS

Dissertation
zur Erlangung des Grades
des Doktors der Naturwissenschaften
der Naturwissenschaftlich-Technischen Fakultät
der Universität des Saarlandes

von

Afra Torge

Saarbrücken

2017

CONTENTS

1. SUMMARY

The eradication of bacteria in cystic fibrosis lungs is often unsuccessful due to biological barriers such as respiratory mucus and bacterial biofilms. Nanoparticles are suitable carriers to transport drugs through these barriers. As nanoparticles show low lung deposition, they need to be converted into microparticles for an inhalation as dry powder formulation.

In this work, different mucus types were evaluated towards pore size and structure. Antibiotic nanoparticles were prepared by loading lipid-core nanocapsules with ciprofloxacin. The nanocarriers showed an improved transport of the drug over the mucus barrier and efficacy against pathogens found in cystic fibrosis lungs. Furthermore, nano-embedded microparticles were prepared as delivery systems for nanoparticles to reach a good lung deposition. Subsequent disintegration of microparticles enables a release of nanoparticles. The influence of a matrix excipient on properties of spray-dried nano-embedded microparticles was investigated. Finally, cylindrical microparticles composed of nanoparticles were prepared by a template-assisted technique and compared with spherical particles.

Concluding, this work elucidates unanswered questions concerning the mucus barrier and presents a promising approach to improve treatment of pulmonary infections in cystic fibrosis.

2. KURZZUSAMMENFASSUNG

Die Eradikation von Erregern bei Mukoviszidose ist aufgrund von biologischen Barrieren wie Mukus und bakteriellem Biofilm oft erfolglos. Nanopartikel sind geeignete Trägersysteme, um Arzneistoffe über diese Barrieren zu transportieren. Da sie jedoch nur unzureichende Lungendeposition aufweisen, müssen sie in Mikropartikel eingebettet werden, um eine Inhalation als Trockenpulver zu ermöglichen.

In dieser Arbeit wurden verschiedene Mukusarten in Hinblick auf Porengröße und Struktur charakterisiert. Antibiotische Nanopartikel wurden durch Einkapselung von Ciprofloxacin in Nanokapseln mit Lipidkern hergestellt. Die Nanopartikel verbesserten den Transport des Arzneistoffs durch den Mukus und zeigten Wirksamkeit gegen Erreger, die Lungeninfektionen bei Mukoviszidose-Patienten hervorrufen. Des Weiteren wurden Nanopartikel in Mikropartikel als Trägersystem eingebettet, um eine gute Lungendeposition zu erreichen. Durch den anschließenden Zerfall der Mikropartikel wird die Freisetzung der Nanopartikel ermöglicht. Der Einfluss eines Matrixbildners auf die Eigenschaften der sprühgetrockneten Nano-in-Mikropartikel wurde untersucht. Zudem wurden zylindrische Mikropartikel bestehend aus Nanopartikeln mittels Templatmethode hergestellt und mit sphärischen Partikeln verglichen.

In dieser Arbeit wurden unbeantwortete Fragen bezüglich Mukus als Barriere geklärt und ein vielversprechender Ansatz für die Behandlung bakterieller Infektionen bei Mukoviszidose-Patienten vorgestellt.

3. INTRODUCTION

Tremendous progress has been made in the last decades in the treatment of cystic fibrosis, a genetic disorder characterized mainly by pulmonary symptoms. The survival age could be significantly increased; nevertheless, there is no cure available yet and patients' lives are still rather short. The main cause of death is pulmonary insufficiency resulting from chronic and recurrent lung infections with *Pseudomonas aeruginosa* [1]. Despite a broad range of different antibiotics with several application routes, efficacy of antibacterial treatment is still limited as the pathogens are forming biofilms inside a thick layer of immobile and viscous mucus covering the airways. Both mucus and biofilm represent biological barriers for antibiotic drugs, impairing the diffusion to their target [2, 3]. A recent approach for overcoming these barriers is the use of nanocarriers that are able to transport drugs through mucus and biofilm [3]. In this thesis, antibiotic-loaded nanoparticles with mucus-permeating properties will be developed. While nanoparticles are well suited delivery systems for drugs, their size is not appropriate for an inhalation as dry powder formulation. Sizes in the lower micrometer range are required for an efficient deposition in the lungs. In this work, nanoparticles shall be converted into microparticles to enable an application of nanoparticles by dry powder inhaler. By spray drying, nanoparticles will be embedded into an excipient matrix. Furthermore, cylindrical nano-embedded microparticles will be prepared by template-assisted technique. The microparticles serve only as delivery system to transport the nanocarriers into the lungs and are supposed to disintegrate after deposition to release the nanoparticles (Fig. 3.1). These nano-in-micro drug delivery systems combine the advantages of two size ranges, the applicability of microparticles as dry powder formulation as well as the improved drug transport by nanoparticles. Due to higher drug amounts reaching the site of action and a sustained release provided by the nanoparticles, both the overall dose and the dosing frequency might be reduced. The efficacy of the antibacterial therapy may be enhanced with at the same time decreased systemic side effects. Nano-embedded microparticles hence feature the perspective to improve the therapy of bacterial infections in cystic fibrosis and in consequence also to increase survival and quality of life of patients.

In the following chapter the scientific background will be presented more detailed.
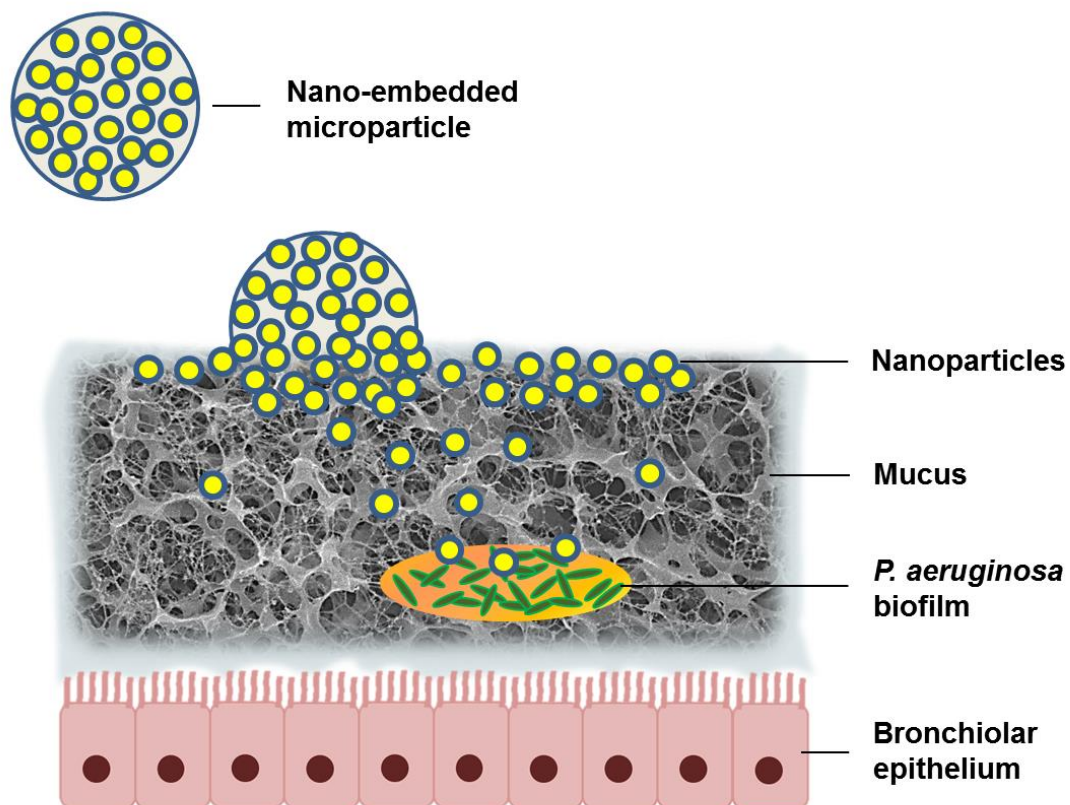
Fig. 3.1. The principle of nano-embedded microparticles: Microparticles are inhaled as dry powder formulation and transport the embedded nanoparticles into the lungs. After deposition in the airways, the microparticles disintegrate and release the nanoparticles. By permeating through the mucus network, the nanoparticles can transport the drug to the site of action, the bacterial biofilms.

3.1. Scientific background

3.1.1. *Cystic fibrosis*

Cystic fibrosis (CF) is the most common life threatening autosomal recessive disorder under Caucasians with an incidence of 1 case per 2500 births [4, 5]. The gene defect in CF concerns the Cystic Fibrosis Transmembrane Conductance Regulator (CFTR) gene, resulting in absence or malfunction of a protein regulating the ion transport through cell membranes. As consequence of a defective chloride transport, the water content in secretions decreases as well [4, 5]. Thickened and viscous secretions lead to dysfunctions of many organs in the whole body such as lungs, gall, pancreas and male sexual organs. Thus, CF is a multiorgan disease. Cystic fibrosis patients suffer for instance from exocrine pancreas insufficiency, intestinal obstructions, malnutrition, infertility and secondary diseases such as diabetes mellitus and osteoporosis [1, 4]. However, their quality of life is mainly affected by pulmonary symptoms. Due to the viscosity and stickiness of the pulmonary mucus, the mucociliary clearance is impaired and bacterial colonization is facilitated [5]. In addition, immune response is inadequate [5, 6]. Hence, patients suffer from recurrent lung infections. In consequence of the infections, exaggerated inflammatory responses lead to bronchiectasis and progressive obstructive airway disease. The resulting pulmonary insufficiency is cause of most CF-related deaths [5]. Especially infections with *Pseudomonas aeruginosa* are associated with a decrease in lung function and lower survival rates [1].

Cystic fibrosis is not curable yet. Causal therapy approaches include gene therapy and CFTR correctors. Though, even if being investigated in clinical studies, gene therapy is still in its infancy [6]. The first CFTR potentiator, *ivacaftor*, is already on the market; however, only around 4% of CF patients carry the mutations responding to this drug [6]. Thus, CF treatment consists mainly of symptomatic therapy. In terms of the lung disease, therapy aims on the one hand for increased mucociliary clearance. Mucolytics such as *dornase alfa* (recombinant human DNase), hypertonic saline and mannitol are used [5-7]. On the other hand, treatment and prophylaxis of bacterial infections are indispensable. Antibiotics such as tobramycin, colistin and ciprofloxacin are applied orally, by inhalation or intravenously [4, 5].

Thanks to improvements in CF therapy in the last decades, the median life expectancy of CF patients in Germany could already be increased from 18.1 years in 1995 to 31.1 years in 2012 [1]. Nonetheless especially the successful eradication of bacteria is still limited by several drawbacks and further progress is needed to improve life quality and expectancy of CF patients.

3.1.2. Limitations of antibacterial therapy – Biological barriers in CF lungs

Treatment of lung infections is a main pillar of CF therapy. Antibiotics can be applied systemically or locally by inhalation. As the application by inhalation delivers the drug directly to the lungs, lower doses are necessary. Higher local drug concentrations are reached and at the same time systemic side effects are reduced. However, the inhalative application of antibiotics suffers from limitations impeding the successful therapy. After being delivered to the lungs, a drug still needs to cross two biological barriers to reach its site of action: bronchiolar mucus and bacterial biofilm.

Mucus is a secretion covering epithelial surfaces in many organs of the body such as the respiratory, gastrointestinal and urogenital system. Its main function is the protection of epithelial cells. In the lungs protection is achieved by the mucociliary clearance: inhaled particles and pathogens are trapped by mucus and subsequently removed together with the mucus by continuous cilia beating towards the pharynx. Mucus is a hydrogel consisting of water, mucins (glycoproteins), non-mucin proteins, salts, lipids and cellular debris [8-10]. The mucins are responsible for the main characteristics of mucus such as pathogen binding, adhesion to cells and also for the high viscosity and structure of mucus [8]. Mucin fibers form a mesh structure (Fig. 3.2) with spacings ranging from about 100-1000 nm [9]. Regarding the rheology, mucus shows a viscoelastic behavior; depending on the shear it can act as elastic solid or viscous liquid [8]. With all these properties, mucus represents a perfect barrier for bacteria.
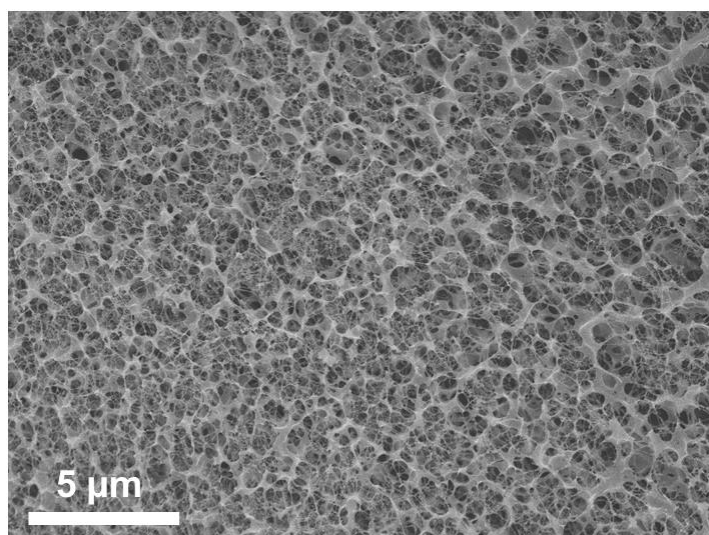
Fig. 3.2. Human tracheal mucus imaged by cryogenic scanning electron microscopy.

However, in cystic fibrosis, due to the abnormal thick and viscous mucus, mucociliary clearance is impaired and bacterial colonization even favored. Inside the immobile mucus microorganisms find a perfect environment to settle. In this situation, mucus serves more

for protection of bacteria than of the host. The pathogens are shielded against immune response as well as against antimicrobial drugs. Antibiotics suffer from limited diffusion through mucus. Likely reasons for this are binding to glycoproteins, obstruction by mucin fibers, increased viscosity and a decrease of the free water fraction [2]. The permeability inhibition was shown to be even more pronounced in cystic fibrosis mucus [11]. In addition to the hindered diffusion also activity of drugs can be reduced in mucus. Antibiotics such as aminoglycosides and β-lactams can show a decreased bioactivity due to high ion concentrations and low pH in mucus or due to binding to DNA or proteins [12].

Even if the drug reaches the site of infection, there is another biological barrier to overcome. A bacterial protection mechanism is the formation of biofilms. Biofilms are matrix-enclosed communities of differentiated bacteria, adherent to each other and/or to surfaces or interfaces [13]. Certain biofilm forming bacteria such as *Pseudomonas aeruginosa* are able to determine the density of bacteria by chemical communication via a quorum sensing system. When a high population density is reached, bacterial phenotype change is induced by quorum sensing and biofilm formation is triggered [3, 14]. These highly organized bacterial communities, which are protected by an extracellular alginate matrix, can hardly be eradicated. In comparison to planktonic cells, bacteria in biofilms are showing increased resistance and tolerance against antibiotics [14]. Resistance has been reported to be at least 500 times higher in biofilms [13]. In addition, bacteria in biofilms are protected from an immune response [14]. If bacterial infections are not treated in a planktonic state, bacteria can form biofilms and lead to chronic infections [3]. 60-75% of adult CF patients are chronically infected with *P. aeruginosa*, a Gram negative biofilm forming bacterium. It is the most important pathogen in CF, as chronic infections are strongly associated with inflammation, decline in lung function and lower survival rates [4, 15]. Among young CF patients, *Staphylococcus aureus* (Gram positive) is the most prevalent bacterium, being one of the first pathogens colonizing CF lungs. In children it is also associated with inflammatory responses and a decreased lung function. In adults it is considered less detrimental than *P. aeruginosa* even if it also has high prevalence [15, 16]. In all cases bacterial infections need to be treated in early stage to prevent pulmonary insufficiency as consequence of bronchiectasis and progressive obstructive airway disease due to the exaggerated immune response [5].

To improve the outcome of CF patients and to increase life expectancy, more efficient antibacterial therapies that are less influenced by the biological barriers are urgently needed.

3.1.3. Overcoming biological barriers by nanoparticles

A novel approach to overcome the mucus and biofilm barrier is the use of nanoparticles as drug delivery system. By encapsulating antibiotics into nanoparticles, the following advantages can be reached: (1) permeation through mucus, (2) penetration into biofilm matrix, (3) protection of the drug inside mucus and biofilm, (4) reduced clearance from the lungs and (5) controlled and sustained drug release [17]. The combination of these benefits can result in a decreased toxicity and at the same time improved efficacy in comparison to conventional formulations.

As described above, mucus has a mesh structure with pore sizes ranging from 100-1000 nm [9]. Given the size of the spacings it may appear evident that particles in the submicron size range are able to pass through this network and a mucus-penetrating effect has already been described for different kinds of nanoparticles [18-21]. However, it strongly depends on particle properties that influence the interaction with mucus such as size, charge and hydrophobicity [8, 9]. Thus, knowledge about retention mechanisms in mucus is indispensable for the development of mucus-penetrating nanoparticles. There are two main mechanisms that can lead to retention of nanoparticles in the mucus network: the size exclusion effect and biophysical or biochemical interactions [22]. The size exclusion effect represents a simple filtering mechanism by size. Depending on the density of the hydrogel-forming polymer a cut-off size is determined. Smaller particles are able to diffuse through the network while larger particles are trapped in the meshes [22]. Nevertheless it may also happen that small particles are retained for longer time as they can diffuse in smaller holes [8]. Furthermore, particles from all sizes can be retained by the mucus network due to interactions with the biopolymers. In mucus mostly electrostatic interactions with the negatively charged mucins occur, but also hydrophobic interactions are possible [22]. Positively charged nanoparticles tend to interact electrostatically with the negatively charged mucins, thus they are showing mucoadhesive properties. Negatively charged nanoparticles are rather repelled from the mucus, while neutral particles can show good permeation properties due to lacking electrostatic interactions. However, neutral nanoparticles might be as well hindered by hydrophobic interactions [23].

For negatively charged nanoparticles size dependence has been shown. 124 nm polystyrene particles were reported to be able to pass through the mucus network while 560 nm particles were retained [24]. However, also larger negatively charged nanoparticles can permeate mucus when their surface is covered by polyethylene glycol (PEG). This coating shields the particles from both electrostatic and hydrophobic interactions, making the particles "muco-inert" [8, 19, 25-27].

To summarize, a drug's permeability through mucus can be increased by encapsulation into nanoparticles, as long as the particles display the right properties. In addition, the encapsulation also protects the drug from deactivation in mucus.

The bacterial biofilm is a hydrogel with negatively charged polymers as well. It contains polysaccharides, proteins, lipids and nucleic acids. Thus, similar to mucus, size exclusion and electrostatic interactions occur [22]. Advantages of nanoparticulate drug delivery systems such as liposomes and polymeric nanoparticles have also been shown in biofilms [14]. The nanoparticles can be able to promote the penetration into the biofilm matrix and to protect the drug from enzymatic degradation. For some antibiotic-loaded liposomes reduced minimal inhibitory concentrations (MIC) in comparison to the free drug were reported. PEGylation of particles has been shown to be advantageous as well for biofilm penetration [14].

Apart from the low permeation through mucus and biofilm, free antibiotics show the disadvantage of a rapid clearance in the lungs. By encapsulation into nanoparticles a longer retention in the lungs is possible, as nanoparticles are not recognized as foreign entities by the lung immune system and thus not subject to uptake by macrophages [17, 28]. The sustained drug release also contributes to the longer retention time. Furthermore, higher local concentrations in proximity to the biofilms can be reached, as the drug is continuously released inside the mucus and not at once before permeating the mucus barrier [17].

To summarize, nanoparticles represent a perfect transport and protection system for antibacterial drugs with the perspective to improve efficacy of antibiotics and to reduce their toxicity.

3.1.4. The challenge of delivering nanoparticles to the lungs

Despite all the advantages of a local antibiotic therapy in the lungs by nanoparticulate drug delivery systems, it is not straightforward to apply nanoparticles to the lungs. For the development of formulations that are applicable by inhalation, knowledge about lung anatomy and physiology and particle deposition mechanisms is necessary.

The lungs are composed of the right and the left lung, which are further divided into three and two lobes respectively. The respiratory system can be classified into three different functional regions: the upper (extrathoracic) airways, the conductive (tracheobronchial) airways and the respiratory (alveolated/pulmonary) airways (Fig. 3.3.). The upper airways comprise the nasal and oral cavity, nasopharynx, oropharynx and larynx. Mean function of this part of the respiratory system is heating and humidifying the inhaled air to body temperature and more than 99% relative humidity [29].

The tracheobronchial airways conduct the air till the alveoli. Their structure can be compared with an inverted tree: the trachea is the trunk which is split into the two main bronchi. The main bronchi are further divided into bronchi, then into bronchioles and finally into terminal bronchioles, the finest branches of the "tree". From the trachea to the terminal bronchioles, the airway diameter decreases from 1.8 cm to 0.06 cm and at the same time the total cross sectional area increases from 2.54 cm^2 to 180 cm^2 [29]. The tracheobronchial epithelium is mainly composed from columnar ciliated cells. Mucus is secreted from submucosal glands and goblet cells and covers the tracheobronchiolar airways as a blanket. In combination with the continuous cilia beating, mucus is responsible for the mucociliary clearance. Hence, another function of the tracheobronchiolar airways is the protection of the lungs from inhaled pathogens and particles.

The respiratory airways start with the respiratory bronchioles, which are followed by alveolar ducts and finally the alveolar sacs. The huge surface area of 100-190 m^2 is responsible for the gas exchange [29]. The alveolar epithelium consists of very flat, squamous type I cells and cuboidal type II cells producing pulmonary surfactant. Mucus is not present in the respiratory airways [29].
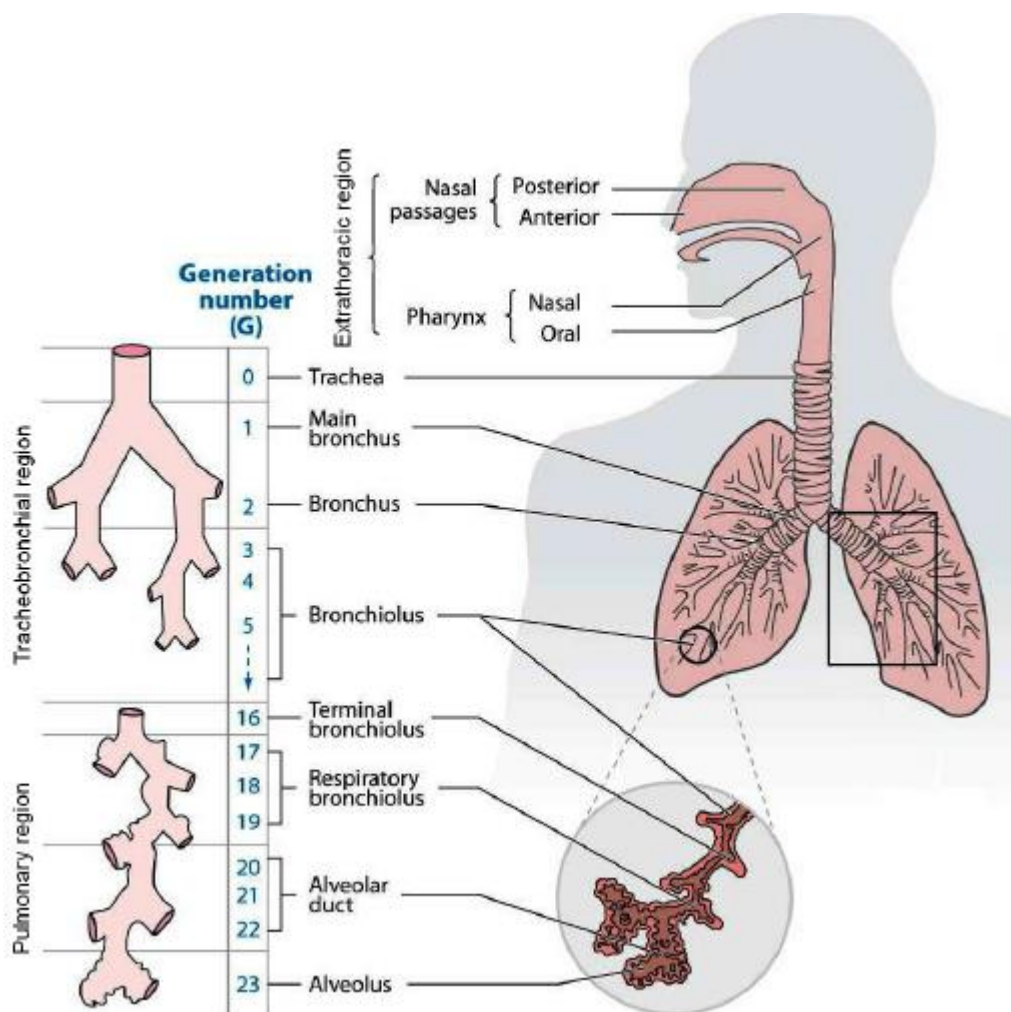
Fig. 3.3. Anatomical regions and airway generations according to the ICRP (International Commission on Radiological Protection) model. Reprinted with permission from [30].

When particles are inhaled, they can be subject to different deposition mechanisms: inertial impaction, gravitational sedimentation, Brownian diffusion, interception and electrostatic precipitation (Fig. 3.4). The type of deposition is mainly dependent from size and shape of particles.

Impaction occurs in the extrathoracic airways such as at the right angle bend of the pharynx and at airway bifurcations. When particles have too much inertia due to their size or velocity and the airstream is changing direction, it may happen that they are not able to follow the flow but hit the airway wall instead. As with the increasing total cross sectional area the flow velocity decreases more and more during its way through the lungs, impaction happens less often in the lower lungs [29, 31, 32].

Gravitational sedimentation is dominant in the small airways and the alveolar region, because airstream velocity is low there. During slow breathing or breath-holding, particles can settle down due to gravity. Sedimentation rate is so fast that around 3 seconds of breath-holding are sufficient to achieve settling of a 5 µm particle [29, 31, 32].

Submicron particles undergo the random Brownian motion. The smaller the particles are, the faster they move. A 50 nm particle for instance can move 120 µm within one second [31]. Both impaction and sedimentation occur mainly for particles with an aerodynamic diameter between 1-10 µm, diffusion for particles below 1 µm [29].

Non-spherical particles such as elongated particles can further deposit by interception. Interception happens when the center of gravity is in the airstream, but a distal end of the particle touches the airway wall. In consequence the whole particle can attach to the airway wall. Interception occurs mainly when the airway diameter is in the same size range as the particle length and mostly in larger bending airways, when aspherical particles are propelled out of the airstream due to their momentum [31, 33].

Electrical forces to charged particles are expected to influence the particle deposition as well, however, knowledge about electrostatic precipitation is still limited [29, 31].
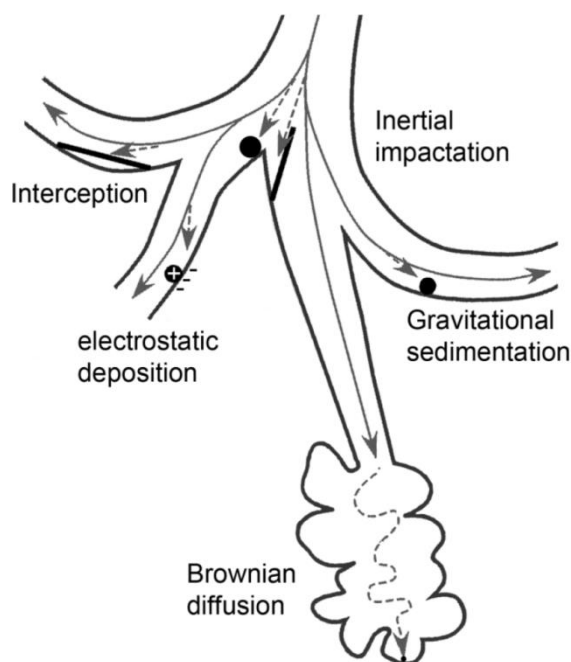
Fig. 3.4. Particle deposition mechanisms. Reprinted with permission from [34].

As described above, most deposition mechanisms depend on the aerodynamic particle size. Particles above 1 µm deposit mainly by sedimentation and impaction, while deposition by diffusion is increased the smaller the particles are. These findings correlate with the ICRP (International Commission on Radiological Protection) deposition model, where the total deposition shows two peaks (Fig. 3.5) [32]. One peak is in the lower nanometer range, representing the particles depositing by diffusion, the other one around 1-10 µm with the impacting and sedimenting particles. For an alveolar and tracheobronchiolar targeting we can see that sizes between 1-10 µm are favorable, although the main part of the particles deposits in the non-thoracic region. Particles

larger than 10 μm deposit nearly completely in the head airways. In principle also particles below 100 nm show good pulmonary deposition. However, such small nanoparticles might not be useful for drug delivery, as particles would tend to form aggregates due to high specific surface. Between 0.1-1 μm total deposition is the lowest. As particles in this size show slow diffusion and are too small for impaction and sedimentation, they are mostly exhaled again before being able to deposit [32]. Most polymeric nanoparticles intended for drug delivery show a size above 100 nm, thus are in the range of the lowest deposition and are not suitable for direct inhalation as dry powder formulation.
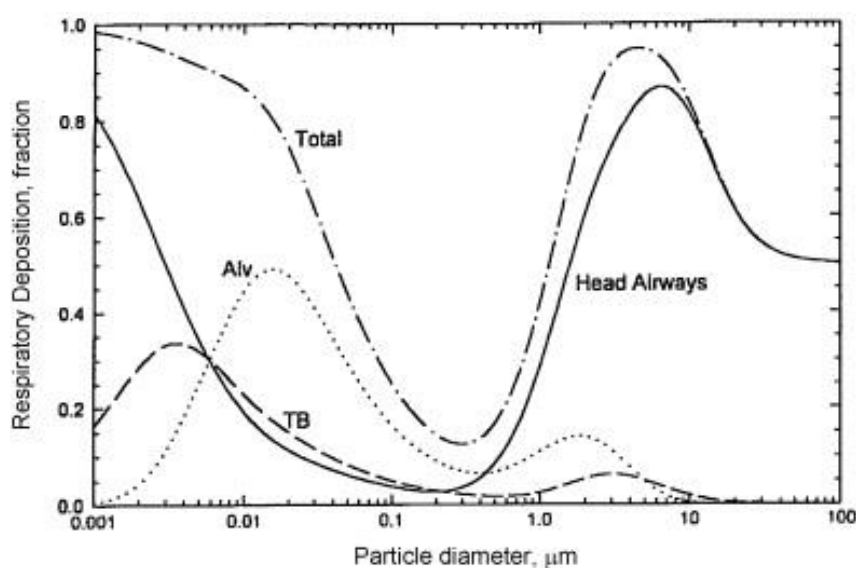
Fig. 3.5. Total and regional deposition based on the ICRP (International Commission on Radiological Protection) deposition model. Highest deposition is predicted for particles below 100 nm and between 1 and 10 μm, respectively. Alv: alveolar region; TB: tracheobronchial region. Reprinted with permission from [32].

However, nanoparticles might be applied as nanosuspension via nebulization. Nebulizers create aerosols from solutions or suspensions e.g. by compressed air or ultrasound and thus are able to create droplets in an appropriate size for pulmonary delivery. Nevertheless, also the application of nanoparticles by nebulization is disadvantageous. From technological sight it would be a challenge to develop a long term stable nanosuspension without high microbiological contamination and nanoparticle aggregation. From the patient's perspective most nebulization devices show disadvantages such as limited portability, time-consuming application, high bacterial contamination risk and poor reproducibility [35, 36]. Thus, handy devices with a short inhalation time such as dry powder inhalers are often preferred.

3.1.5. Microparticles as pulmonary delivery system for nanoparticles

For an easy and fast application by inhalation, dry powder inhalers are well suited. To guarantee a good lung deposition, microparticles with an aerodynamic diameter of 1-10 µm are required. A prominent approach to deliver nanoparticles by dry powder inhaler is thus to prepare nano-embedded microparticles, also called Trojan particles [37-39]. Those microparticles serve as carrier for the nanoparticles and can transport them into the lungs. In the lungs the nanoparticles are supposed to be released again to benefit from the advantages of a nanoparticulate drug delivery system.

To convert nano- into microparticles, spray drying is the method of choice, as nanosuspensions can be dried into particles of appropriate sizes for pulmonary delivery. To ensure redispersibility after landing in the lungs, the use of water-soluble matrix excipients is favorable. The approach of nano-embedded microparticles has already been followed by different research groups. Spray drying into microparticles has been performed with nanoparticles consisting from materials such as poly(lactic-co-glycolic acid) (PLGA), chitosan, gelatin, poly-ε-caprolactone (PCL), polyacrylate, polybutylcyanoacrylate and silica. For the matrix, excipients such as mannitol, lactose, trehalose, cyclodextrin, leucine and phospholipids have been used [40-46].

Another method to prepare microparticles composed of nanoparticles is the template-assisted technique. The pores of a track etch membrane are filled with nanoparticles which are subsequently interconnected to form cylindrical particles. These can be released by dissolving the membrane. Recently, the preparation of rod-shaped microparticles composed of nanoparticles has been performed with non-biodegradable silica nanoparticles [47, 48]. Nanoparticles were interconnected by agarose or the layer-by-layer technique using polyallylamine hydrochloride (PAH) and poly(sodium 4-styrenesulfonate) (PSS) as charged polymers [47, 48]. As these interconnecting materials are not soluble in water, a disintegration into nanoparticles is not easily possible. However, the template technique represents an innovative and promising approach to prepare microparticles composed of nanoparticles, as elongated particles are expected to show better deposition in deeper lung regions compared to spheres of the same volume [33].

Both spray drying and template technique enable the preparation of nano-embedded microparticles and thus represent promising drug delivery systems for the treatment of bacterial infections in cystic fibrosis. Microparticles can be easily applied by dry powder inhaler and show a good distribution in the lungs. After deposition, the microparticle matrix is supposed to dissolve and to release the nanoparticles, which can then penetrate

the mucus barrier and release the drug in a controlled way. By this innovative drug delivery system efficacy of pulmonary antibacterial therapy in CF patients might be improved.

3.2. Techniques of interest

In the following subchapter selected preparation and analytical methods with relevance for this work will be presented.

3.2.1. Nanoparticle preparation

In this work two common methods to prepare polymeric nanoparticles were used, the nanoprecipitation and the emulsion-diffusion-evaporation technique.

The nanoprecipitation, also called solvent displacement or interfacial deposition method, is a fast and easy nanoparticle preparation method. Two miscible solvents are necessary, from which one is a solvent for the polymer and the other one a nonsolvent. The polymer solution (solvent) is slowly added to the nonsolvent containing a stabilizer. As consequence of the rapid diffusion of the solvent into the nonsolvent, interfacial turbulences occur and droplets are reduced in size. Due to the desolvation, polymer chains aggregate to form nanoparticles [49, 50]. In the case of gelatin nanoparticles, gelatin is dissolved in water (solvent) and added to an organic poloxamer solution (acetone or ethanol). As gelatin is water-soluble, an additional crosslinking step is necessary to enable stability of nanoparticles in an aqueous medium. Glutaraldehyde is used to crosslink the gelatin molecules in the nanoparticles. After a certain incubation time, nanoparticles are transferred to an aqueous environment by centrifugation and redispersion in water [49]. Lipid-core nanocapsules are as well prepared by nanoprecipitation. The solvent (acetone) contains the polymer (e.g. poly-ε-caprolactone), the core components (oil, sorbitan monostearate) and the lipophilic drug. The solvent is injected into the aqueous polysorbate solution (nonsolvent) and nanocapsules are formed by a mechanism of self-assembly. Subsequently the organic solvent is removed under reduced pressure and the nanosuspension further concentrated [51, 52].

For the emulsion-diffusion-evaporation technique the solvent and the nonsolvent must not be miscible, but the solvent needs to be partially soluble in the nonsolvent. The polymer is dissolved in an organic volatile solvent and added to the aqueous stabilizer solution. Emulsification can be performed by a high-energy shearing source such as an ultrasonic or ultra turrax homogenizer. A subsequent dilution step with a high amount of nonsolvent enables the solvent in the emulsion droplets to diffuse out and precipitation of the polymer occurs. Finally, the organic solvent is evaporated [53]. For the preparation of PLGA nanoparticles ethylacetate can be used as solvent for the polymer and polyvinylalcohol (PVA) as stabilizer. Subsequent washing steps are performed by centrifugation and redispersion.

3.2.2. Microparticle preparation

Preparation of microparticles in an appropriate size range for pulmonary application is challenging. Common methods are milling, spray drying, spray-freeze-drying and precipitation by supercritical fluids [54]. A novel technique is the preparation of cylindrical particles by template technique [47]. The methods used in this work will be presented more detailed.

Spray drying

Spray drying is a drying process that converts dissolved or suspended substances into solid, dry particles by the following three fundamental operations: atomization - drying - separation. The solution or (nano-)suspension is atomized by a nozzle or vibrating mesh to small droplets, which expose their large surface immediately to a heated gas. By the rapid evaporation of the liquid in the droplets, solid dry particles are formed. The dried particles are then separated from the drying gas by a cyclone or electrostatic precipitator [54, 55].

In this work two different types of devices were used: the Nano Spray Dryer B-90 and the Mini Spray Dryer B-290 (both from Büchi, Flawil, Switzerland). The two spray dryers show differences regarding atomization technique, construction of drying chamber and separation.

The Mini Spray Dryer B-290 is one of the traditional spray dryers with pneumatic atomization (Fig. 3.6). In a two-fluid nozzle the liquid feed comes in contact with pressurized air at the nozzle orifice and a spray cone is created. The sprayed liquid enters the drying chamber from the same direction as the drying gas, in co-current [54, 55]. The droplets dry during their way through the drying chamber and follow the air stream around a 90° bend towards the cyclone. Larger, undried droplets will deposit in the collector under the drying chamber. Between drying chamber and cyclone the outlet temperature is measured. The air stream with the dried particles enters the cyclone tangentially. In consequence, centrifugal forces act on the particles, which will impact the cyclone walls and will be removed from the air stream. The particles are collected in the bottom vessel, while the air stream is flowing upwards together with the finest particles [54, 55].
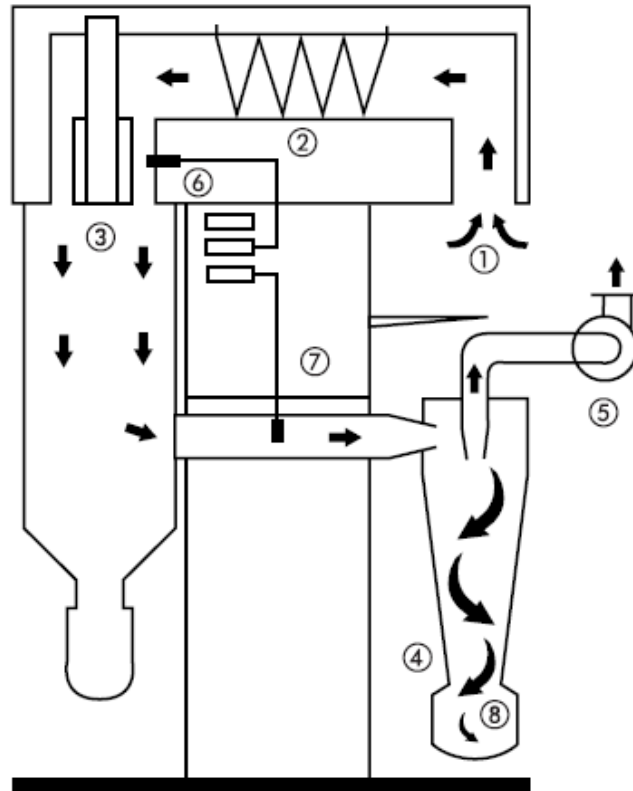
Fig. 3.6. Schematic of a conventional spray dryer. 1) Aspirating Port, 2) Heating, 3) Entry of drying gas into drying chamber, 4) Cyclone, 5) Aspirator, 6) Inlet temperature sensor, 7) Outlet temperature sensor, 8) Collector. Reprinted with permission from Büchi (Flawil, Switzerland) [56].

The Nano Spray Dryer B-90 (Fig. 3.7) contains several novel features. First of all, atomization is performed by a vibrating mesh. The spray mesh is a membrane with an array of precise holes in a size of 4.0, 5.5 or 7.0 µm. The mesh is vibrating due to a piezoelectric driven actuator and produces droplets with a precise size and narrow size distribution. This technique allows the production of particles in the submicron range, starting from 300 nm, thus far smaller than particles prepared with the traditional spray drying technique [55, 57]. The second innovation is the cylindrical one-piece-construction. Due to the laminar air stream and minimal dead volume, substance loss is reduced and spray drying of small sample amounts is possible. Finally, the B-90 has a novel particle separation technique, an electrostatic particle collector. Dried particles are electrostatically charged and then collected by the oppositely charged collector electrode. From this cylindrical collector the particles can be scraped off. Due to this separation technique also small particles are collected and high yields even with small sample amounts are possible [55, 57].
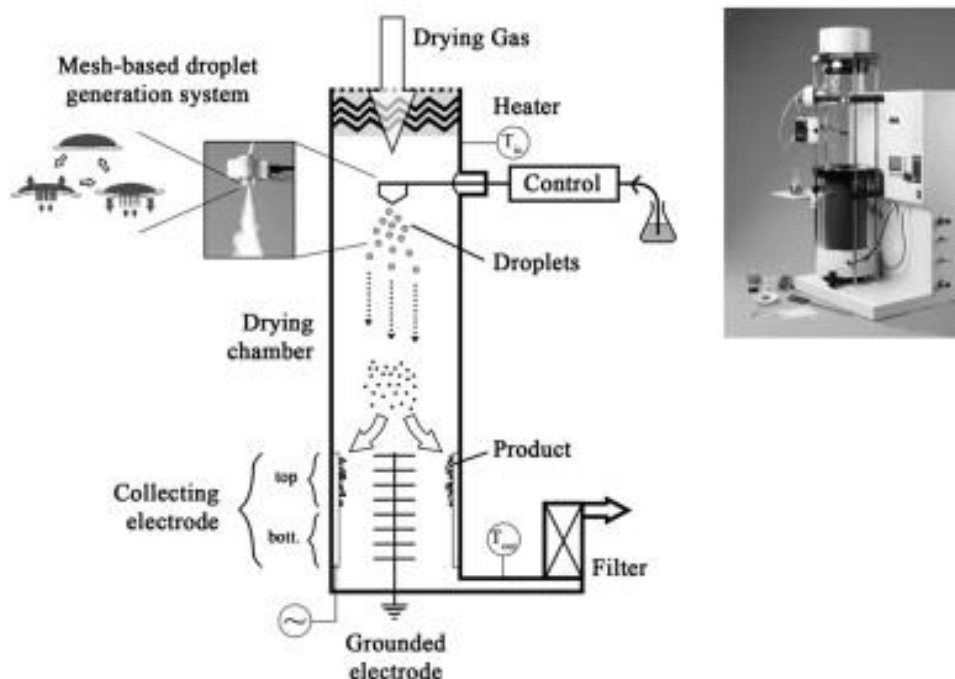
Fig. 3.7. Schematic of the Büchi Nano Spray Dryer B-90. Reprinted with permission from [57].

Important parameters in spray drying are inlet and outlet temperature, feed rate, composition and concentration of the spraying liquid as well as drying gas flow and spray gas flow. These parameters allow tuning of the produced particles, e.g. in terms of size, shape and density and therefore also of the aerodynamic diameter [54]. Particles prepared by spray drying are often spherical, but can also have irregular structures such as raisin shape [54]. Depending on the spray drying parameters and the ingredients of the formulation, hollow particles can be prepared [58]. These low density particles are well suited for pulmonary drug delivery. In general spray drying is an appropriate preparation technique for microparticles intended for inhalation as the particle properties and thus the lung deposition can easily be influenced.

Template-assisted technique

The template-assisted technique is a recently developed method to prepare aspherical particles. The approach of the inverted template method is to fill a mold of a certain shape with a material that is subsequently released from the template with the desired shape (Fig. 3.8) [59]. By using polycarbonate track-etched membranes with cylindrical pores, rod-shaped particles or fibers can be produced. The size of the resulting particles is defined by the thickness of the membrane and the pore diameter. The pores can be filled with a nanosuspension by an infiltration technique. The template membrane is placed in a filter holder with a blocking membrane beneath. The blocking membrane has a pore size below the nanoparticle size and thus allows only the water to pass, while nanoparticles are accumulated inside the template pores. After the filling of the membrane, the nanoparticles need to be interconnected to maintain the microparticle shape. In consequence, the rods can be released by dissolving the polycarbonate membrane with an appropriate solvent.
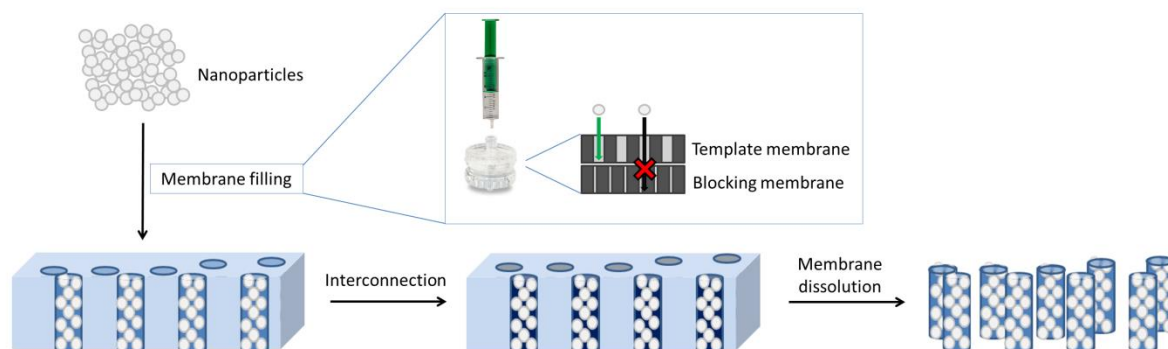
Fig. 3.8. Schematic of the template-assisted technique.

3.2.3. Characterization of aerodynamic properties

Particles intended for inhalation are characterized by their aerodynamic properties. Not only the geometric diameter, but also the shape and density have an influence on the flying properties. Thus, the aerodynamic diameter combining these three parameters is used for characterization. The aerodynamic diameter (d_{ae}) is defined as the diameter of a unit density sphere settling with the same velocity [31, 32]. It is described by the following equation (3.1):

$$d_{ae} = d_{geo} \cdot \sqrt{\rho/\chi} \qquad (3.1)$$

with χ being the shape factor, d_{geo} the geometric size and ρ the particle density [60]. The shape factor is usually < 1 for non-spherical particles [60]. To report the characteristics of a powder for inhalation the mass median aerodynamic diameter (MMAD) is used together with the geometric standard deviation (GSD). The MMAD is the cut-off size at which 50% of the particle mass is smaller and 50% larger. The GSD allows estimating the size distribution. It is dimensionless and defined by the following equation (3.2):

$$GSD = \sqrt{D_{84.1}/D_{15.9}} \qquad (3.2)$$

$D_{84.1}$ and $D_{15.9}$ are the cut-off sizes under which 84.1% and 15.9%, respectively, of the aerosol mass resides [29].

Another parameter to evaluate a powder's aerodynamic properties is the fine particle fraction (FPF). The FPF is the mass fraction of the powder released from the inhaler with an aerodynamic diameter below 5 µm and is expected to represent the percentage of the formulation reaching the lungs [29].

Impactors are the devices of choice to characterize powders for inhalation in terms of their flying properties, as they can classify particles according to the aerodynamic diameter. The Next Generation Impactor (NGI) is a novel device with a horizontal layout (Fig. 3.9). It consists of seven stages and a micro-orifice collector representing the final filter. The aerosolized powder enters the impactor by a 90° angled induction port that is mimicking the throat. Subsequently it is led through the pre-separator in which larger particle aggregates are collected before the powder enters the impactor stages [61]. The air with the aerosolized powder flows through the impactor in a saw tooth pattern. Each stage contains a nozzle and a collection cup for impacted powder. The air and particles small enough to follow the airstream leave the stage by the exhaust cavity in the lid (Fig. 3.10). Larger particles impact in the collection cup. By progressively reduced nozzle diameters the airstream velocity is increased during its way through the impactor and

particles are impacting depending on their size [61]. The cut-off diameters for the different stages are defined by the used air flow rate. The impacted powder can be quantified after rinsing the collection cups. By calculating the cumulative mass fractions for the different cut-off diameters, the MMAD can be interpolated and the GSD and FPF can be determined.
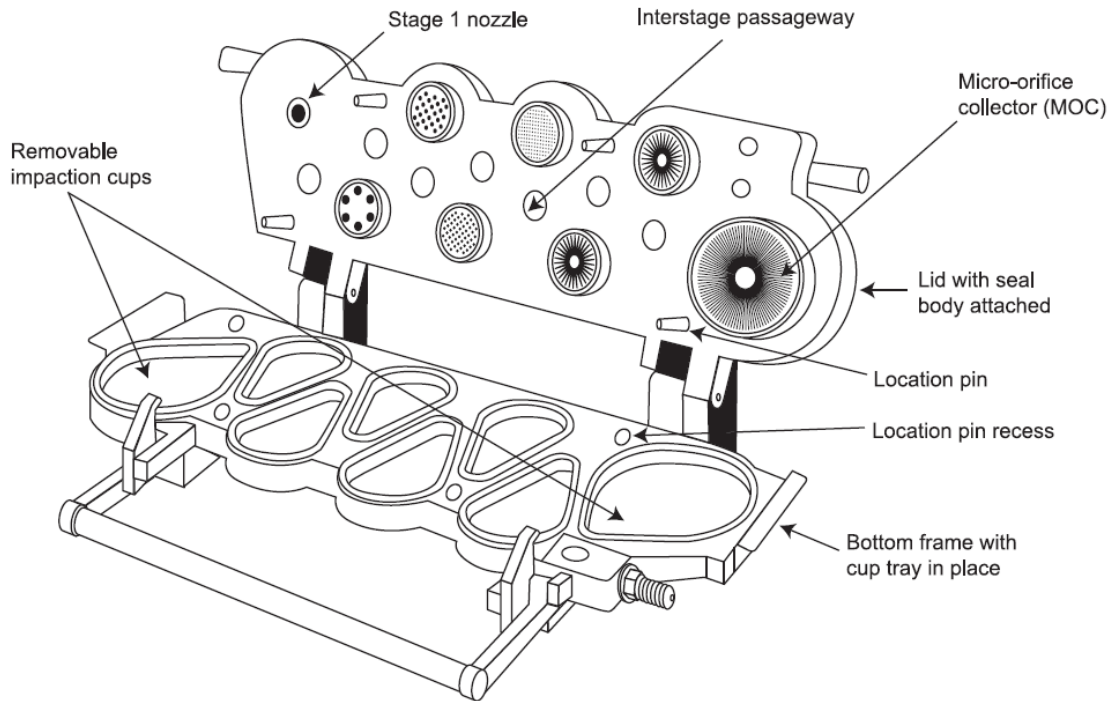
Fig. 3.9. Next Generation Impactor (NGI) in opened state (without induction port and pre-separator). Reprinted with permission from Ph. Eur. 5.1 [62].
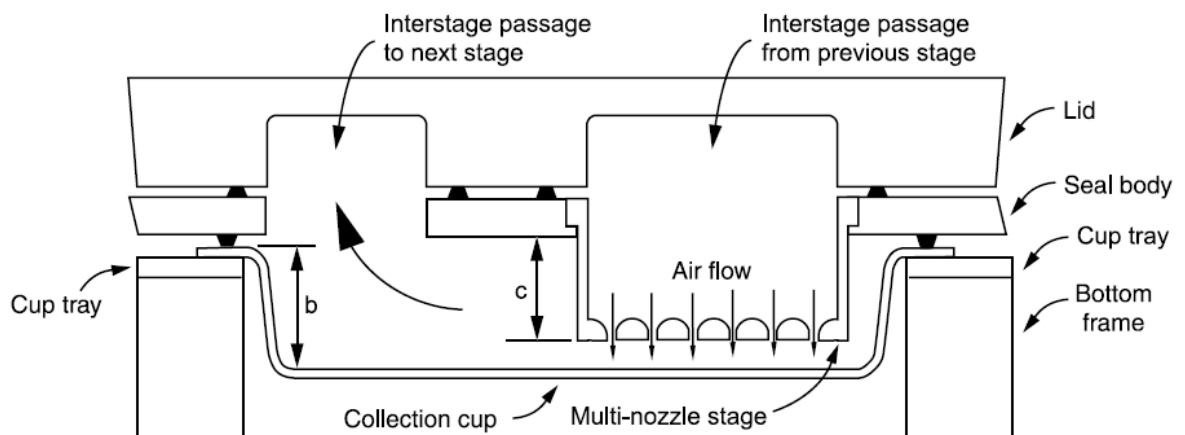
Fig. 3.10. Cross section of one NGI stage. Particles above a certain aerodynamic cut-off diameter impact in the collection cup, while smaller particles fly to the next stage together with the air. Reprinted with permission from Ph. Eur. 5.1 [62].

4. AIM OF THIS WORK

Respiratory mucus is one of the main barriers impeding a successful eradication of bacteria colonizing cystic fibrosis patients' lungs. Nanoparticles with low mucus interaction can improve the transport of a drug through mucus and thus represent a promising drug delivery system for antibiotics in cystic fibrosis. However, for an application as dry powder formulation, nanoparticles need to be converted into microparticles. After deposition in the lungs, these microparticles disintegrate and the released nanoparticles deliver the drug across the mucus barrier. A common method to prepare microparticles composed of nanoparticles is spray drying, yielding spherical particles. An innovative approach is the preparation of aspherical particles. Elongated particles such as fibers are expected to show good aerodynamic properties.

The overall objective of this thesis is to tackle the challenges to overcome the mucus barrier and to deliver nanoparticles into the lungs by using microparticles composed of nanoparticles. To achieve this goal, the following four aims are stated:

I) Characterization of different mucus models
II) Development of antibiotic-loaded mucus-penetrating nanoparticles
III) Embedding of nanoparticles into microparticles optimized for inhalation and redispersibility
IV) Comparison of different geometries and preparation techniques for microparticles composed of nanoparticles

The first aim focuses on the characterization of mucus to gain essential information for developing mucus penetrating nanoparticles. Especially pore sizes are of relevance as nanoparticles can be retained due to size-exclusion effects.

The second objective comprises the development and characterization of antibiotic-loaded nanocapsules. A crucial parameter for nanoparticles intended for the treatment of bacterial infections in cystic fibrosis is the ability to penetrate in mucus without being entrapped. A sustained drug release is favored as it can enable a reduction of the dosing frequency.

The third aim was to prepare nano-embedded microparticles by spray drying with optimized aerodynamic properties and disintegration behavior. For an appropriate testing of the redispersibility, a model to investigate the disintegration of nano-embedded microparticles under conditions similar to the lungs shall be established.

The fourth objective aims to compare cylindrical with spherical microparticles composed of nanoparticles. Spray drying and template-assisted technique shall be compared in terms of tunability of the particle size, aerodynamic properties, nanoparticle content and disintegration behavior.

5. VISUALIZATION OF MUCUS

Porcine and human mucus samples used in this work were collected and processed by Xabier Murgia and Jenny Juntke (Helmholtz Institute for Pharmaceutical Research Saarland). Analysis of human tracheal mucus was performed together with Xabier Murgia.

5.1. Introduction

Mucus as biological barrier for pulmonary drug delivery has been extensively researched in the past years. Despite a high level of knowledge on the mucus composition on a molecular level, the structural array of mucin fibers and other components such as proteins and lipids remains relatively unclear. However, the inner structure of mucus plays an important role for the penetration by nanoparticles as particles are reported to be retained in the mucus network by size exclusion effects if they are larger than the mesh spacings [22]. Hence, it is of high interest to know the pore sizes of the mucus network. Furthermore, as stability and availability of fresh mucus samples are limited, it is relevant to know if preservation methods such as freeze drying or freezing will change the mucus structure and if alternative mucus sources may be used.

The imaging of mucus by conventional scanning electron microscopy is only possible after extensive sample preparation due to the high water content and the dynamic structural arrangement of mucin fibers [9]. Imaging of respiratory mucus has been performed so far by several groups after chemical fixation of mucus by glutaraldehyde and osmium tetroxide and subsequent drying of the samples [24, 63, 64]. This preparation method however results in images with mucin fibers that are about 10-fold thicker than the biochemically determined diameter [9]. This effect might be due to aggregation or condensation of mucin fibers or adsorption of proteins to the fibers during fixation [9]. Thus, it is unclear how much the resulting images reflect the actual mucus structure. Another drawback of SEM imaging after fixation is the limitation on the mucus surface. The surface of mucus might differ from the interior of the hydrogel as it has an interface to the air space potentially covered by surfactants.

To avoid chemical fixation and associated artefacts, cryogenic scanning electron microscopy (CSEM) can be applied. Samples are thermally fixated by rapid cooling such as freezing in liquid nitrogen. By imaging at cryogenic temperatures, hydrogels can be imaged in their hydrated, native state. Furthermore, the CSEM sample preparation enables freeze fracturing of samples and sublimation of surface water and thus allows the

imaging of the internal structure. CSEM has been used so far for imaging of equine respiratory mucus [10, 65] and porcine intestinal and biosimilar mucus [66].

In this work, CSEM was applied to investigate the influence of preservation methods on the pore size of mucus and to compare mucus types from different sources. First, the mucus structure of porcine tracheal mucus in fresh state and after freeze drying and rehydration was compared. Second, imaging was performed for fresh and thawed frozen human tracheal mucus and pore sizes were determined. Finally, equine respiratory mucus was imaged to evaluate the comparability with human mucus.

5.2.   Experimental details

5.2.1. Materials

Samples of fresh and freeze-dried porcine tracheal mucus and fresh human tracheal mucus were obtained as kind gift from Helmholtz Institute for Pharmaceutical Research Saarland (HIPS). Porcine mucus was collected from the tracheas of slaughtered pigs and human mucus from endotracheal tubes used during surgery. Before imaging, freeze-dried porcine mucus was rehydrated with MEM medium (containing FCS, NEAA and glucose; obtained from HIPS) to reach the original liquid content (85.7%; determined experimentally by evaluating the weight loss upon lyophilization). To investigate the influence of freezing, fresh human mucus was frozen overnight or longer at -20°C. Horse lung mucus was obtained by bronchoalveolar lavage with saline and kept in frozen state until use. After thawing, samples were centrifuged (3,000 x g, 10 min) and the aqueous supernatant was taken off to remove contained saline.

5.2.2. CSEM Imaging

Mucus was placed between two metallic freezing tubes (Gatan, Abingdon, UK) and frozen by immersion into liquid nitrogen (Fig. 5.1). The upper tube was knocked off inside the cryo transfer system (Alto 2500, Gatan) to create a fractured surface and sublimation was performed (-95°C, 15 min). Subsequently samples were sputter-coated with platinum at -140°C and transferred to the SEM cryo-stage (JSM-7500F, JEOL, Tokyo, Japan). Imaging was performed at -140°C and 5 kV acceleration voltage. For human tracheal mucus, each three samples of fresh and frozen mucus from different patients were imaged.
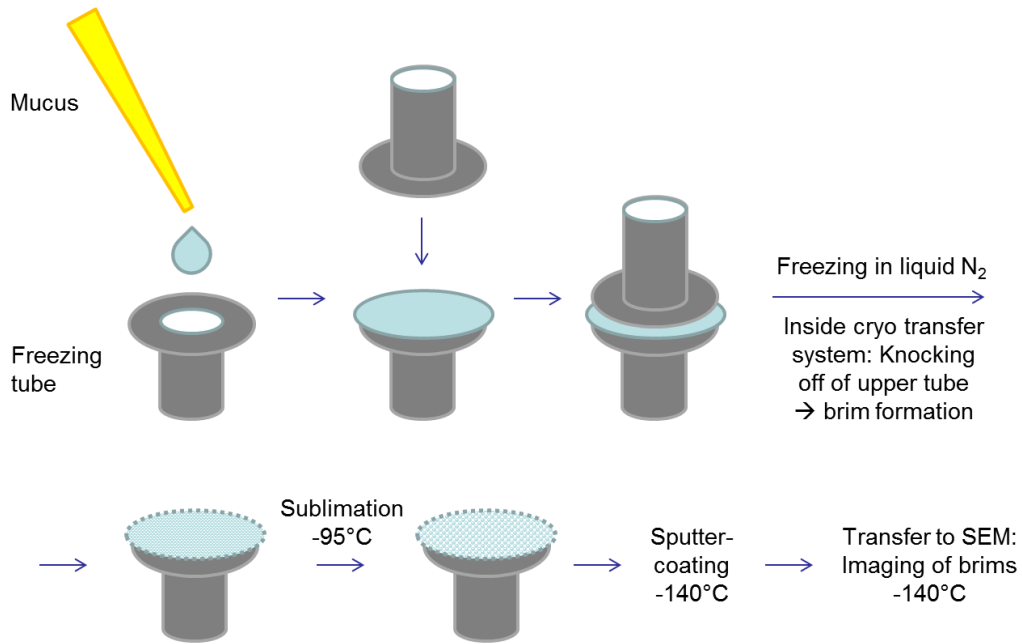
Fig. 5.1. Preparation of mucus samples for CSEM imaging.

5.2.3. *Image analysis*

Pore sizes were determined by ImageJ 1.48v software (National Institutes of Health, USA) (Fig. 5.2). Image contrast and brightness were adjusted and a threshold was set appropriately to clearly distinguish the inside of the pores from the pore walls (Fig. 5.2 B). Pore areas were determined by the "Analyze Particles" function (Fig. 5.2 C) and converted to equivalent circular area diameters. For fresh and rehydrated freeze-dried porcine mucus each 200 pore sizes were measured. Each 12 images for both fresh and frozen human mucus were analyzed. For equine mucus analysis was performed for 5 images.
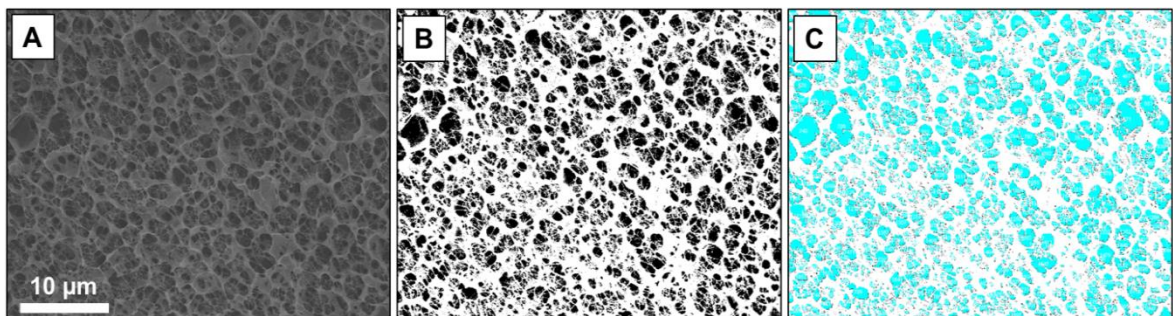
Fig. 5.2. Pore size determination: The original CSEM images (A) were processed and a threshold was applied (B). The measured pore areas are displayed in light blue (C).

5.3. Results and discussion

5.3.1. Influence of freeze drying on porcine tracheal mucus

Porcine tracheal mucus was imaged in fresh state and after freeze drying and rehydration. In both cases a foam-like structure with a rigid scaffold building the pore walls was observed (Fig. 5.3). In comparison, SEM images obtained after chemical fixation show a network formed by entangled fibers [63, 64]. Differences in the structures of the two types of porcine mucus can be observed. The fresh porcine mucus shows a longitudinal orientation which might be due to shear strain during sample preparation. The pore walls in the freeze-dried and rehydrated sample appear thicker and denser. This might be attributed to the relatively slow freezing step during freeze drying, which is expected to lead to aggregation of mucin fibers [9]. The determined pore sizes are nevertheless comparable in the two samples. Both show similar size distributions with most pores between 1-5 µm (Fig. 5.4) and a median pore diameter of 2.3-2.4 µm (Table 5.1). A student's t-test revealed no significant difference between the pore sizes of the two samples. Thus freeze drying might be an appropriate method to preserve mucus for investigation of nanoparticle retention due to size exclusion effects. Nevertheless, CSEM images reveal structure changes that might have an influence on the interaction of nanoparticles with mucus. As retention of nanoparticles due to interaction with mucus components plays an important role for the motion of nanoparticles inside mucus, the use of rehydrated freeze-dried mucus for permeation studies is not recommended. Furthermore, it can be observed that the pore sizes of porcine tracheal mucus differ strongly from those of human tracheal mucus (Fig. 5.7, Tab. 5.2). Thus, the use of porcine mucus is in general not advisable to simulate the *in vivo* situation in humans.
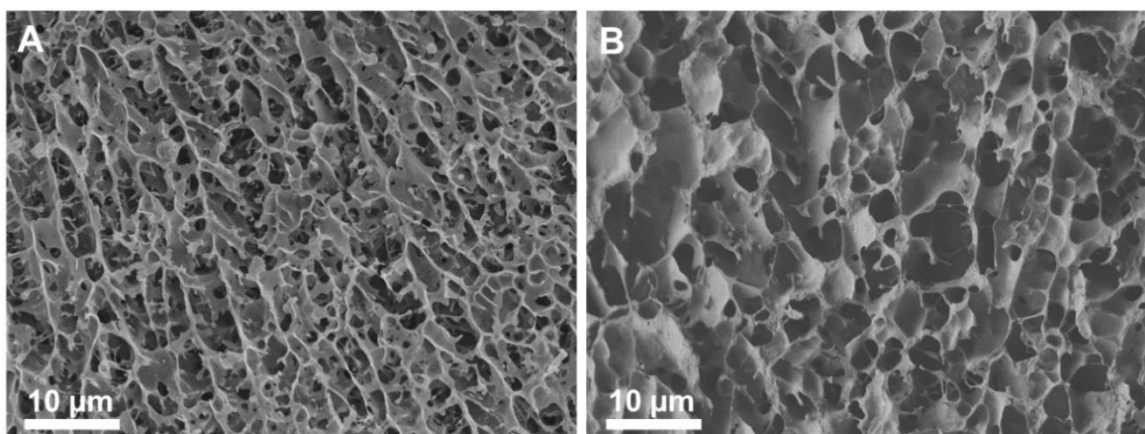
Fig. 5.3. CSEM images of porcine tracheal mucus in fresh state (A) and after freeze drying and rehydration (B).
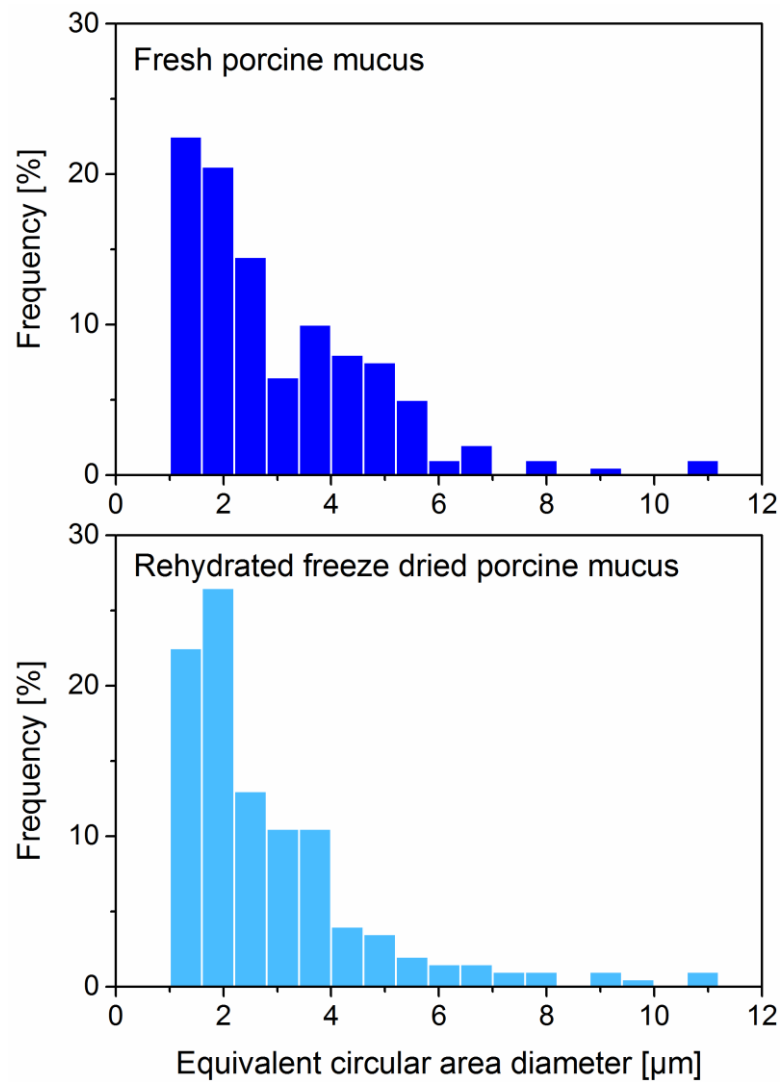
Fig. 5.4. Histogram of pore size distribution of fresh and rehydrated freeze-dried porcine mucus. For each sample 200 pore sizes were measured.

Porcine tracheal mucus	Dn10 [µm]	Dn50 [µm]	Dn90 [µm]
Fresh mucus	1.31	2.39	5.25
Rehydrated freeze-dried mucus	1.31	2.30	5.20

Table 5.1. Pore size distribution parameters for porcine tracheal mucus in fresh state and after freeze drying and rehydration. The Dn-values are the cut-off diameters at which 10%, 50% and 90% of the pores show a smaller equivalent circular area diameter.

5.3.2. Suitability of freezing for preservation of human tracheal mucus

Human tracheal mucus was imaged in fresh state and after freezing and thawing. A high variability of pore sizes within one mucus sample was observed. In the overview image displayed in Figure 5.5 A different types of regions can be seen. While there are pores with a diameter of around 10 µm visible, other areas of the freeze fractured surface appear rather smooth. On a closer look, these smooth areas are composed of fine structures (Fig. 5.5 B) and very filigree fiber networks (Fig. 5.5 C). Besides the fiber networks, other regions are characterized by rigid pore walls (Fig. 5.5 D) or a mixture of both (Fig. 5.5 B). This heterogeneity of mucus structure has not yet been described so far by SEM imaging after chemical fixation. On Figure 5.5 D both the inner structure and the surface of mucus can be seen. In the surface there are only few openings with a crack-like structure. It cannot be excluded that these cracks only appeared during sample preparation and imaging due to the present vacuum. Mucus might actually be lacking openings at the air interface or pores might be covered by a thin layer of mucus constituents. This shows that imaging of mucus without a fracturing step is not advisable as the surface differs from the inner structure.
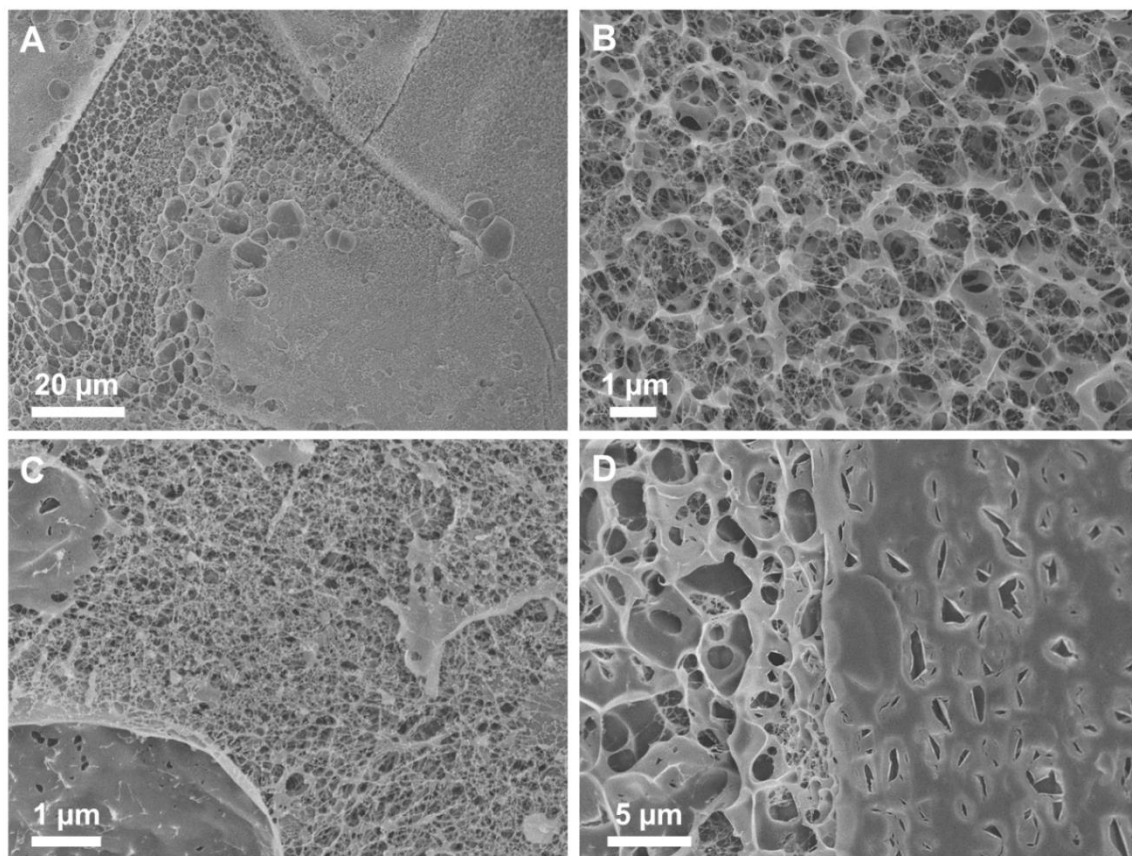
Fig. 5.5. CSEM images of fresh human tracheal mucus. A) Overview image showing the high variability within one sample; B) and C) Close-ups of regions with different pore sizes; D) The mucus surface (right side) shows less pores in comparison to the interior of mucus (left side).

After freezing and thawing, human tracheal mucus still displays a high heterogeneity of the pore structure (Fig. 5.6 A). Different types of regions can be found as in the fresh mucus samples, also the fine fibers are preserved (Fig. 5.6 B).
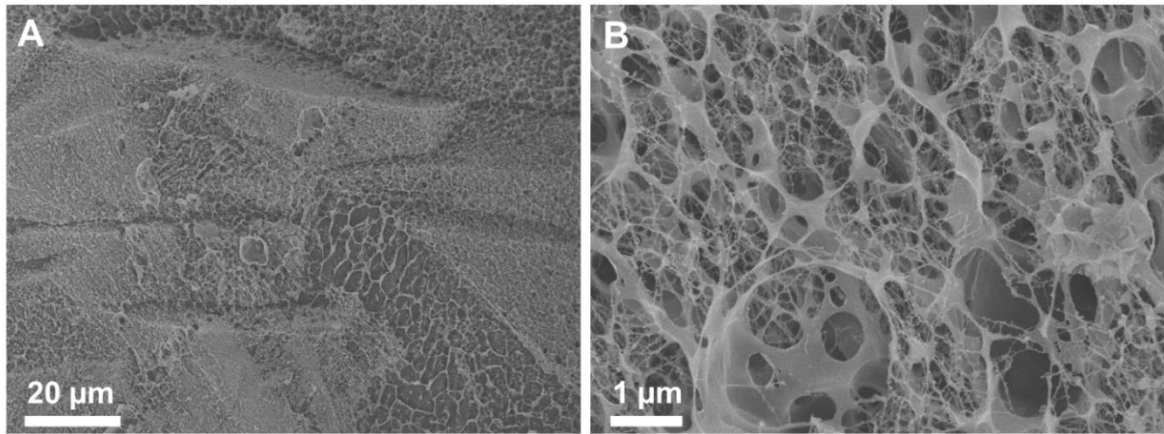
Fig. 5.6. CSEM images of thawed frozen human tracheal mucus. A) Highly heterogeneous structure as observed in the fresh samples; B) The fine fiber structures were not affected by the freezing.

For a better comparison of fresh and frozen human mucus, pore size distributions were analyzed. Both show a comparable distribution with most of the pores smaller than 500 nm (Fig. 5.7 and Table 5.2). A student's t-test did not show any significant difference. As no structural changes were observed, freezing is considered as appropriate preservation method for human tracheal mucus.
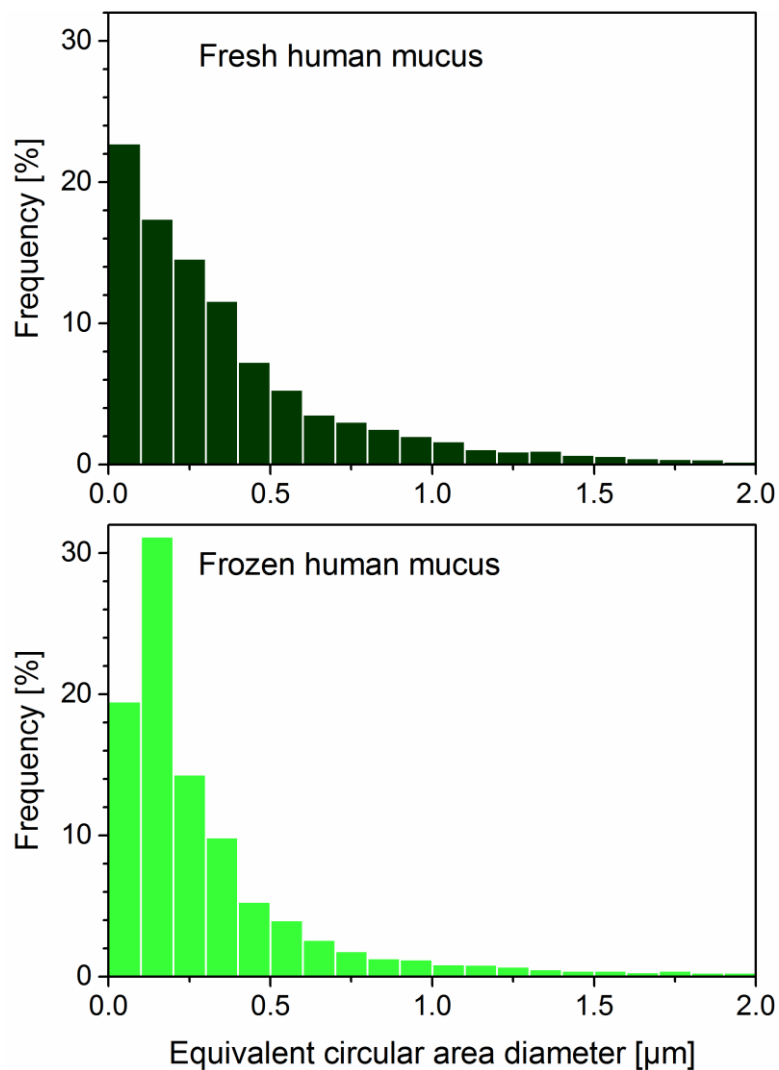
Fig. 5.7. Histogram of pore size distribution of fresh and thawed frozen human tracheal mucus. Each three different patient samples were imaged and 13524 pores for fresh and 8519 pores for frozen mucus were measured.

Human tracheal mucus	Dn10 [µm]	Dn50 [µm]	Dn90 [µm]
Fresh mucus	0.05	0.26	1.00
Frozen mucus	0.07	0.20	0.91

Table 5.2. Pore size distribution parameters for human tracheal mucus in fresh state and after freezing and thawing.

5.3.3.   Visualization of equine respiratory mucus

Respiratory horse mucus was imaged by CSEM to evaluate the suitability as model mucus. Samples were used after storage in frozen state, as freezing was evaluated as suitable preservation method. As already observed for human mucus, horse mucus shows as well high structural variability. Both dense areas with rigid pore walls and areas with fine fiber networks were detected (Fig. 5.8).

Similar to human mucus, most pores showed a size below 500 nm (Fig. 5.9). A slight shift to larger pore sizes was observed in comparison to human mucus (Fig. 5.9, Table 5.3).
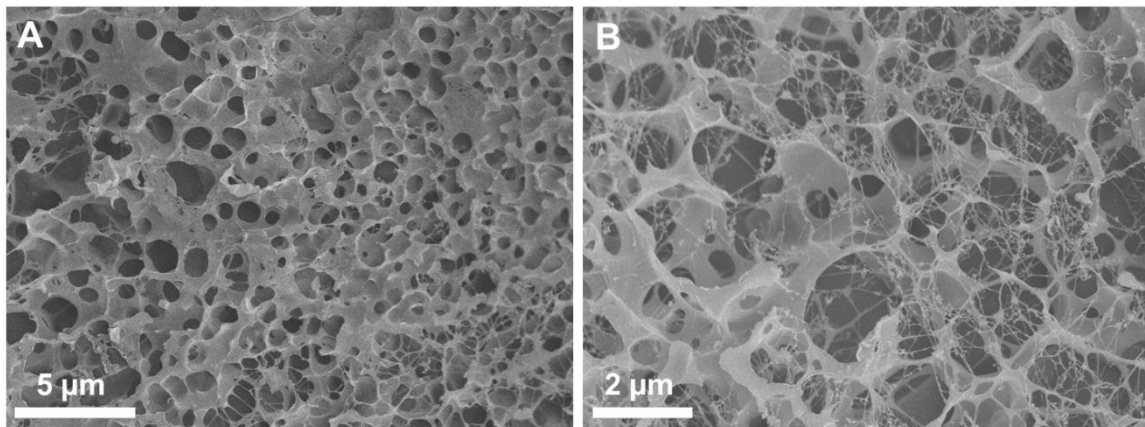
Fig. 5.8. CSEM images of respiratory mucus. Areas with rigid pore walls (A) were found as well as fine fiber-like structures (B).
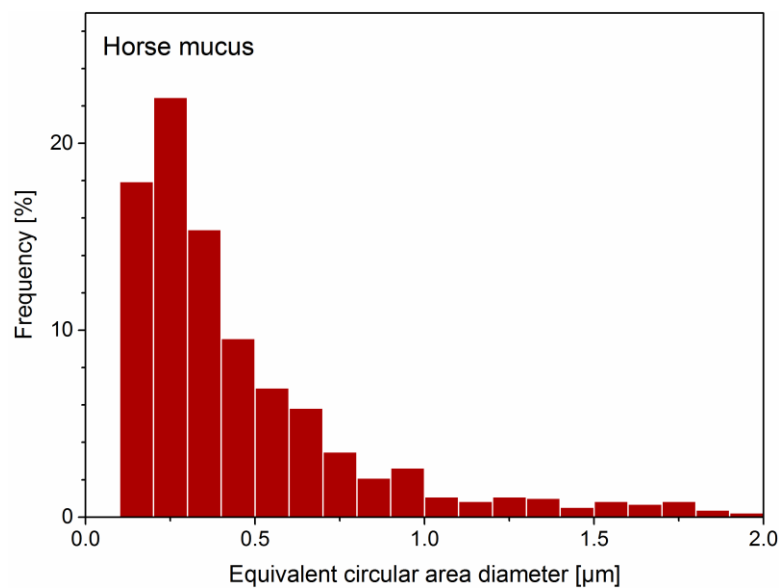
Fig. 5.9. Histogram of pore size distribution of respiratory horse mucus. 1286 pore sizes were measured.

	Dn10 [µm]	Dn50 [µm]	Dn90 [µm]
Horse mucus	0.15	0.35	1.34

Table 5.3. Pore size distribution parameters for horse mucus.

In comparison with porcine tracheal mucus, respiratory horse mucus shows higher correlation with human mucus in terms of the pore sizes. Thus, based on these data, horse mucus is better suited as model to investigate permeation of nanoparticles through mucus. As the pores are slightly larger than pores in human mucus, the obtained permeation rates may not exactly reflect the permeation in human mucus. Nevertheless, a good permeation behavior of nanoparticles in horse mucus indicates that nanoparticles may also permeate through human mucus without being entrapped.

5.4. Conclusion

Cryogenic scanning electron microscopy is an appropriate technique to image mucus in its hydrated state and to elucidate its inner structure. However, it can also be subject to artefacts. In samples with high water content large ice crystals can be formed due to too low cooling rate during plunging into liquid nitrogen. These crystals can cause damages [67]. As artefacts might occur, it cannot be definitely concluded that the visualized structures correspond completely to the real situation. Nevertheless, the artefact potential of CSEM is estimated to be lower than for SEM with chemical fixation. CSEM allows the comparison of different samples and an estimation of the pore size.

Most pores in human tracheal mucus had a pore size below 500 nm. However, a distinct cut-off size for nanoparticles cannot be given based on the images, as a high heterogeneity of regions with different pore sizes was observed. These diverse regions might also differ from their composition and thus show varying interaction potential with nanoparticles. Thus, it cannot be predicted through which regions nanoparticles might permeate easily or where they might be trapped. Porcine tracheal mucus showed larger pore sizes than human mucus and is thus not advisable for permeation experiments. In comparison, equine respiratory mucus may be used to evaluate nanoparticle-mucus interactions due to comparable pore sizes. Concluding from the performed experiments, the use of freeze drying as preservation method for mucus is not recommended due to visible structure changes. Freezing in comparison is considered as appropriate for storage of mucus.

6. CIPROFLOXACIN-LOADED LIPID-CORE NANOCAPSULES

Bacterial growth assays were conducted by Dr. Stefanie Wagner, Helmholtz Institute for Pharmaceutical Research Saarland (HIPS), Chemical Biology of Carbohydrates, Saarbrücken, Germany. Cryo-TEM measurements were performed by Dr. Marcus Koch, INM Leibniz Institute for New Materials.

6.1. Introduction

The prophylaxis and treatment of bacterial lung infections are essential components of cystic fibrosis therapy. The broad spectrum fluoroquinolone ciprofloxacin is one of the established antibiotics as it shows efficacy against CF-relevant bacteria such as *Pseudomonas aeruginosa* and *Staphylococcus aureus*. Ciprofloxacin can be administered orally or intravenously. However, the systemic application involves as well systemic side effects, which limit the use of ciprofloxacin mainly to adults. A long term use in children is not recommended due to safety concerns [68]. By applying the antibiotic by inhalation, the drug is delivered directly to the site of infection. Higher local concentrations allow a reduction of dose and thus involve lower systemic side effects. The pulmonary application might also enable the use of ciprofloxacin for pediatric patients. In clinical studies a ciprofloxacin dry powder formulation is currently being investigated and efficacy of inhaled ciprofloxacin in chronic *P. aeruginosa* infections has already been shown [69].

However, the highly viscous mucus in cystic fibrosis represents a barrier for antibacterial drugs as drug diffusion through mucus is limited and deactivation of antibiotics can occur [11, 12]. The use of nanoparticles as drug delivery system is a promising approach to protect the drug and to enhance mobility in mucus depending on surface properties, charge and size of nanoparticles [3, 19, 24, 70]. Furthermore, nanoparticles may enable a reduced dosing frequency due to a sustained drug release. In this context lipid-core nanocapsules (LNC) are an interesting nanoparticulate carrier system. LNC contain a lipid-core which is formed by an organogel composed of a liquid lipid and sorbitan monostearate. The shell consists of biodegradable and biocompatible polymers such as poly(ε-caprolactone) (PCL). Stabilization is achieved by polysorbate 80. Due to the lipid core, LNC can be efficiently loaded with poorly water soluble drugs [51, 71-73]. The nanocapsules protect the encapsulated drug from chemical and light induced degradation [71]. Furthermore, lipid-core nanocapsules show the ability to cross biological barriers and can enable decreased side effects and high pharmacological

responses [71]. With all these combined advantages, LNC represent a promising carrier system for encapsulation of the poorly soluble ciprofloxacin free base and for targeting bacteria inside mucus.

In this part of the work, the lipid-core nanocapsule formulation was adapted for a loading with ciprofloxacin. Aims for the ciprofloxacin-loaded LNC were a sustained release, high mucus permeability and antibacterial activity against *P. aeruginosa* and *S. aureus*.

6.2. Experimental details

6.2.1. Preparation of nanocapsules

The nanoprecipitation method was used to prepare ciprofloxacin-loaded lipid-core nanocapsules (LNC-CIP) [51, 71]. Poly(ε-caprolactone) (PCL) and sorbitan monostearate were dissolved in acetone and ciprofloxacin previously solubilized in oleic acid was added. The organic phase was injected into aqueous polysorbate 80 solution under magnetic stirring and light protection. After 10 minutes of stirring, the acetone and part of the water were removed by evaporation under reduced pressure (Rotavapor, Büchi) until a volume below 10 mL was reached. Volume was finally adjusted to 10 mL by adding water. For the preparation of blank lipid-core nanocapsules, oleic acid was used without addition of ciprofloxacin. For the cryo-TEM analysis a nanoemulsion (NE-CIP) was prepared by omitting PCL. In addition pure PCL particles without lipid core were prepared. In Table 6.1 the exact compositions are listed.

	LNC-CIP	LNC-blank	NE-CIP	PCL particles
Poly(ε-caprolactone)	0.1 g	0.1 g	-	0.1 g
Sorbitan monostearate	38.5 mg	38.5 mg	38.5 mg	-
Ciprofloxacin	8 mg	-	8 mg	-
Oleic acid	165 µL	165 µL	165 µL	-
Acetone	27 mL	27 mL	27 mL	27 mL
Polysorbate 80	77 mg	77 mg	77 mg	77 mg
Water	54 mL	54 mL	54 mL	54 mL

Table 6.1. Compositions of LNC-CIP, LNC-blank, NE-CIP and PCL particles yielding a final volume of 10 mL nanosuspension.

6.2.2. Testing of interaction between polymer and lipid

Poly(ε-caprolactone) films were prepared by dissolution of the polymer in chloroform and subsequent evaporation of the solvent in a glass petri dish. The film was cut into fragments (n = 3) which were accurately weighed, immersed separately in glass vials filled with oleic acid and stored at room temperature. The films were withdrawn from the oleic acid at predetermined time points (1, 2, 5, 15, 30, 60 days), completely dried with tissues and weighed.

6.2.3. Physicochemical characterization of nanocapsules

To exclude the presence of microparticles, laser light diffraction analysis was performed with a Mastersizer[®] 2000 by dropping the nanosuspensions and ciprofloxacin suspension, respectively, into a wet dispersion unit filled with water. Exact size values and the polydispersity index (PDI) were determined by photon correlation spectroscopy (PCS) (Zetasizer[®] Nanoseries ZS ZEN3600) after 1:500 dilution in filtered water. Zeta potential was measurement by laser Doppler electrophoresis (Zetasizer[®] Nanoseries ZS ZEN3600) after dilution (1:500) with 10 mmol·L^{-1} aqueous NaCl solution. Determination of pH values was performed with a calibrated pH-meter (DM-22, Digimed) in the undiluted formulations.

6.2.4. HPLC method for quantification of ciprofloxacin

Ciprofloxacin was quantified by high performance liquid chromatography with UV detection (HPLC-UV). For the determination of the encapsulation efficiency and for release studies a Shimadzu HPLC system with a Waters Nova-Pak[®] C18 column was used. Quantification for mucus permeation studies was performed by a Dionex UltiMate 3000 HPLC system with LiChrospher[®]100 RP-18 column. Mobile phase consisted of 0.025 mol·L^{-1} ortho-phosphoric acid (pH 3.0, adjusted with triethylamine) and acetonitrile (87:13, v/v) at an isocratic flow rate of 1.5 mL·min^{-1}. Ciprofloxacin was detected at 278 nm at a retention time of 4.5 and 8.5 min for the Shimadzu and Dionex system, respectively. For both systems and each quantification range a validation was performed evaluating linearity, precision (repeatability and intermediate precision) and the limits of detection (LoD) and quantification (LoQ). The LoD and LoQ were calculated using the following equations (6.1) and (6.2), respectively:

$$\text{LoD} = 3.3 \cdot \sigma \cdot S^{-1} \qquad (6.1)$$

$$\text{LoQ} = 10 \cdot \sigma \cdot S^{-1} \qquad (6.2)$$

σ is the standard deviation of the response (peak areas) and S is the slope of the calibration curve. Specificity analysis showed no influence by the blank formulation on the ciprofloxacin assay. All experiments were conducted in triplicate, validation data is given in Table 6.2.

	Shimadzu system (Drug content, EE%)	Shimadzu system (Release studies)	Dionex UltiMate 3000 (Mucus permeation assay)
Injection volume (μL)	20	100	50
Range (μg·mL^{-1})	1-20	0.1-2	1-20
Linearity (Equation and correlation coeff.)	$y = 88244x - 35832$ $R^2 = 0.9978$	$y = 419084x - 16451$ $R^2 = 0.9986$	$y = 3.2797x - 1.2775$ $R^2 = 0.9987$
Repeatability RSD (%)	3.37	2.04	2.59
Intermediate precision RSD (%)	4.42	1.77	4.07
LoD (μg·mL^{-1})	1.365	0.109	1.061
LoQ (μg·mL^{-1})	4.126	0.329	3.216

Table 6.2. Validation data for HPLC analysis.

6.2.5. *Encapsulation efficiency and drug loading*

The total drug content in the formulation (encapsulated and non-encapsulated drug) was determined by dissolving an aliquot of the nanosuspension in acetonitrile and extraction by sonication. After centrifugation, the supernatant was diluted with mobile phase and injected to HPLC. To evaluate if the extraction is sufficient, recovery was calculated by relating the determined value to the initially used drug concentration.

Analysis of encapsulation efficiency was performed indirectly by ultrafiltration-centrifugation using Amicon$^{®}$ Ultra Centrifugal Filters (MWCO 10k) (4,120 x g; 20 min). The non-encapsulated drug can pass the filter during centrifugation and is thus separated from the encapsulated drug, as nanocapsules are retained. The filtrate was analyzed by HPLC after dilution with mobile phase. The encapsulation efficiency (EE%) was calculated by the following equation (6.3):

$$EE\% = \frac{M_{total} - M_{non-encapsulated}}{M_{initial}} \times 100 \quad (6.3)$$

M_{total} is the total drug mass in the nanosuspension and $M_{non-encapsulated}$ the free drug mass, calculated from the concentrations in the nanosuspension and the filtrate, respectively. $M_{initial}$ is the initially used ciprofloxacin mass.

Interaction of ciprofloxacin with the filter would lead to a misinterpretation of the results. Thus, the same ultrafiltration-centrifugation protocol was conducted with a drug solution in mobile phase (concentration 0.8 mg·mL^{-1}). Drug loading was reported as encapsulated ciprofloxacin per gram of nanocapsules. All experiments were performed in triplicate.

6.2.6. Determination of the presence of drug crystals

Upon nanoprecipitation the simultaneous formation of nanocrystals can occur [74]. To detect the presence of such, one batch of nanosuspension was split into equal volumes and stored in two different vials at room temperature and under light protection. One flask was shaken before sampling and HPLC analysis, while the other flask was immobilized and samples were withdrawn from the top. Drug contents were analyzed at predefined time points (0, 5, 10, 20 days).

6.2.7. Visualization of nanocapsules

Atomic force microscopy was performed in tapping mode in air. After dilution of the samples with water, they were dropped onto a freshly cleaved mica surface. The liquid was taken off with a paper tissue after 5 minutes of incubation. Samples were visualized by a Bioscope BS3-Z2 AFM with a Nanoscope IV controller (Bruker Corporation) and by using silicon cantilevers with tetrahydral tips (OMCL-AC160TS, Olympus, nominative force constant 42 Nm^{-1}, resonance frequency around 300 kHz). Size analysis was performed with the NanoScope Analysis 1.40 software.

For conventional transmission electron microscopy samples were diluted in ultrapure water (1:10, v/v) and dropped onto grids. Staining was performed with uranyl acetate (2%). After complete drying, the samples were analyzed by a JEOL JEM 1200-ExII TEM at an accelerating voltage of 80 kV.

For cryo-TEM imaging 3 µL of the nanosuspension were plotted onto a holey carbon TEM grid (type S147-4, Plano, Wetzlar, Germany) and plunged into liquid ethan using a Gatan CP3 Cryoplunger. The frozen sample was transferred under liquid nitrogen into a Gatan 914 cryo-TEM holder. TEM imaging was performed at T = 93 K and 200 kV accelerating voltage using a JEOL JEM-2100 (high resolution pole piece) with LaB$_6$ cathode and a Gatan Orius SC1000 camera.

6.2.8. Mucus permeation assay

To determine the capability of LNC to permeate mucus, diffusion through respiratory horse mucus was investigated in a Transwell® setup (polyester membrane, 12 mm diameter, pore size 3.0 μm, Corning Incorporated). Horse lung mucus was obtained by bronchoalveolar lavage with saline. Mucus samples were kept in frozen state until use. After thawing, samples were centrifuged (3,000 x g, 10 min) and the aqueous supernatant was taken off to remove contained saline. As barrier 200 μL of horse mucus were homogeneously distributed onto each Transwell® membrane. The thickness of the mucus barrier was estimated to be around 1.8 mm. The donor compartment consisted of 200 μL LNC-CIP nanosuspension previously mixed with 100 μL horse mucus and was placed on top of the mucus barrier. The mixing with mucus was performed to reduce viscosity differences between donor and barrier and thus to avoid bypassing of the nanosuspension between Transwell® wall and mucus. The same experiment was conducted in parallel using an aqueous ciprofloxacin suspension with the same drug concentration (0.8 mg·mL^{-1}). As acceptor 400 μL PBS-buffer were placed in each well. The well plate was stored in a shaker at 37°C and gentle shaking. Samples were withdrawn from the acceptor medium at predetermined time points (2, 4, 6, 8, 10 h) and replaced by an aliquot of preheated PBS-buffer. Drug contents of the samples were analyzed by HPLC after extraction with acetonitrile and sonication. Experiments were performed in triplicate. The 10 h-samples were additionally analyzed by dropping onto freshly cleaved mica surfaces, air drying and imaging by AFM.

6.2.9. In vitro drug release study

Determination of ciprofloxacin release was performed by direct dialysis bag method. In parallel the release of a ciprofloxacin solution in 0.14% ortho-phosphatidic acid (0.8 mg·mL^{-1}) was conducted to ensure that the drug release behavior is not dominated by the dialysis membrane. Simulated lung fluid (SLF 3) was used as release medium [75]. Dialysis tubing cellulose membrane bags (MWCO=14,000) were filled with each 2 mL nanosuspension or ciprofloxacin solution and located into 150 mL simulated lung fluid. The release setup was kept under continuous stirring at (37 ± 1)°C and under light exclusion. Sink conditions were ensured. Samples of the release medium were withdrawn at predetermined time points (1, 2, 4, 6, 8, 24 h) and replaced by preheated medium. Drug contents were analyzed by HPLC and the cumulative release was calculated. All experiments were performed in triplicate. For prediction of the release mechanism and evaluation of kinetics, the Scientist® software (MicroMath®) was used.

6.2.10. Antibacterial growth assays

Antibacterial efficacy was evaluated in growth assays for *P. aeruginosa* PA01 (DSMZ) and *S. aureus* Newman. Three independent assays were conducted for *P. aeruginosa* and two for *S. aureus*. In each assay duplicates were measured. All tested formulations (LNC-CIP, LNC-blank and ciprofloxacin solution) were prepared aseptically. The ciprofloxacin solution contained polysorbate 80 in the same concentration as the LNC formulations. Inoculation of bacterial pre-cultures was performed from single colonies in 5 mL LB medium and bacteria were grown for 6-8 hours or overnight at 37°C to stationary phase. 200 µL of the formulations (nanosuspensions and drug solution) at double the highest concentration to be tested were added to a 96-well plate (GreinerBioOne) and serially diluted (1:2) in LB medium, resulting in 100 µL per well. Bacteria in LB medium were used as positive control and LB medium with ciprofloxacin or LNC-CIP as negative control. Bacterial pre-cultures were diluted in fresh LB medium to an OD600 of 0.04 and 100 µL diluted culture was given to each well (final OD600 of 0.02). Incubation was performed at 37°C with shaking at 180 rpm for 16-18 hours. Bacterial growth was monitored by absorbance measurement at 600 nm with a FLUOstar Omega microplate reader. The supernatant from the wells containing *S. aureus* were in addition measured after 1:1 dilution with medium in a fresh plate.

Release properties in antibacterial growth assay conditions were investigated. LNC-CIP was diluted with LB-medium to different concentrations and incubated for 18 hours at 37°C and 200 rpm. By ultrafiltration-centrifugation (Amicon® Ultra Centrifugal Filters, MWCO = 10k), the released drug was separated from the nanocapsules and quantified by HPLC.

6.2.11. SEM analysis of S. aureus aggregates

The antibacterial growth assay was repeated with ciprofloxacin solution with a drug content of 0.2 µg·mL^{-1}, LNC-CIP with the same ciprofloxacin concentration and 3.715 µg·mL^{-1} oleic acid and LNC-blank similarly diluted (same oleic acid concentration). *S. aureus* were incubated in 8-well microscope slides (Sarstedt) with the formulations at 37°C and 180 rpm for 16-18 hours. Fixation for SEM analysis was performed by 2.5% glutaraldehyde for two hours and subsequent three times washing with PBS. Samples were sequentially dehydrated with ethanol dilutions (10%, 30%, 40%, 50%, 60%, 70%, 80%, 90%, 96%, 100%, 100%). Incubation time was 10 minutes for each dilution. After complete drying the samples were sputter coated with gold and imaged with a JEOL JSM-7000F scanning electron microscope (accelerating voltage 20.0 kV).

6.3. Results and discussion

6.3.1. Interaction testing between polymer and lipid

Lipid-core nanocapsules contain a lipid core surrounded by a polymeric shell. Usually oils such as vegetable oils or caprylic/capric triglycerides are used as core lipid, enabling high drug loading for lipophilic drugs [71]. For an optimized loading with ciprofloxacin, oleic acid was used as lipid in this work. Oleic acid has a less lipophilic character in comparison to triacylglycerols. Hence, ciprofloxacin exhibits higher solubility in oleic acid than in typically used oils [76]. In addition, ciprofloxacin can interact with oleic acid by forming ionic chemical bonds or hydrogen bonds due to its amine and carboxylic acid functional groups, respectively.

However, as oleic acid is a not a usual excipient for the formation of lipid-core nanocapsules, its compatibility with the polymer needs to be investigated. The core constituents must be non-solvents for the polymer to avoid instabilities of the LNC [71, 77]. The suitability of oleic acid as core lipid was tested by analyzing weight changes of the polymer during incubation with oleic acid. The PCL weight increased about (7.50 ± 0.97)% within 24 hours and then remained constant over 2 months (Fig. 6.1). As no weight decrease was observed, oleic acid is a non-solvent for PCL and thus suitable for the preparation of lipid-core nanocapsules.
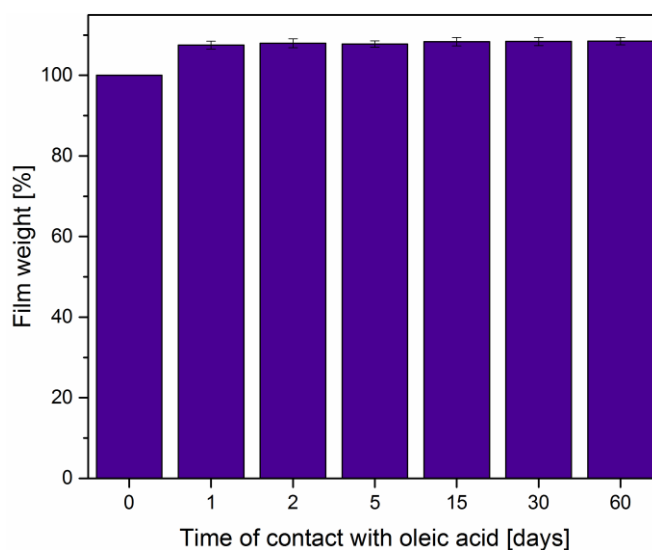
Fig. 6.1. Interaction testing: The PCL film weight increased about 7.5% within one day of incubation with oleic acid. No further uptake was observed over 60 days (*n* = 3).

6.3.2. Physicochemical characterization

Ciprofloxacin-loaded and blank lipid-core nanocapsules were prepared by interfacial deposition of the polymer. For physicochemical characterization particle size, size distribution, pH and zeta potential were measured. For LNC-CIP the encapsulation efficiency and drug loading was additionally determined.

Blank and drug loaded nanocapsules exhibited both mean hydrodynamic diameters of about 180 nm as measured by PCS and a narrow size distribution (PDI < 0.2). By laser light diffraction analysis the presence of microparticles could be excluded. pH values were slightly acidic and the zeta potential negative due to carboxylate groups at the particle surface (Table 6.3). In general, stabilization of lipid-core nanocapsules is mainly achieved by steric hindrance of the stabilizer, the polysorbate molecules [78]. The mean particle size is in the desired range, as negatively charged nanoparticles larger than 200 nm are reported to be disadvantageous in terms of the mucus permeability [8, 24].

	Size (nm)	PDI	pH	Zeta potential (mV)
LNC-blank	182.2 ± 3.2	0.125 ± 0.018	5.49 ± 0.25	-30.0 ± 4.3
LNC-CIP	181.8 ± 10.7	0.140 ± 0.010	5.85 ± 0.10	-21.3 ± 2.6

Table 6.3. Physicochemical parameters of LNC-CIP and LNC-blank (*n* = 3).

In the case of an indirect determination of the encapsulation efficiency by ultrafiltration-centrifugation, several factors can lead to a misinterpretation of the results. Thus, potential pitfalls have to be addressed to ensure correct results.

First of all, a possible retention of the drug by the filter membrane due to interaction of absorption needs to be detected. Thus a ciprofloxacin solution (0.8 mg·mL^{-1} in mobile phase) was filtered through the ultrafiltration-centrifugation tube. As the drug was completely recovered in the filtrate, drug membrane interactions could be excluded.

Furthermore, the presence of nanocrystals needs to be excluded. Drug nanocrystals can be formed simultaneously during nanoprecipitation when poorly water-soluble drugs are used [74]. These crystals might be retained by the filter during ultrafiltration and thus this drug amount would be determined as encapsulated drug. Nanocrystals tend to agglomeration and would subsequently precipitate or sediment as larger crystals or aggregates. The drug contents of immobile and shaken LNC-CIP nanosuspensions were analyzed in parallel. If drug crystals or aggregates were present, decreasing concentrations would be measured over time for the immobile sample, as the

sedimented crystals would not be included for quantification. During storage over 20 days, no difference was detected in the drug contents of the shaken and immobile samples. Thus the absence of drug crystals or aggregates can be concluded.

As an interaction of the drug with the filter membrane and the formation of nanocrystals can be both excluded, the indirect determination of the encapsulation efficiency is validated.

The total drug content of the LNC-CIP formulation was (0.794 ± 0.028) mg·mL^{-1}, which corresponds to a recovery of $(99.24 \pm 3.57)\%$ of the initially used drug. The complete extraction of ciprofloxacin by the used method can be concluded. The determined encapsulation efficiency was $(86.90 \pm 0.83)\%$, and thus the drug loading (18.5 ± 0.8) mg per g LNC. By using oleic acid as core lipid, high encapsulation efficiency could be reached for ciprofloxacin. This is probably due to the interactions between oleic acid and ciprofloxacin such as ionic chemical bonds and hydrogen bonds.

Ciprofloxacin has been reported to show a water solubility between 0.086 and 0.22 mg·mL^{-1} at neutral pH [79-81]. By using lipid-core nanocapsules, the apparent solubility of ciprofloxacin could be significantly increased, reaching a drug content of 0.8 mg·mL^{-1} in aqueous phase.

In both TEM and AFM images, spherical particles were found (Fig. 6.2). Sizes in the AFM images were analysed and found to range from 112 to 271 nm. Thus, sizes correspond to the values obtained by PCS. The particle heights determined by AFM were smaller than the diameter. This might be a due to an adhesion to mica or collapsing polymeric structures in ambient conditions [82, 83]. Particle surface was found to be smooth in the AFM images.
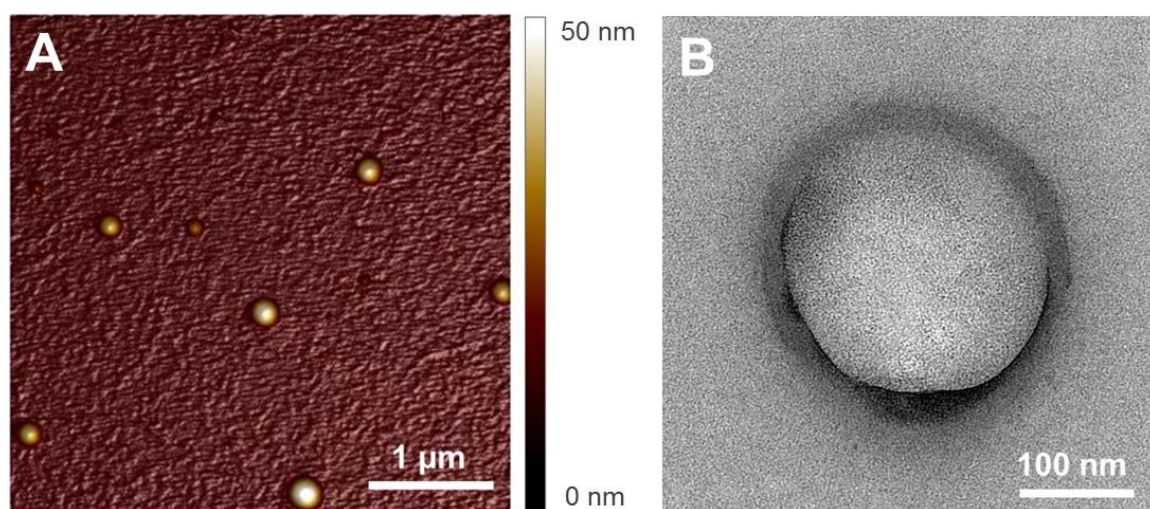
Fig. 6.2. Nanocapsule morphology: LNC-CIP imaged by AFM (A) and TEM (B).

Imaging by cryogenic transmission electron microscopy (cryo-TEM) did not clearly reveal a core-shell-structure. However, by analyzing the behaviors of particles composed of different materials under the influence of the electron beam, conclusions can be drawn on the structural composition of LNC-CIP. PCL particles without lipid core were relatively stable in the beam, while the nanoemulsion (lipid core without shell) resulted in bubble formation while being treated with the electron beam (Fig. 6.3). The formation of bubbles was also observed for LNC-CIP, however, the bubbles could not easily exit these particles as they were most likely retained by the shell. The particles inflated and finally the interior oozed out, probably through leaks in the shell. The comparison of the different behaviors in the electron beam strengthens the presumption that LNC-CIP are composed of a shell and a core as conventional lipid-core nanocapsules.
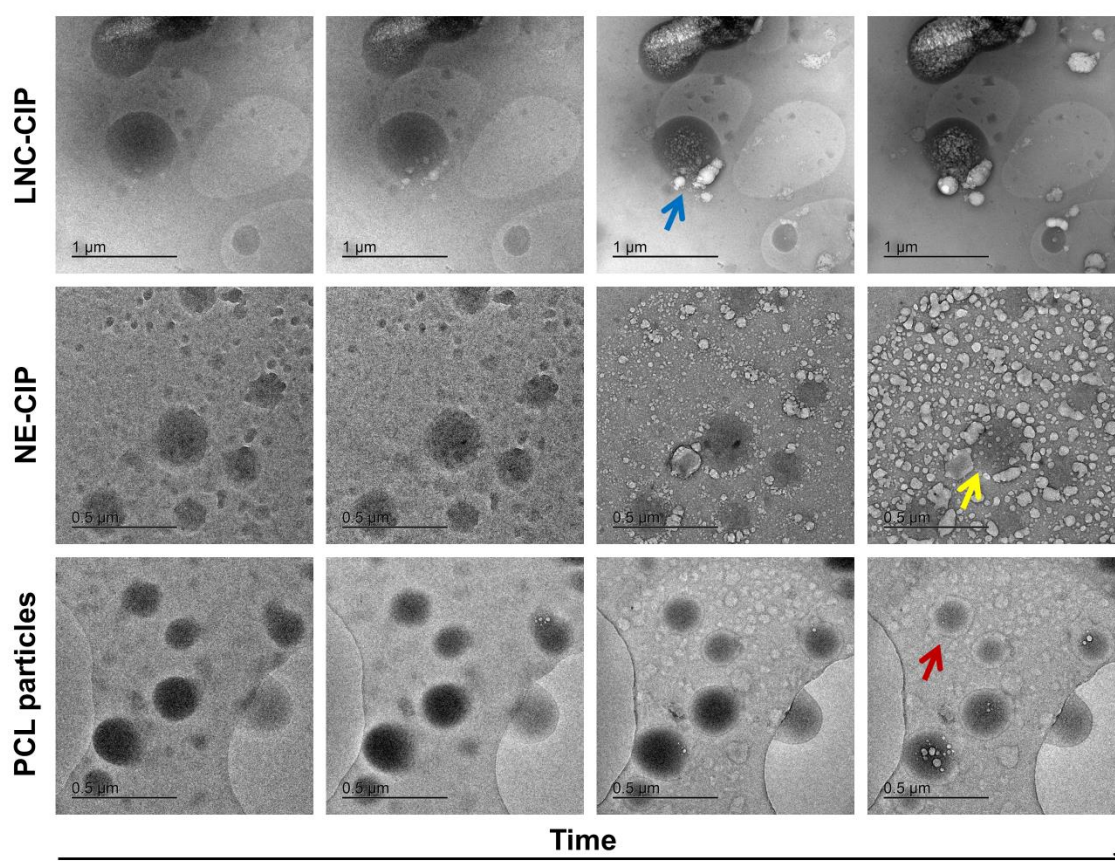
Fig. 6.3. Lipid-core nanocapsules (LNC-CIP), nanoemulsion (NE-CIP) and PCL particles imaged by cryo-TEM. Different behaviors were observed under the influence of the electron beam. LNC-CIP inflated upon formation of bubbles in the interior, until the content oozed out (blue arrow). NE-CIP also reacted with formation of bubbles, which moved out of the particles without being retained by a shell (yellow arrow). PCL particles in comparison were relatively stable and reacted by shrinkage (red arrow). Only few bubbles were formed for the particles without lipid core.

6.3.3. Mucus permeation assay

An essential prerequisite for a successful eradication of bacteria inside the mucus is the capability of the nanoparticles to permeate mucus without being entrapped in the network. Thus a diffusion experiment was performed to investigate the permeation of ciprofloxacin-loaded lipid-core nanocapsules through respiratory horse mucus. A Transwell® setup as previously established by Friedl et al. was used [84]. The diffusion behavior of the non-encapsulated drug was examined as well for comparison. An aqueous ciprofloxacin suspension with the same drug concentration was used, as ciprofloxacin is poorly water soluble at neutral pH. The use of a ciprofloxacin solution with the same drug content would only have been possible by modifying the pH, which would have also influenced the barrier properties of mucus. Permeated drug was quantified by HPLC analysis after extraction of the drug. The drug concentration in the acceptor compartment was monitored over time.

Within 10 hours, (50.6 ± 2.7)% of the drug was present in the acceptor compartment when LNC-CIP had been applied on the mucus barrier, while only (32.8 ± 1.3)% of the ciprofloxacin from the suspension permeated the mucus within the same time. The permeation curves could be fitted by linear equations with a high correlation ($R^2 > 0.995$) (Fig. 6.4).

The apparent permeability coefficients (P_{app}; in cm·s^{-1}) were calculated by equation (6.4).

$$P_{app} = \frac{dQ}{dt} \cdot \frac{1}{A \cdot c_0} \quad (6.4)$$

with dQ/dt being the drug appearance rate in the acceptor (µg·s^{-1}), A the surface area of the membrane (cm^2) and c_0 the initial drug concentration in the donor (µg·mL^{-1}) [85].

The determined apparent permeability coefficients were (3.73 ± 0.20) x 10^{-6} cm·s^{-1} for the lipid-core nanocapsules and (2.41 ± 0.09) x 10^{-6} cm·s^{-1} for the ciprofloxacin suspension, hence the permeation was increased by 50% by encapsulation of ciprofloxacin into LNC.

A

B
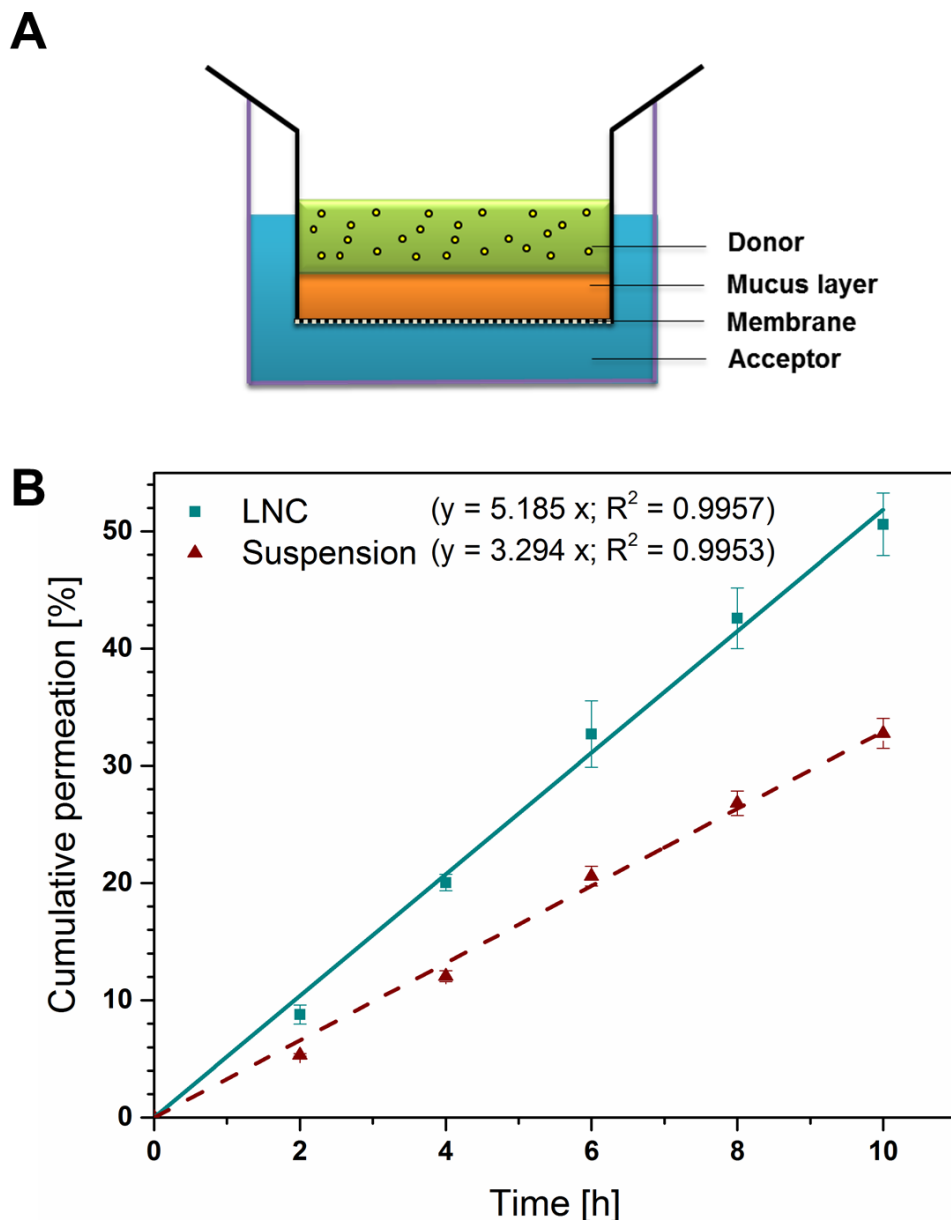
Fig. 6.4. Mucus permeation assay: A) Schematic of the Transwell® setup; B) Cumulative permeated drug through respiratory horse mucus; LNC-CIP showed faster permeation in comparison to the suspended drug ($n = 3$).

By extracting the drug with acetonitrile and sonication, we determined the encapsulated drug together with the released drug by HPLC. To exclude that only released drug permeated through the mucus and to ensure that LNC are present in the acceptor, samples of the acceptor compartment were additionally analyzed by AFM after 10 hours of experiment time. Nanocapsules were successfully visualized in the LNC-samples, showing the permeation of LNC through respiratory horse mucus (Fig. 6.5 A). However, visualization was hampered by impurities on the mica surface, which were probably due

to mucus components that were able to diffuse into the acceptor. AFM analysis was performed as well for samples from the ciprofloxacin suspension. There, a certain background structure was observed as well; however, no nanoparticulate structures were found (Fig. 6.5 B).

The size of permeated nanocapsules measured in the AFM images for LNC samples was with (102.9 ± 19.6) nm (n = 15) slightly smaller than sizes determined from native nanoparticles. Increased permeability of smaller particles has been previously described for negatively charged particles [8, 24]. The larger nanocapsules might be retained in the mucus network for longer time due to size exclusion effects.

Besides the size exclusion effects, interaction filtering is the second important retention mechanism for particles in biological hydrogels [22]. In the case of the ciprofloxacin-loaded nanocapsules, interaction with mucus components is unlikely, as high permeability rates could be observed in total.
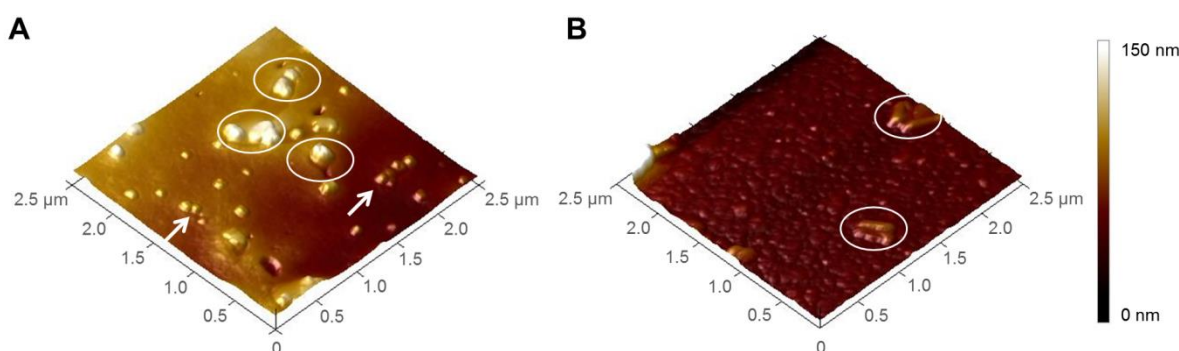
Fig. 6.5. Samples taken from the acceptor compartment visualized by AFM: A) Spherical particles were found in the acceptor compartment from the LNC-samples (labelled by arrows); impurities were found as well (labelled by circles); B) Ciprofloxacin suspension samples from the acceptor compartment: a background structure was visible due to mucus components; however, no nanocapsules were found.

The low interaction with mucus is supposed to result from the used stabilizer, polysorbate 80, which is containing polyoxyethylene chains. High mucus permeability has been reported for the so-called muco-inert nanoparticles having a PEGylated surface and neutral charge [19, 25-27]. There is also evidence that by just using surfactants with polyoxyethylene chains, the interaction with mucus is already reduced. An influence of the type of stabilizer on the diffusion of solid lipid nanoparticles has been described. The use of polyvinyl alcohol (PVA) was disadvantageous for mucus permeation, whereas nanoparticles with stabilizers containing polyoxyethylene chains (poloxamer 407 and polysorbate 80) showed diffusion into mucus [70, 86]. Furthermore, mucus penetration

has been described for poloxamer-modified liposomes, poloxamer-stabilized nanolipoparticles and nanoparticles stabilized by PEG-based surfactants [87-89]. For polysorbate 80 micelles no interaction with mucin was observed [90].

Thus a correlation between polyoxyethylene chains on the nanoparticle surface and high mucus permeability due to low interaction with mucin is hypothesized. The stabilization of LNC-CIP by polysorbate 80 might be responsible for the high diffusion rates through respiratory horse mucus.

The reason for the slow permeation observed for the ciprofloxacin suspension is the low aqueous solubility of the drug. The size of the ciprofloxacin particles was determined by laser diffraction and found to be in the lower micrometer range. With this large size, no diffusion of the suspended particles through the mucus network can be expected. Most probably, the particles form a reservoir in the donor and release the drug slowly. Only the dissolved drug is hence able to diffuse through the mucus barrier.

To summarize, the encapsulation of a drug with low aqueous solubility into lipid-core nanocapsules can considerably increase its mobility through mucus.

6.3.4. *In vitro drug release*

Besides the capability to permeate mucus, another aim for the antibiotic nanocapsules was a sustained drug release at the site of action. The *in vitro* drug release was studied by direct dialysis method with simulated lung fluid type 3 as release medium, representing the composition of lung lining fluid [75]. The actual *in vivo* release in mucus is expected to occur even more slowly, due to the limited fluid volume.

A fast concentration increase in the medium was observed for the ciprofloxacin solution with (97.9 ± 7.1)% of the drug reaching the measurement compartment within the first 4 hours. The drug is supposed to diffuse freely, while in the LNC samples the drug needs to be released from the nanocapsules first. In the same time frame, only (66.9 ± 2.7)% of the drug from the nanosuspension was detected in the medium. The complete release from the LNC was achieved after 24 hours (96.0 ± 3.3%) (Fig. 6.6).
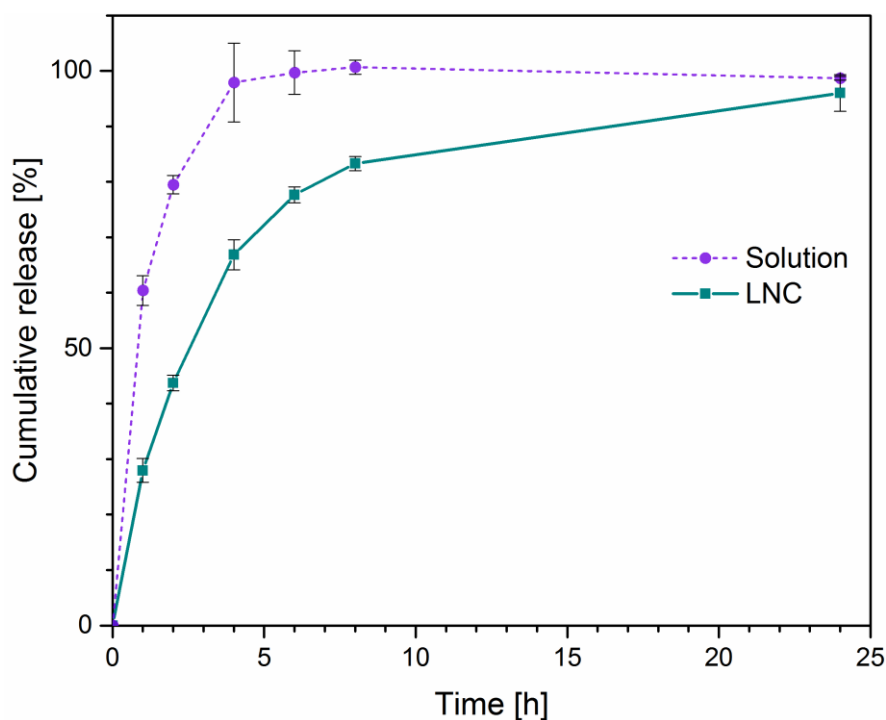
Fig. 6.6. Release study: Cumulative release of LNC-CIP and ciprofloxacin solution in simulated lung fluid (*n* = 3).

The release data was analyzed in terms of the release mechanism and kinetics. The release curve of the LNC-CIP was fitted to the following equation described by Ritger and Peppas (6.5) and the diffusional exponent n was determined [91].

$$M_t/M_\infty = k' \cdot t^n \qquad (6.5)$$

M_t and M_∞ are the drug amounts released at time t and infinite time, respectively. k' is the kinetics constant and t the release time [91].

The determined diffusional exponent was n = 0.302 (Table 6.4). For spherical non-swellable controlled release system, a diffusional exponent of n = 0.43 is related to Fickian diffusion. However, this is only valid for samples without any size distribution. The authors determined the exponent for a sample with size distribution and obtained a n-value of 0.30 ± 0.01 [91]. As the LNC-CIP display a size distribution as well, a release following Fick's law of diffusion is proposed.

The diffusion is assumed to be the sole release mechanism. The fitting of the release data assuming a monoexponential release strengthened this expectation. The monoexponential release is described by equation (6.6):

$$c = c_0 \cdot (1-e^{-kt}) \qquad (6.6)$$

with c being the drug amount released at time t, c_0 is the initial total ciprofloxacin content and k the kinetic rate constant.

Determined parameters and coefficients of determination are shown in Table 6.4. 50% of the ciprofloxacin solution's drug reached the medium within around 48 minutes, while it took more than 2.5 h for the nanocapsules to release the same drug fraction. In summary, the ciprofloxacin-loaded nanocapsules showed a sustained drug release and might thus enable a reduced dosing frequency.

	Release parameters	LNC-CIP	CIP solution
Determination of release mechanism by Ritger and Peppas [91]	k' (h^{-1})	40.00 ± 1.25	
	Diffusional exponent n	0.302 ± 0.015	
	R^2	0.9848 ± 0.0062	
Monoexponential release	k (h^{-1})	0.268 ± 0.010	0.873 ± 0.058
	t$_{50\%}$ (h)	2.59 ± 0.10	0.80 ± 0.05
	R^2	0.9971 ± 0.0011	

Table 6.4. Drug release parameters obtained by fitting the equation described by Ritger and Peppas [91] and a monoexponential equation to the release data (n = 3).

As reported in literature the sustained drug release from LNC can be related mostly to diffusion from the core to the outer phase, which is influenced by the concentration of sorbitan monostearate affecting the core viscosity. The impact of the polymer shell is in contrast negligible for low polymer concentrations [51, 71]. Often a biphasic release is observed for nanocapsules prepared with triacylglycerol or mineral oil as core lipids. The drug located on the nanocapsule surface undergoes an initial burst release and subsequently the encapsulated drug is released in a sustained way [51, 71]. In the case of the LNC-CIP no burst effect was observed. A strong interaction of ciprofloxacin with oleic acid by ionic chemical bonds and/or hydrogen bonds is suggested, preventing a burst release.

To summarize, the LNC-CIP showed the desired sustained release, which might enable a reduced dosing frequency.

6.3.5. Antibacterial activity

The biological activity is a key parameter for the LNC-CIP formulation. To evaluate if efficacy of ciprofloxacin is preserved after encapsulation, antibacterial growth assays were performed with *P. aeruginosa* PAO1 and *S. aureus* Newman. The tested formulations were LNC-CIP, LNC-blank and a ciprofloxacin solution. Within the time of the experiment, the complete drug amount was released from the LNC-CIP in dilutions with ciprofloxacin concentrations up to 6.4 µg·mL^{-1} (Table 6.5).

Concentration (µg/mL)	Released drug (%)
25.6	81.8 ± 3.4
12.8	88.3 ± 3.2
6.4	95.8 ± 2.8
3.2	98.8 ± 2.6
1.6	103.8 ± 7.8

Table 6.5. Percentage of drug released from LNC-CIP in LB-medium after 18 h of incubation. Complete release is reached in concentrations below 6.4 µg/mL (*n* = 3).

The LNC-CIP showed a similar efficiency as the free ciprofloxacin in *P. aeruginosa*, while no growth inhibition was observed for LNC-blank (Fig. 6.7 A). For *S. aureus* comparable minimal inhibitory concentrations (MIC) were observed for the free drug and LNC-CIP as well (Fig. 6.7 B, D). However, higher OD600 values were determined for higher concentrations of ciprofloxacin solution due to aggregated large structures at the bottom of the wells (Fig. 6.7 C). After transferring the supernatant of these wells to a fresh 96-well plate, absence of bacterial growth in the supernatants was determined (Fig. 6.7 D).

S. aureus samples were further analyzed by scanning electron microscopy (SEM) to elucidate this aggregation phenomenon. For the visualization, *S. aureus* was incubated for 16 hours with ciprofloxacin solution, LNC-CIP and LNC-blank (concentration of 0.2 µg·mL^{-1} ciprofloxacin and 3.72 µg·mL^{-1} oleic acid, respectively). Samples were fixed, dehydrated and imaged after sputter coating.
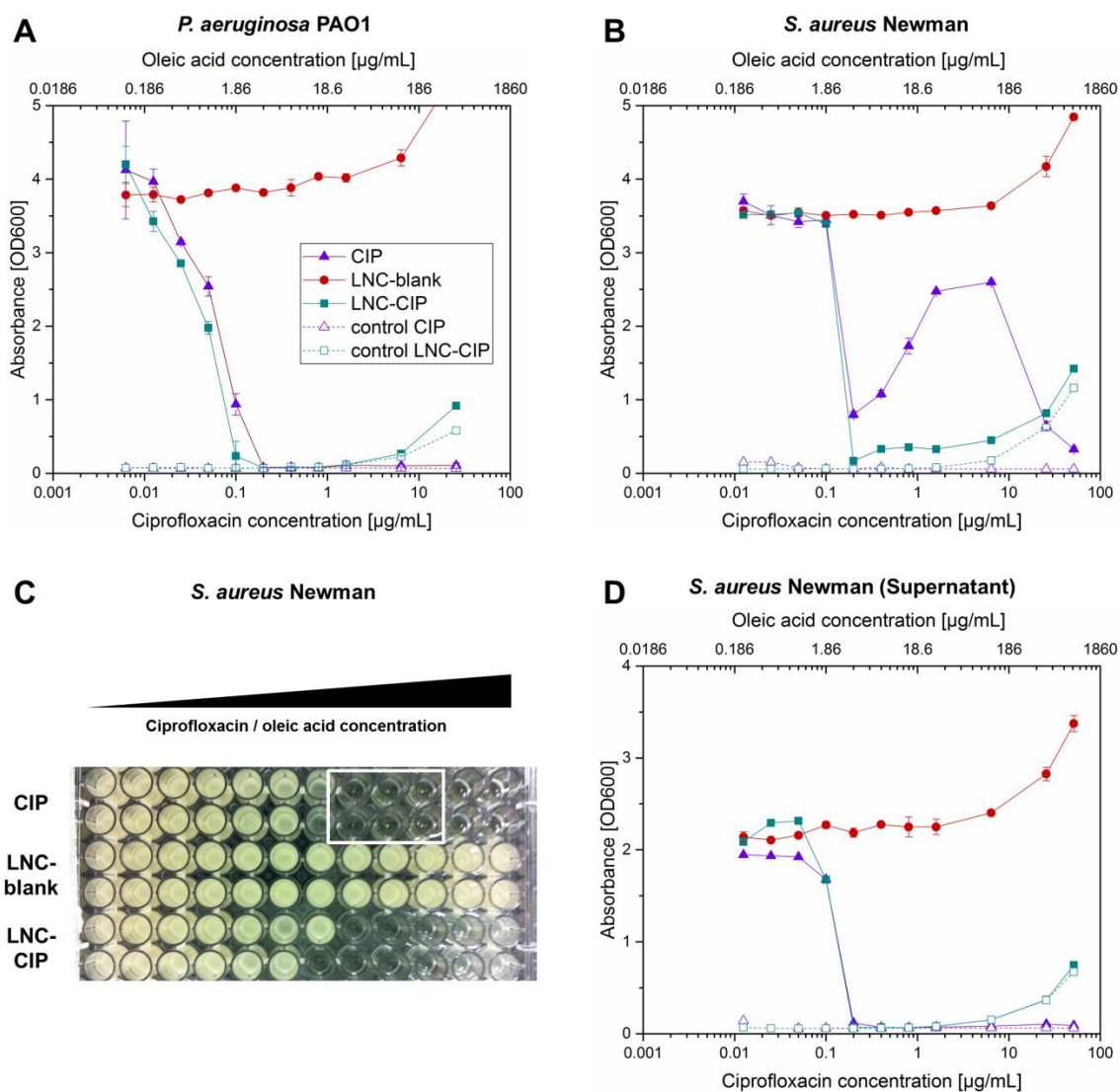
Fig. 6.7. Bacterial growth of *P. aeruginosa* (A) and *S. aureus* (B, D) in presence of different concentrations of ciprofloxacin (CIP), blank nanocapsules (LNC-blank) or ciprofloxacin-loaded lipid-core nanocapsules (LNC-CIP), measured after 16-18 hours of incubation. LNC-CIP showed similar antimicrobial activity as the free drug against both pathogens. Corresponding concentrations of LNC-CIP (control LNC-CIP) and ciprofloxacin (control CIP) were measured as controls without bacteria. Increase of OD600 values in higher concentrations of LNC-CIP and LNC is caused by the turbidity of the nanosuspensions. Aggregates were observed for *S. aureus* treated with higher concentrations of ciprofloxacin (B, C). Wells with aggregates are labelled by the white box (C). No bacterial growth was observed in the supernatants of these wells after measuring the absorbance in the supernatants (D).
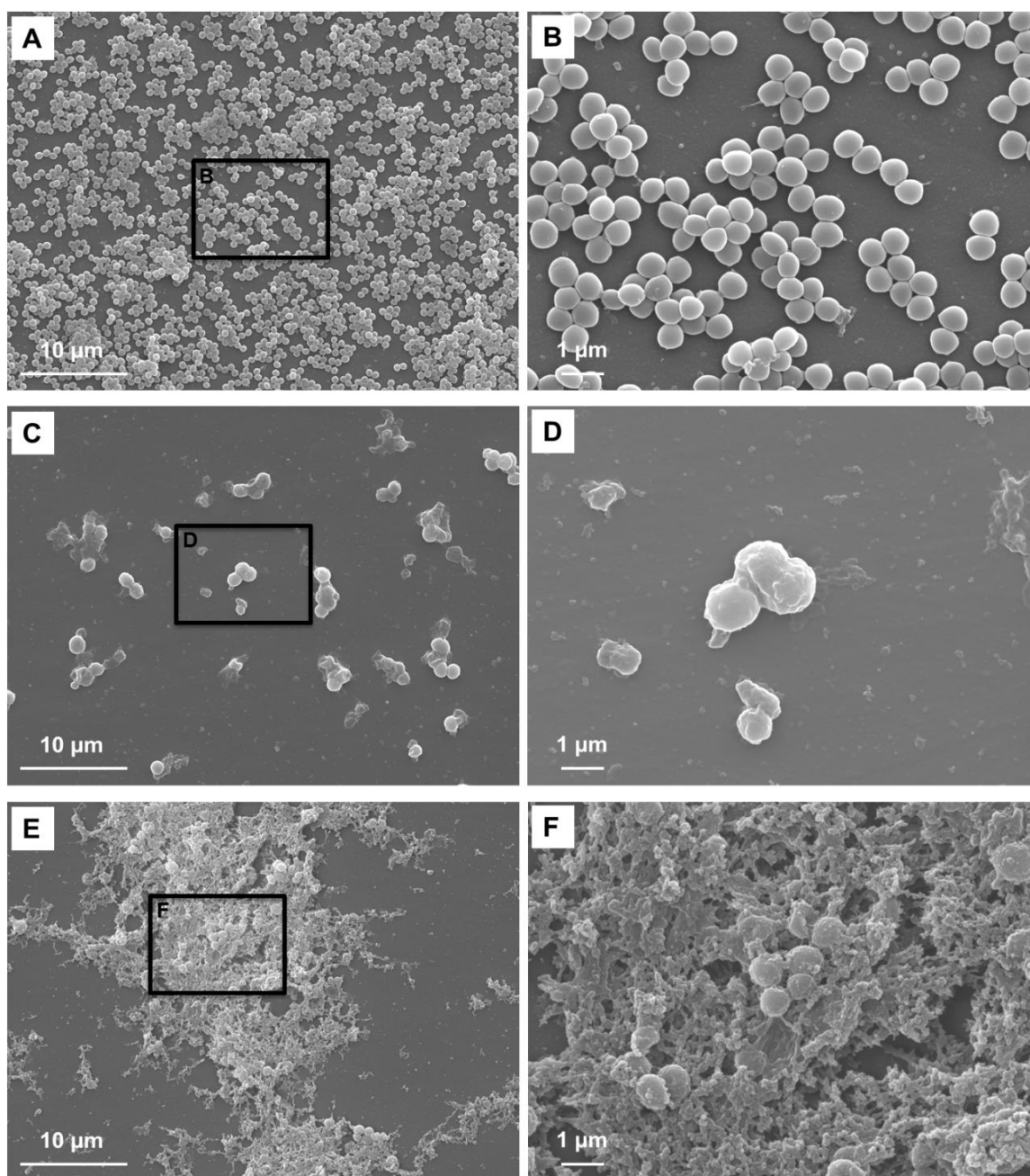
Fig. 6.8. *S. aureus* imaged by SEM: (A, B) After treatment with LNC-blank planktonic bacteria were observed; (C, D) Few enlarged bacteria after exposure to LNC-CIP; (E, F) Biofilm-like structures were formed upon incubation with ciprofloxacin solution.

After incubation with LNC-blank, planktonic bacteria with normal morphology at a high bacterial density were observed, indicating ongoing growth (Fig. 6.8 A, B). The treatment with LNC-CIP yielded in contrast only few but enlarged *S. aureus* and small aggregates of approximately 3-5 bacteria were found (Fig. 6.8 C, D). The enlargement of *S. aureus* upon exposure to antibiotic drugs has already been reported in literature [92]. Interestingly, an increased number of bacteria was observed for *S. aureus* incubated with free ciprofloxacin, which were embedded in matrix-like structures that are most likely biofilms

(Fig. 6.8 E, F). *S. aureus* aggregates have been reported to show higher resistance to antibiotics such as ciprofloxacin in comparison to planktonic bacteria [93].

A comparable efficacy of free and encapsulated ciprofloxacin against *P. aeruginosa* and *S. aureus* has been observed in antibacterial growth assays. However, higher drug concentrations at the site of infection can be expected for the use of nanocapsules, due to the higher mucus permeability of LNC-CIP in comparison to the non-encapsulated drug. Furthermore, a surprising prevention of antibiotic-resistant aggregates was observed for ciprofloxacin-loaded nanocapsules, whereas formation of biofilm-like structures was even induced by ciprofloxacin solution.

6.4.   Conclusion

Ciprofloxacin-loaded lipid-core nanocapsules with a mean size of around 180 nm were prepared with high encapsulation efficiency, reaching a considerably increased apparent solubility. Due to the small size and an appropriate stabilizer, a by 50% increased mucus permeability was observed in comparison to ciprofloxacin suspension. Protection of the drug from deactivation and the mobility inside mucus are essential prerequisites for an effective delivery of antibiotics for the treatment of bacterial infections in cystic fibrosis. Furthermore, the antibiotic nanocapsules showed a sustained drug release. The combination of these advantages might enable a reduction of dosing frequency and overall dose at the same time. Encapsulation of the drug into LNC did not affect antibacterial activity against CF relevant pathogens. Interestingly, formation of biofilm-like *S. aureus* aggregates could be prevented by treatment with LNC-CIP. In summary, ciprofloxacin-loaded LNC showed several benefits over the non-encapsulated drugs, giving a promising perspective to improve antibacterial therapy of pulmonary infections in cystic fibrosis.

7. SPRAY-DRIED NANO-EMBEDDED MICROPARTICLES

7.1. Introduction

Nano-embedded microparticles represent a promising drug delivery system for the pulmonary application. Nanoparticles are widely investigated for a delivery of drugs across the mucus barrier, as they have been shown to permeate mucus depending on their physicochemical properties [8, 9]. As nanoparticles are in a size range with low deposition efficiency, they need to be converted into microparticles to enable an inhalation as dry powder.

By spray drying a nanosuspension together with a matrix forming excipient, nanoparticles can be embedded into microparticles [39, 55]. Spray drying has already been used for the preparation of microparticles containing nanoparticles from various materials [41-46]. A well suited polymer for nanoparticle preparation is poly(lactic-co-glycolic acid) (PLGA), a biodegradable and biocompatible polymer that is already established for parenteral use [94]. It has not yet been approved for pulmonary use. Nevertheless, PLGA nanoparticles intended for pulmonary application are widely investigated and are considered as non-toxic for the lungs [39, 94]. As only few materials are approved so far for pulmonary use, new appropriate materials are needed. Being a safe and biodegradable material, PLGA is therefore a promising polymer for nanoparticle preparation.

For the preparation of nano-embedded microparticles it is crucial to use an appropriate matrix excipient enabling the disintegration of the microparticles in the lungs and release of nanoparticles. Sugar alcohols and sugars such as mannitol, trehalose and lactose are widely applied due to their safety and aqueous solubility [42-46]. Mannitol is of special interest regarding the treatment of pulmonary infections in cystic fibrosis. It is even approved in the EU as mucolytic drug for the add-on therapy in adult cystic fibrosis patients (Bronchitol®). Applied as dry powder formulation, mannitol shows an osmotic effect that is supposed to modify the viscoelastic properties of mucus and to increase its liquid content. In consequence, the mucociliary clearance is enhanced [95]. In addition, mannitol has been reported to increase the sensitivity of persister bacteria in *P. aeruginosa* biofilms against antibiotics [96].

The matrix excipient is supposed to separate the nanoparticles upon spray drying by forming bridges. This is necessary to prevent irreversible aggregation of approaching nanoparticles inside the drying droplet, which might occur when attractive forces overcome electrostatic repulsion. The matrix is supposed to dissolve in contact with aqueous media to release morphologically unchanged nanoparticles. This step is

indispensable to achieve the benefits provided by the nanoparticles such as enhanced drug transport through pulmonary biological barriers.

Despite the high relevance of the redispersibility, the disintegration behavior of microparticles lacks thorough investigation. Most groups working with nano-embedded microparticles investigated the redispersibility by dispersing the powder in aqueous solution and subsequent size determination; in some cases the fraction of redispersed powder was additionally determined [42-46]. However, these methods do not reflect the *in vivo* conditions. The amount of fluid present in the lungs is limited, with estimated 15-70 mL of total liquid volume in the lungs. Only a 5-10 µm thick layer of lung lining fluid covers the airways and even less liquid is present in smaller airways and alveoli [97]. Furthermore, no strong mechanical forces act on inhaled particles. Investigating the disintegration by dispersing nano-embedded microparticles in a large volume of fluid and applying mechanical forces by mixing or stirring is hence not advisable. Ruge et al. addressed this issue by investigating the redispersibility of the particles after deposition on a mucus layer. Particles that easily disintegrated in aqueous solution, were not redispersible after deposition on the mucus, whereas agitation of the mucus enabled disintegration [37]. The presented model reflects the *in vivo* situation. The realization of this experiment though may be impeded due to the limited availability of mucus and low comparability of mucus models with native mucus. In addition, a complex setup is required to enable a homogeneous particle distribution on the mucus layer.

In the following chapter a simplified *in vitro* system to investigate the redispersibility of nano-embedded microparticles under conditions similar to the lungs is presented. Furthermore, the influence of mannitol on morphology, aerodynamic properties and disintegration behavior of nano-embedded microparticles is evaluated.

7.2. Experimental details

7.2.1. *Nanoparticle preparation and characterization*

Emulsion-diffusion-evaporation technique was applied to prepare coumarin 6-loaded PLGA nanoparticles. The solvent consisted of 50 mg PLGA and 7.5 µg coumarin 6 in 2.5 mL ethylacetate. 5 mL 2.5% polyvinylalcohol (PVA) solution were added to the solvent and subsequently the emulsion was homogenized by ultrasound (30%, 30 s; Sonopuls UW3100 with MS73 sonotrode). The primary nanoemulsion was diluted by 25 mL water and left for evaporation of ethylacetate overnight under continuous stirring and light protection. The next day, the nanosuspension's volume was adjusted to 40 mL by water and centrifuged (20,000 g, 15 min). The pellet was redispersed in 40 mL water and the

formulation was centrifuged a second time. Finally the pellet was redispersed in 7.5 mL water. By lyophilization (Alpha 2-4 LSC, Christ) of the nanosuspension and weighing of the pellet, the nanoparticle concentration was determined. The nanosuspension was diluted to yield a nanoparticle concentration of 5 mg·mL^{-1}.

By photon correlation spectroscopy (PCS) and laser Doppler velocimetry, respectively, the hydrodynamic diameter and the zeta potential of the nanoparticles were analyzed. The nanosuspension was diluted 1:100 with water and measured with a Zetasizer Nano-ZS (Malvern Instruments).

The pH was determined from the undiluted nanosuspension by a Seven compact pH meter (Mettler Toledo).

7.2.2. Preparation of nano-embedded microparticles

An excipient solution containing 5 mg·mL^{-1} mannitol and 5 µg·mL^{-1} rhodamine B was prepared. PLGA nanosuspension and excipient solution were mixed in different ratios to prepare the spraying feed liquids. According to their nanoparticle content (0%, 20%, 33%, 50% and 100%), the resulting microparticulate powders were named MP 0, MP 20, MP 33, MP 50 and MP 100, respectively. For each ratio spray drying was performed in triplicate.

Spray drying was conducted with a Nano Spray Dryer B-90 (Büchi). The tall glass construction with the spray head in 45° bent position and a 7.0 µm spray mesh were used. The inlet temperature was set to 80°C and the gas flow rate to 140 L·min^{-1}. 80 mL feed liquid were used for each spray drying run. Prior to spray drying, the liquids were filtrated (Acrodisc$^®$ 25 mm syringe filter with 1 µm glass fiber membrane) to avoid blocking of the vibrating spray mesh due to aggregates. The feed liquids containing nanoparticles were exposed to an ice bath during spray drying to prevent instabilities due to a temperature increase of the spray head, which is exposed to the hot drying gas. The used spray rate was (0.918 ± 0.086) mL·min^{-1} (relative spray rate of 45%) and the resulting outlet temperature ranged between 32-39°C. After collecting the spray-dried powder, it was further dried in a desiccator for several days.

7.2.3. Morphology analysis by SEM and CLSM

For SEM analysis, spray-dried powders were distributed onto conductive carbon discs. After sputter coating with gold (Quorum Q150R ES), imaging was performed with an EVO HD 15 SEM (Zeiss) at an accelerating voltage of 3.5 kV. ZEN 2012 (blue edition) software (Zeiss) was used to determine geometric particle sizes. Each 500 particle diameters were measured for the different microparticle types.

For CLSM analysis, the microparticles were dispersed on a microscope glass slide in immersion oil and covered by a cover slip. Imaging was performed with a LSM 710 AxioObserver confocal microscope with a C-Apochromat 63x objective (Zeiss) at excitation wavelengths of 458 and 514 nm. Fluorescence was detected at 470-551 nm and 551-703 nm, respectively.

7.2.4. Evaluation of aerodynamic properties

By aerosolization on a Next Generation Impactor (NGI; Copley Scientific), the aerodynamic properties of the spray-dried microparticles were analyzed. The gas flow was adjusted to 60 L·min^{-1} by a M1A flowmeter (Copley Scientific). The impactor cups were coated prior to the experiment by a Brij$^®$-Coating (mixture of 40% of 15% Brij$^®$ 35 in ethanol and 60% glycerol) and the pre-separator was filled by 10 mL water. Approximately 20 mg of the powders was filled into hard gelatin capsules (size 3). The capsules were placed in a HandiHaler$^®$ (Boehringer Ingelheim) and punctured. The powder contained in the capsule was aerosolized by a 4 seconds gas flow using a vacuum pump and critical flow controller (both from Erweka). Subsequently, the cups and the induction port were rinsed with a defined volume of water. The powder concentrations in induction port, pre-separator and cups were determined by fluorescence spectroscopy (infinite 200, Tecan). For powders containing mannitol, fluorescence was measured at λ_{ex} = 565 nm and λ_{em} = 625 nm (quantified by rhodamine B) and for MP 100 at λ_{ex} = 440 nm and λ_{em} = 520 nm (quantified by coumarin 6). Calibration curves were generated for the different powders after dispersion in water (concentration range of 0.01-1 mg·mL^{-1}). After measuring the powder concentrations, the cumulative mass fractions were determined for each stage and converted into probit values. The probit values were plotted against the log cut-off diameter. Linear regression was applied for the curve points including a probit of 5 and a log cut-off diameter of 0.7. The mass median aerodynamic diameter (MMAD) is the diameter corresponding to the cumulative mass fraction of 50% and hence to a probit of 5. The geometric standard deviation (GSD) is defined by the square root of the ratio of d_{84} to d_{16} (also see equation (3.2)). d_{84} and d_{16} are the cut-off diameters corresponding to probits of 5.99 and 4.01, respectively. For calculating the fine particle fraction (FPF), the mass fraction of particles smaller 5 µm was determined by converting the probit value for a log cut-off diameter of 0.7. As for the FPF the total powder released from the capsule needs to be considered, the mass of particles below 5 µm in the impactor cups was related to the complete powder found in all cups, the pre-separator and the induction port.

7.2.5. Evaluation of redispersibility in simulated lung fluid

A quantitative evaluation of the redispersibility was performed in simulated lung fluid (SLF). SLF 3 was prepared as previously described in literature [75]. For each prepared powder 10 mg were weighed into Eppendorf tubes of known weight. 2 mL SLF were added to the powder and the Eppendorf tubes were located in horizontal orientation in a shaker under gentle shaking (150 rpm, 30 min, 37°C). Subsequently, the dispersions were centrifuged to separate non-disintegrated microparticles from dissolved mannitol and free nanoparticles (2,000 x g, 10 min). 1.5 mL of the supernatant were taken off and replaced by 1.5 mL of water without further mixing. The supernatant was diluted by water and the size and PDI of the contained particles were determined by PCS (Zetasizer Nano-ZS, Malvern Instruments). Centrifugation was repeated for the Eppendorf tubes and three more washing steps were conducted by removal of the supernatant, addition of water and centrifugation. Finally, the supernatant was discarded and the pellet was freeze-dried (Alpha 2-4 LSC, Christ). After complete drying, the pellet weight was determined. The redispersed powder fraction was calculated by relating the difference between total powder mass and pellet weight to the total powder mass. Mannitol was considered to be completely dissolved. Hence, the pellet was assumed to contain only nanoparticles that are forming non-disintegrated microparticles or larger aggregates. The nanoparticle mass present in the supernatant was thus calculated as difference between redispersed powder mass and mannitol amount. By relating the redispersed nanoparticle mass to the theoretical nanoparticle content, the redispersed fraction of nanoparticles was determined.

7.2.6. Disintegration under conditions similar to the lungs

Agarose was dissolved in water under heating (1.5 mg·mL^{-1}) and the hot solution was poured into petri dishes. A gel pad was formed upon cooling. Spray-dried microparticles were spread on a membrane (NC 05, Schleicher & Schuell) and the membrane pieces were placed on the gel pads. The samples were stored in an incubator (37°C, 90-98% relative humidity) for predefined time periods (10 min, 30 min, 60 min). White light interferometric measurements (NewView^{TM} 7300 3D Optical Surface Profiler, Zygo Corporation) were performed to analyze the membrane surfaces. In addition, powders distributed on the membranes without exposure to high relative humidity (time point 0 min) and membranes without powder were analyzed as well. Three membranes were prepared for each powder type and for each membrane 10 areas of 0.7 x 0.53 mm were analyzed. Roughness analysis was done by MetroPro 8.3.5 software (Zygo Corporation). Furthermore, the membranes were visualized by SEM (EVO HD15) after sputter coating.

7.3. Results and discussion

7.3.1. Nanoparticle characterization

PLGA-nanoparticles were prepared by emulsion-diffusion-evaporation technique and loaded with the fluorescent dye coumarin 6 as lipophilic model drug. With a mean hydrodynamic diameter of around 170 nm and a negative surface charge (Table 7.1), the PLGA-nanoparticles might be well-suited to deliver drugs across the mucus barrier. For negatively charged nanoparticles, a size smaller 200 nm has been reported to be advantageous for a mucus-penetrating effect [8, 24]. The negative zeta potential is caused by carboxylic groups at the particle surface that are deprotonated at the slightly acidic pH value. The particles showed a narrow monodisperse size distribution as defined by the polydispersity index (PDI) < 0.1 [98].

| Size [nm]	PDI	Zeta potential [mV]	pH
169.5 ± 1.8	0.033 ± 0.019	-27.1 ± 4.9	4.96 ± 0.26

Table 7.1. Results of physicochemical characterization of PLGA-nanoparticles loaded with coumarin 6 (n = 3).

## 7.3.2. Morphology of spray-dried particles

The PLGA-nanoparticles were converted into microparticles by spray-drying with mannitol. By SEM and CLSM, the morphologies of the spray-dried particles were investigated.

An influence of the mannitol content on the morphology could be observed by SEM visualization (Fig. 7.1). By spray drying pure mannitol, spherical particles were produced (MP 0). The addition of nanoparticles resulted in raisin-shaped particles (MP 20, MP 33, MP 50). With increasing nanoparticle content, the degree of buckling increased. When no mannitol was used for spray drying (MP 100), collapsed microparticles were observed. Most particles containing both nanoparticles and mannitol (MP 20, MP 33, MP 50) were hollow as seen in CLSM images (Fig. 7.1). These hollow particles display a distinct shell composed of both matrix and nanoparticles, as can be observed by the co-localization of the green (nanoparticles) and red fluorescence (matrix). Most particles prepared only from mannitol (MP 0) were in comparison solid spheres. An irregular distribution of the fluorescence can be seen in the particles. This might be due to crystal formation during spray drying. Crystal structures are as well visible on the particle surfaces in SEM images (Fig. 7.2 A). The crystallinity of spray dried mannitol has already been reported in

literature [99]. MP 100 appeared dense in CLSM images as they were lacking voids due to collapsing (Fig. 7.1). By SEM imaging, the inner structure of broken particles could be visualized. The nanoparticles in MP 100 particles were densely packed (Fig. 7.2 C), whereas they were embedded in a matrix of mannitol for MP 50 particles (Fig. 7.2 B). To prevent the irreversible aggregation of nanoparticles and thus to facilitate the disintegration of the microparticles, the formation of excipient bridges between the nanoparticles is crucial.
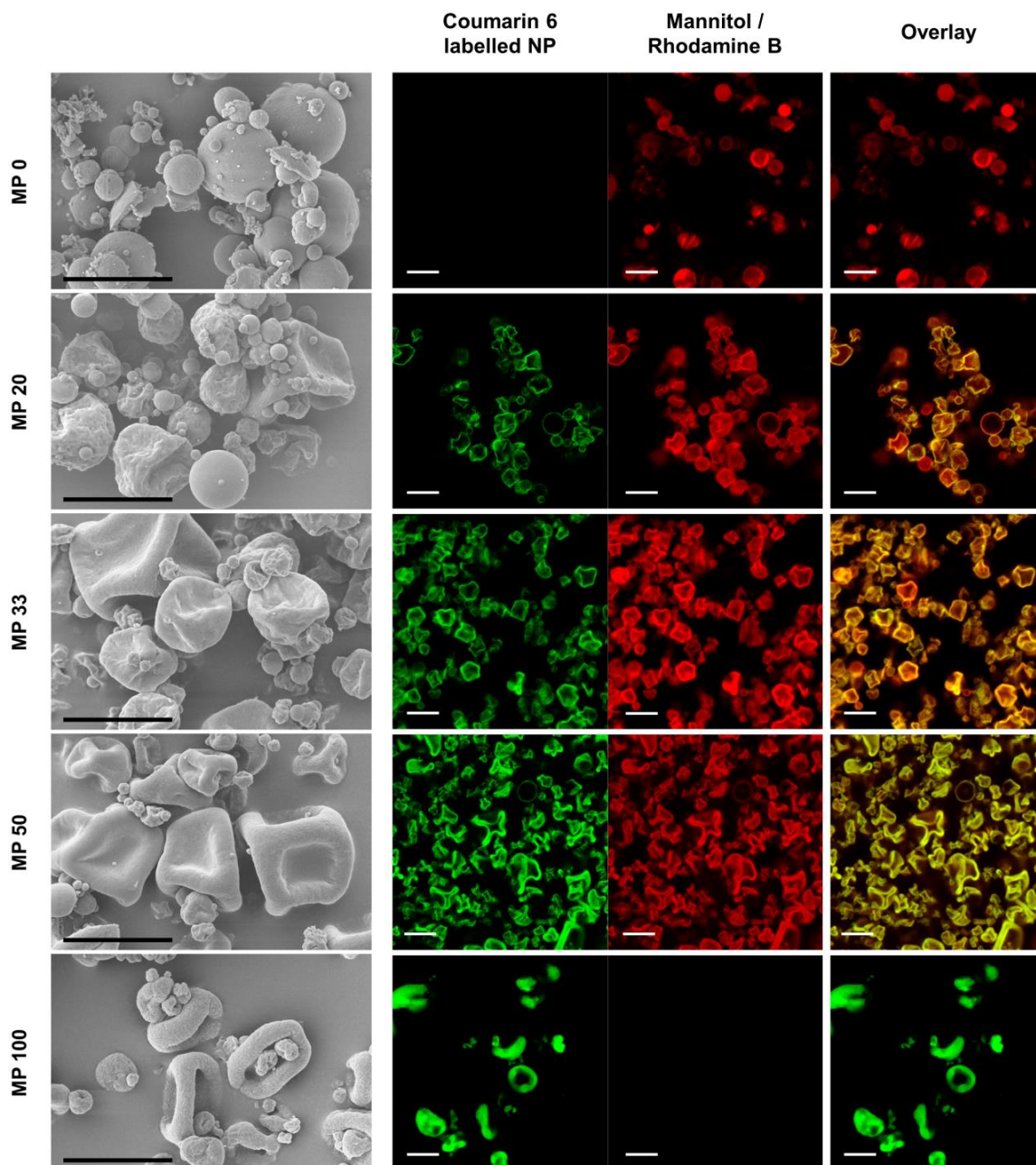
Fig. 7.1. Spray-dried microparticles visualized by SEM and CLSM. An increasing degree of buckling was observed for increasing nanoparticle content. The left row of the CLSM images shows green fluorescence of the coumarin 6-loaded nanoparticles; the second row displays the red matrix fluorescence (rhodamine B) and the overlay is seen in the right row. Scale bars represent 10 µm.
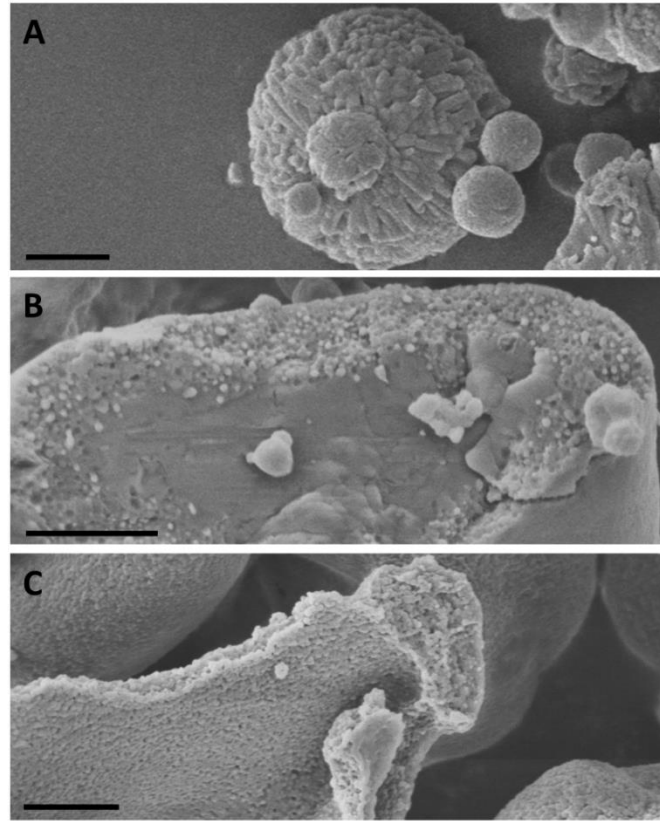
Fig. 7.2. Close-ups of spray-dried microparticles (SEM); A: Crystal structures on the MP 0 particle surface; B: Embedding of nanoparticles into the matrix (MP 50); C: Nanoparticles are densely packed in the shell by spray drying without excipient (MP 100). Scale bars represent 2 µm.

To understand how the different morphologies develop depending on the mannitol and nanoparticle content, the processes occurring during the drying of a droplet in the spray dryer need to be considered. While an evaporating droplet is shrinking, the concentration of the substances increases at the surface. A concentration gradient is generated and thus a diffusional flux from the droplet surface to the center is induced. Crucial are here the velocities of these two processes, the drying-induced transport of components to the droplet surface on the one hand, and the diffusion to the droplet center on the other hand. Different morphologies occur, depending on which of these two processes predominates [100-102]. The Péclet number (Pe) describes the ratio of a substance's diffusion time over a characteristic distance (τ_{diff}) to the drying time (τ_{dry}). The Péclet number is dimensionless and defined by the following equation:

$$Pe = \frac{\tau_{diff}}{\tau_{dry}} = \frac{\kappa}{8 D_i} \qquad (7.1)$$

κ is the evaporation rate and D_i is the diffusion coefficient defined by Stokes-Einstein equation [100-102].

As all parameters besides the ratio of components were kept constant upon spray drying, an equal evaporation rate (κ) is assumed. The diffusion coefficients are 2.9 x 10^{-8} cm^2·s^{-1} (25°C) for the nanoparticles (determined by PCS) and 6.6 x 10^{-6} cm^2·s^{-1} (25°C) for mannitol [103]. The ratio of the diffusion coefficients represents the reciprocal ratio of the Péclet numbers of the two components. Hence, the nanoparticles have a more than 200 times higher Péclet number in comparison to mannitol.

Low Péclet numbers are found for materials with fast diffusional motion. As the diffusion into the droplet center occurs faster than the drying, dense particles without voids are formed. This behavior was observed for the particles containing only mannitol (MP 0). Substances with high Péclet numbers diffuse only slowly so that the droplet surface shrinking predominates. Due to the drying effect the components are transported to the surface and accumulate at the droplet-air interface. In consequence, a shell is formed [100-102]. A shell formation was observed in all microparticle samples containing nanoparticles. In Figure 7.3 B, nanoparticles are mostly seen in the outer part of the particle, whereas mannitol also filled the inner part. Due to its low Péclet number, mannitol could diffuse towards the droplet center, while slow nanoparticle diffusion did not allow moving away from the surface. Nevertheless, mannitol was also found in the shell, preventing the aggregation of the nanoparticles by separating them. Most probably, the dissolved mannitol already started to crystallize, when the saturation concentration at the droplet surface was reached, before attracting forces could overcome electrostatic repulsion between the nanoparticles. In addition, formation of hydrogen bonds between mannitol and the nanoparticle stabilizer polyvinylalcohol might have facilitated the presence of mannitol between the nanoparticles.

The difference in the Péclet numbers of mannitol and nanoparticles allows to explain the formation of either dense particles or solid shells. However, to understand the final morphology of a hollow particle, the mechanical properties of the shell need to be considered [104]. A viscoelastic behavior has been reported for the shell formed upon drying of colloidal suspensions. As long as the shell shows viscous behavior, the droplet shrinks isotropically. At a certain point it becomes elastic. As soon as a solid shell is formed, the buckling starts [100, 104, 105]. For the particles spray-dried from mannitol and PLGA-nanoparticles, more pronounced deformation of the particles occurred with higher nanoparticle content. With increasing nanoparticle concentrations, the shell solidifies faster and the onset of buckling is earlier.

The geometric sizes of the particles were analyzed from SEM images. A trend to larger particle sizes can be seen with increasing nanoparticle content (Fig. 7.3 and Tab. 7.2). This tendency can also be explained by the fact, that a solid shell is formed earlier for higher

nanoparticle contents. If the nanoparticle concentration is lower, the onset of buckling is later. Hence, the longer time of isotropic shrinkage allows the particles to reach smaller final sizes.

	Dn10 [µm]	Dn50 [µm]	Dn90 [µm]
MP 0	1.084	1.953	6.064
MP 20	1.159	2.445	6.264
MP 33	1.398	3.205	7.181
MP 50	1.166	2.641	7.022
MP 100	1.932	3.678	7.207

Table 7.2. Size distribution parameters: The Dn-values are the cut-off sizes at which 10%, 50% and 90%, respectively, of the number of particles show smaller sizes ($n = 500$).
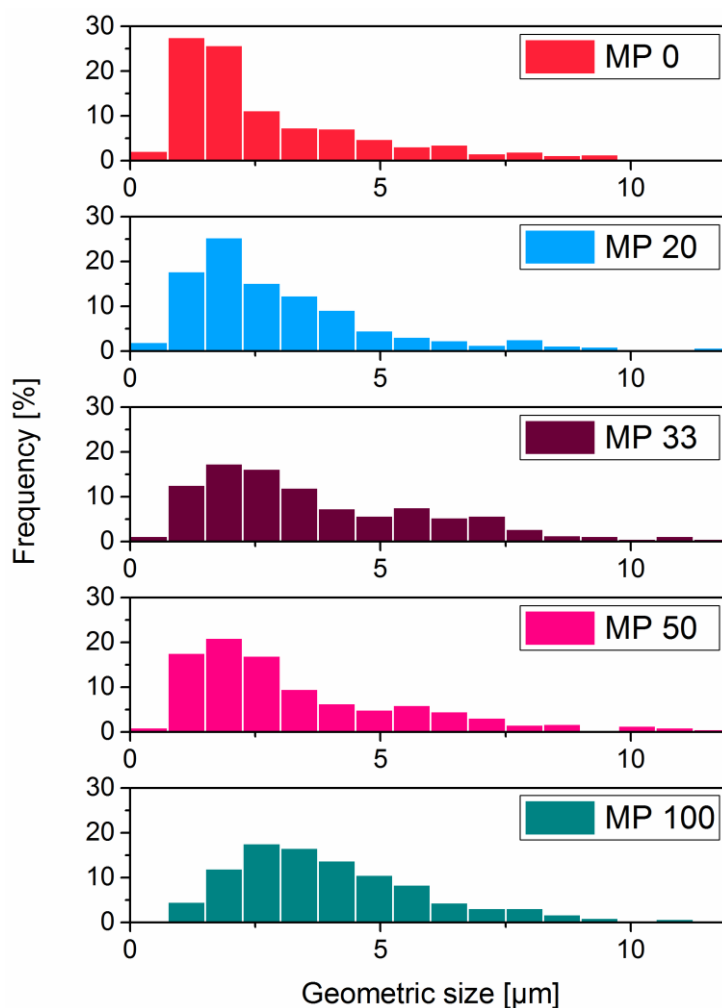
Fig. 7.3. Geometric size distributions of spray-dried microparticles ($n = 500$).

7.3.3. Aerodynamic properties

Dry powder formulations intended for inhalation require appropriate aerodynamic properties for a good deposition in the lungs. Next generation impactor (NGI) experiments were performed to determine the mass median aerodynamic diameter (MMAD), the geometric standard deviation (GSD) and the fine particle fraction (FPF). All samples containing mannitol (MP 0, MP 20, MP 33, MP 50) displayed comparable MMAD values between 5.04 and 5.41 µm (Tab. 7.3). Despite their largest geometric size, the MP 100 particles had with 3.61 µm a considerably smaller MMAD in comparison to particles containing mannitol. Most probably a different surface texture causes a lower aggregation tendency and thus a lower aerodynamic diameter. The fine particle fraction was also highest for MP 100.

Ideally, particles should be distributed on the conducting airways for an optimal therapy of chronic lung infections in cystic fibrosis [106]. Particles with a MMAD of 1-5 µm are reported to deposit in small airways and alveoli. Among these, particles showing a MMAD below 3 µm deposit mostly in the alveolar region and are thus not appropriate for targeting the conducting airways [106]. MMAD values of 5-10 µm are associated with a deposition in the oropharyngeal region and large conducting airways [106]. Showing MMAD values between 3.61 and 5.41 µm, all spray-dried powders have hence the appropriate aerodynamic size for a therapy of lung infection in cystic fibrosis, as they would deposit preferably in the conducting airways.

The powders showed GSD-values above 1.5. Hence, all powders can be considered as polydisperse, as typically the case for most pharmaceutical aerosols [29].

	MMAD [µm]	GSD	FPF [%]
MP 0	5.04 ± 0.05	1.99 ± 0.14	25.7 ± 2.2
MP 20	5.41 ± 0.12	1.65 ± 0.06	22.5 ± 0.4
MP 33	5.21 ± 0.20	1.70 ± 0.02	19.9 ± 2.7
MP 50	5.17 ± 0.18	1.67 ± 0.07	20.8 ± 4.9
MP 100	3.61 ± 0.22	1.76 ± 0.14	28.6 ± 2.7

Table 7.3. Aerodynamic properties of spray-dried microparticles (*n* = 3).

7.3.4. Quantitative evaluation of redispersibility

After reaching the airways, the spray-dried microparticles are supposed to disintegrate so that nanoparticles are released. The disintegration behavior was first tested by dispersing the powders under shaking in an excess of simulated lung fluid. The size and PDI of the nanoparticles in the supernatant were measured by PCS. Nanoparticles spray dried with mannitol showed only a slight increase of size and PDI after spray drying and redispersion in comparison to the untreated nanoparticles (Fig. 7.4). If no mannitol was used for spray drying, the initial size and PDI were not recovered after redispersion suggesting an irreversible aggregation of the nanoparticles upon spray drying.
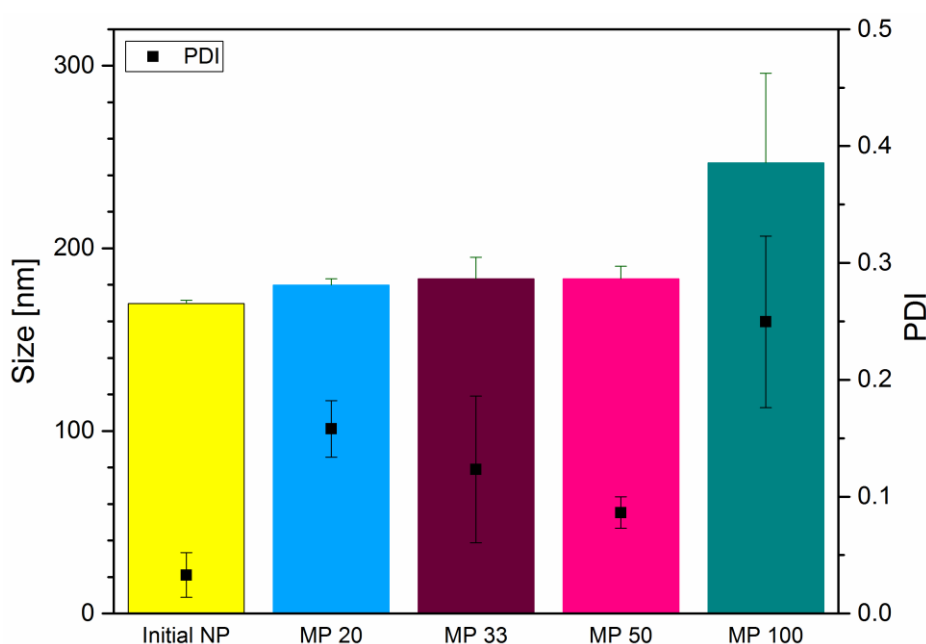
Fig. 7.4. Size and PDI of nanoparticles of initial nanoparticles and after spray drying and redispersion. The initial nanoparticle size was only recovered for samples containing mannitol, whereas a clear increase in size and PDI was observed for MP 100 ($n = 3$).

The fraction of the powder that was not redispersed was determined gravimetrically after lyophilization of the pellet. As mannitol is water soluble, the MP 0 powder was completely redipersed (Tab. 7.4). The redispersed nanoparticle fraction was determined by assuming the contained mannitol to be completely dissolved. The highest fraction of redipersed nanoparticles was achieved for the MP 20 powder, hence for the highest mannitol content. For MP 33 and MP 50 powders only around 16% of the nanoparticles were found to be redispersed. Nearly no nanoparticles were released from MP 100 particles. Nevertheless, the size measurement from the supernatant yielded a size value in the nanometer range.

	Redispersed powder fraction [%]	Redispersed NP fraction [%]
MP 0	99.83 ± 0.29	-
MP 20	84.80 ± 0.78	24.02 ± 3.92
MP 33	72.16 ± 0.32	15.63 ± 0.98
MP 50	57.85 ± 1.50	15.69 ± 2.99
MP 100	3.41 ± 2.59	3.41 ± 2.59

Table 7.4. Redispersed fractions of powder and nanoparticles (NP) after dispersion of the powders in simulated lung fluid (n = 3).

7.3.5. Disintegration under conditions similar to the lungs

The investigation of the disintegration behavior in simulated lung fluid gives a first impression of the redispersibility of nano-embedded microparticles and eventual size changes of the nanoparticles can be detected. However, the *in vivo* situation is not reflected, as liquid is used in excess and mechanical forces are applied. In this project, the disintegration should be evaluated under conditions similar to the lungs. The air in the lungs has 100% relative humidity at 37°C. The inspired air is conditioned to these conditions upon breathing. Complete conditioning is usually already achieved in the larger conducting airways [107]. A relative humidity of 100% at 37°C was hence considered to be the relevant parameter for the redispersibility of nano-embedded microparticles. The spray-dried particles were distributed on a membrane located on an agarose gel and exposed to > 90% relative humidity at 37°C. The function of the membrane was to take up the dissolved mannitol while retaining released nanoparticles and undisintegrated microparticles on the surface. Without using the membrane, the mannitol would recrystallize again and influence the roughness values and hinder the proper imaging of the released nanoparticles. White light interferometry was applied to evaluate the results. This profilometric technique allows to measure a large surface area and to determine its roughness with a vertical resolution < 1 nm [108]. Higher roughness values correspond to larger deviations from the surface in z-direction and hence indicate the presence of larger objects such as microparticles on the membrane surface. By disintegration of nano-embedded microparticles, the roughness value decreases with optimally only a smooth layer of nanoparticles remaining on the membrane. Visualization of the membranes by SEM was additionally performed to support the white light interferometric measurements.

All untreated powders (t = 0 min) displayed high roughness values with large standard deviations (Fig. 7.5). Within 10 minutes of incubation, the roughness of the MP 0 sample decreased to the roughness value of the membrane (0.499 ± 0.049 µm). In SEM images, no particles were seen any more after 10 min, confirming the complete dissolution of the mannitol and uptake into the membrane (Fig. 7.6). For MP 20, MP 33 and MP 50 a strong decrease of the roughness was observed as well, indicating that disintegration occurred also in these samples (Fig. 7.5). A plateau was reached for the MP 20 sample within 10 min at a comparable roughness value as the MP 0 powder. SEM imaging revealed few remaining, collapsed microparticles and the released nanoparticles were distributed over the membrane surface (Fig. 7.6). The roughness of the MP 33 sample was decreasing till 30 min of experiment time, whereas no plateau was reached for MP 50 within 60 min. More microparticulate remnants were observed for MP 33 and MP 50 in comparison to the MP 20 powder. The MP 100 powder, consisting only of nanoparticles, displayed a high roughness over the 60 minutes of experiment, with only slight reduction in the last 30 minutes. In SEM images, no disintegration was observed for MP 100 particles, which remained morphologically unchanged and did not release any nanoparticles. The slight decrease of the roughness might be caused by a rearrangement of the microparticles or aggregates of those.
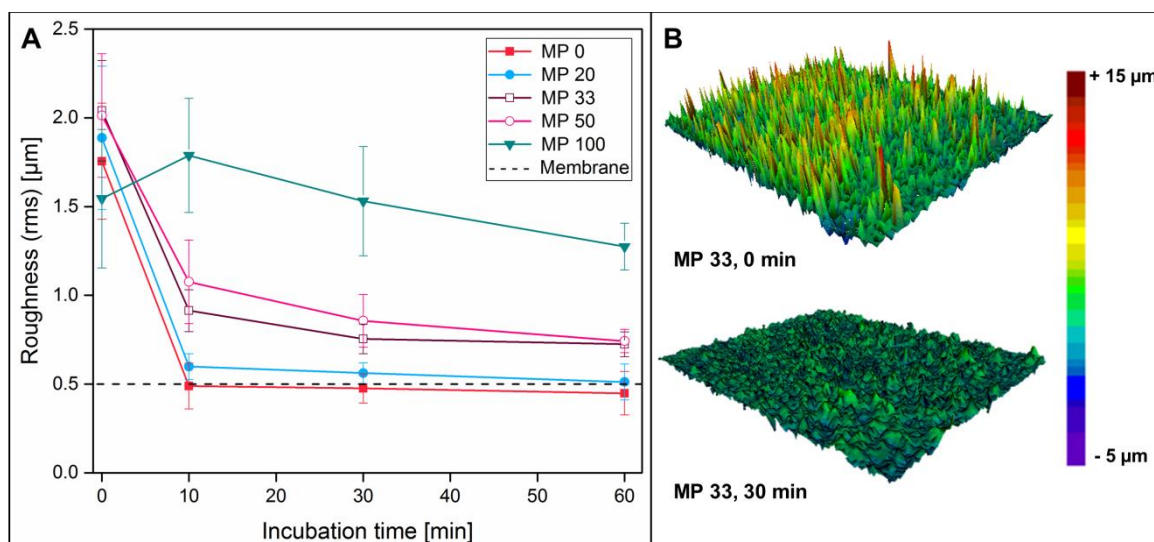
Fig. 7.5. Disintegration behavior of spray-dried microparticles in high relative humidity monitored by white light interferometry. A) The roughness values (root mean square roughness) of the membranes were plotted against the time of incubation. 10 positions for each 3 membranes per sample were analyzed. B) Exemplary 3D white light interferometric images. A decrease of the roughness after 30 min of incubation can be observed. The shown areas represent a surface of 0.7 x 0.53 mm.
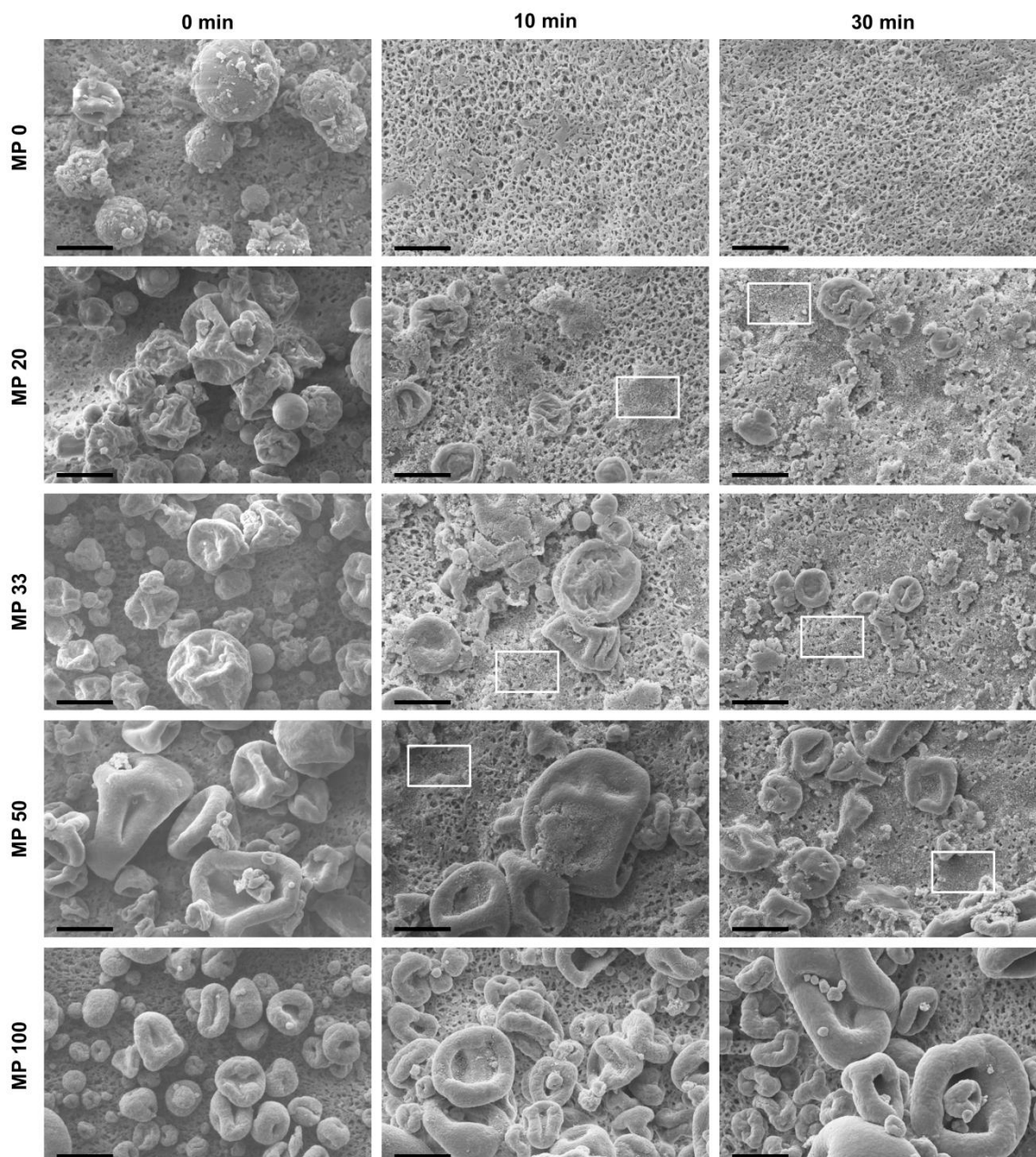
Fig. 7.6. Spray-dried microparticles before and after 10 and 30 min of exposure to > 90% relative humidity. MP 0 particles disappeared completely within 10 min. Microparticles composed of nanoparticles and mannitol disintegrated faster and to a higher degree for higher mannitol contents. Areas that are covered by nanoparticles are exemplarily labelled by white boxes. No change of the morphology of MP 100 particles was observed over the 60 min. Scale bars represent 5 μm.

In summary, microparticles containing mannitol were able to disintegrate in > 90% relative humidity. The velocity and degree of the disintegration was revealed to increase with increasing mannitol content. No disintegration was possible for particles without mannitol. Despite the slower and less pronounced disintegration for lower mannitol contents, morphologically unchanged nanoparticles were released. Disintegrated MP 50 powder after 60 min of incubation with high air humidity is displayed in Fig. 7.7. Even if

some microparticulate remnants are present, high amounts of homogeneously distributed nanoparticles are visible. The formation of a smooth nanoparticle layer indicated that no irreversible agglomeration occurred during spray drying.
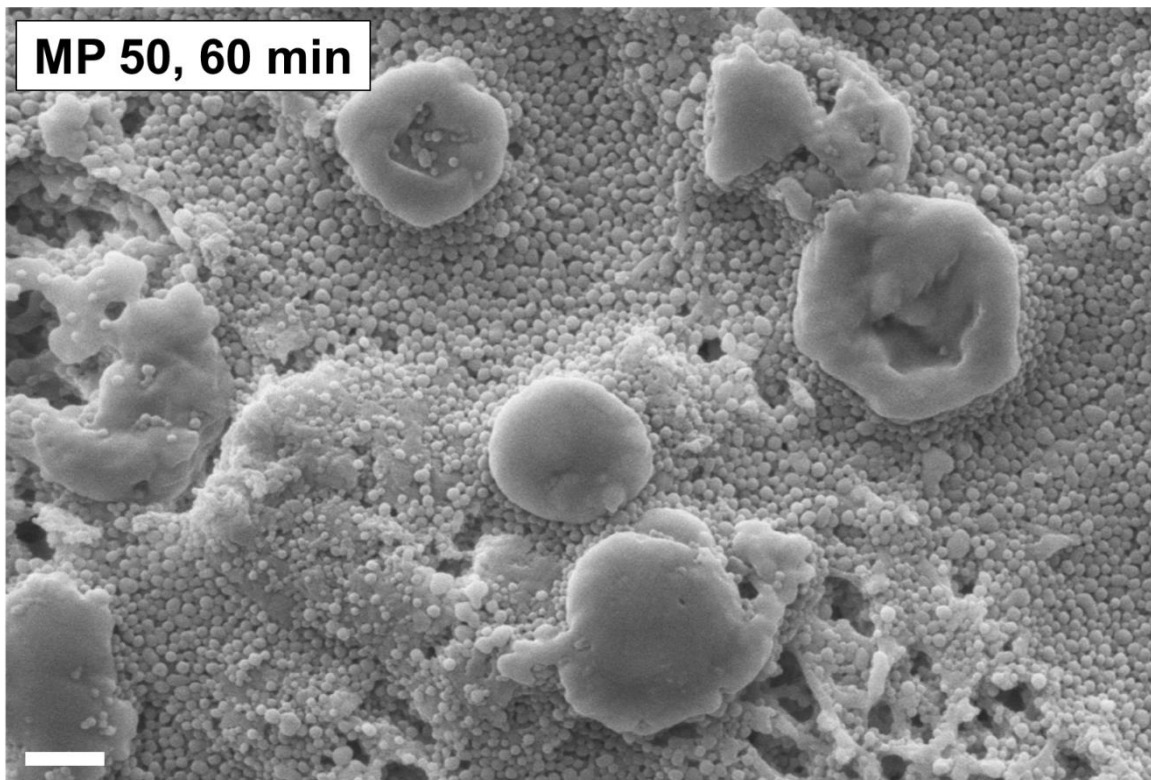
Fig. 7.7. MP 50 particles imaged by SEM after 60 min incubation at > 90% relative humidity; microparticulate remnants are still present, while a smooth layer of released nanoparticles has been formed on the membrane surface. Scale bar 1 µm.

The necessary disintegration time is relevant for the development of nano-embedded microparticles. Slowly disintegrating microparticles might already be removed by the mucociliary clearance before sufficient amounts of nanoparticles are released. The transport rates achieved by the mucociliary escalator are reported to range from 2.4 to 11.4 mm·min^{-1}. In the trachea, mucus velocity is higher in comparison to smaller airways [106, 109]. Hence, as inhaled microparticles may already be transported few centimeters within 10 minutes, a fast disintegration is preferred. In addition, further time is needed for the nanoparticles to penetrate the mucus layer before being transported away. Even if in cystic fibrosis the mucociliary clearance is strongly impeded, a maximum nanoparticle content of 20% is recommended for nano-embedded microparticles with mannitol as excipient, to enable a fast disintegration and release of nanoparticles.

The results obtained from the quantitative investigation of the redispersibility behavior in simulated lung fluid correlates to a large extent with the data obtained by evaluating the

microparticle disintegration under conditions similar to the lungs. With higher mannitol content, both the highest redispersible fractions in SLF and fastest disintegration in high relative humidity were observed. Nevertheless, to determine only the sizes after redispersion in fluid is not sufficient as it might deliver misleading results. A nanoparticulate size was measured by PCS after dispersing MP 100 powder in SLF, even if no release of nanoparticles was seen after 1 h of exposure to > 90% relative humidity. The use of models reflecting the *in vivo* situation of the lungs is therefore highly recommended.

7.4.   Conclusion

Nano-embedded microparticles consisting of PLGA-nanoparticles and mannitol as matrix were prepared by spray drying. The morphology of the microparticles turned out to be influenced by varying mannitol content. However, the aerodynamic properties were not affected by changing the mannitol to nanoparticle ratio. The disintegration of nano-embedded microparticles is crucial to enable a release of the nanoparticles. The evaluation of the redispersibility by dispersing the powder in fluid under application of mechanical forces is not recommended due to the divergence to the *in vivo* situation. A simplified *in vitro* model was presented to test the redispersibility under lung-relevant conditions. A water soluble matrix excipient such as mannitol was revealed to be indispensable to enable a release of the nanoparticles. High relative humidity turned out to be sufficient to induce a disintegration of microparticles containing mannitol. With higher mannitol content, faster redispersion of nanoparticles could be achieved. To enable the release of nanoparticles before the microparticles are cleared, a maximum nanoparticle content of 20% is advisable.

By embedding PLGA-nanoparticles into a matrix of mannitol by spray drying, a promising drug delivery system for the pulmonary route is created. Due to the appropriate aerodynamic diameter and composition of the microparticles, an efficient deposition in the lungs with subsequent disintegration and release of nanoparticles can be achieved. By using drug-loaded nanoparticles, the drug might benefit from protection from deactivation, improved delivery across the mucus barrier and sustained release.

8. COMPARISON OF CYLINDRICAL AND SPHERICAL MICROPARTICLES COMPOSED OF NANOPARTICLES

8.1. Introduction

The preparation of nano-embedded microparticles is a novel approach to deliver nanoparticles into the lungs. Mostly, spray drying is used for the preparation of spherical microparticles. Though, also the use of aspherical particles such as fibers is of high interest for a delivery to the lungs.

Per definition, fibers have an elongated (approximately cylindrical) shape, a length greater than 5 µm and an aspect ratio (ratio of length to diameter) over 3 [33, 110]. Fiber materials like asbestos and mineral wool are well known for their toxicity as they cause lung diseases such as lung cancer, mesothelioma and fibrosis (asbestosis) [111]. Pott stated that "*A fibre has to be regarded as a physical carcinogen that works by its elongated shape*" [112]. Due to the elongated shape, fibers align in the airflow and are thus easily transported into the deep lungs [111]. Fibers are retained for long time in the alveoli and small non-ciliated airways, as clearance can only be achieved by translocation after ingestion by alveolar macrophages, which is even hindered due to the elongated shape [33, 113]. Disintegration is practically impossible for asbestos and mineral fibers [33, 111]. The long retention time of these persistent materials in the deep lungs is responsible for the toxicological effects.

Despite their high toxicity, these fibers can serve as inspiration for the development of drug delivery systems. By preparing fibers from biocompatible and biodegradable materials, pulmonary drug delivery might benefit from the good lung deposition, while toxicological effects due to retention can be excluded. Promising is as well the use of aspherical nano-embedded microparticles, which disintegrate after deposition into nanoparticles. Hence, the fibers are only used for the transport of the nanoparticles without accumulating in the lungs.

Good aerodynamic properties have been shown so far for needle-shaped particles [114]. The aerodynamic diameter of a fiber is more influenced by its diameter than by its length [110]. For larger particle diameters, however, the length of the cylindrical particle has an increasing influence on the aerodynamic properties [33]. A mathematical approach has been described to predict the aerodynamic diameter of fibers depending on the diameter and aspect ratio [33].

By using templates with appropriate dimensions, custom-tailored particles with the desired aerodynamic diameter, exact shape and narrow size distributions can be prepared. Recently, a nanomolding technology (PRINT, Particle Replication In Non-wetting Templates) has been established with which aspherical particles with narrow aerodynamic size distributions can be prepared [115]. Track-etch membranes have already been used as template for the preparation of cylindrical particles composed of silica nanoparticles [47, 48].

In this chapter, cylindrical microparticles are prepared for the first time from biodegradable and biocompatible nanoparticles. The template-assisted technique will be compared with spray drying in terms of the tunability of the particle size, expenditure of time and feasibility of scale-up. A comparison of the resulting microparticles will be performed regarding size distribution, nanoparticle content, aerodynamic properties and disintegration behavior.

8.2.   Experimental details

8.2.1.   *Nanoparticle preparation and characterization*

Fluorescently labeled gelatin nanoparticles (GNP) were prepared by nanoprecipitation technique [49]. 20 mg of gelatin (type B) and 1 mg of FITC-dextran 70 (Mw 70 kDa) were dissolved in 1 mL of water at 40°C. This solution was added dropwise to a poloxamer 188 solution (450 mg in 1 mL water and 15 mL acetone). Crosslinking was performed by slow addition of 0.5 mL glutaraldehyde solution (2%, w/v). After 6 h of crosslinking time under stirring, GNP were purified by three centrifugation steps and subsequent redispersion in water. The concentration of the resulting nanosuspension was determined by freeze drying (Alpha 2-4 LSC, Christ) and weighing of the pellet.

Nanoparticle size and zeta potential were measured by photon correlation spectroscopy (PCS) and laser Doppler velocimetry, respectively, after 1:100 dilution with water with a Zetasizer Nano-ZS. pH was measured in the undiluted nanosuspension using a Seven compact pH meter (Mettler Toledo).

8.2.2.   *Preparation of cylindrical microparticles*

Polycarbonate membranes (Nuclepore Track-Etch Membranes; Whatman) with different pore size diameters (1, 3, 5 μm) were placed above blocking membranes with 0.05 μm pores and fixed in a Swinnex filter holder (EMD Millipore Corporation). GNP nanosuspension (adjusted to a concentration of 1.5 mg·mL^{-1}) containing 5% (m/v) mannitol and 0.05 mg·mL^{-1} rhodamine B was infiltrated into the upper membrane by a

syringe pump (Legato 210; KD Scientific). Subsequently, membranes were cleaned with a humid tissue and dried overnight at 30°C. Membrane filling was repeated till no further filling was possible. Fresh blocking membranes were used for each filling step. For 1 µm and 3 µm pore size membranes 5 filling steps were necessary, for the membranes with 5 µm pores 7-9 filling cycles were required. After complete filling, the GNP inside the pores were interconnected by placing each membrane onto 250 µL interconnection solution dropped onto a glass slide. The interconnection solution consisted of 20% (m/v) mannitol solution containing 10 mg·mL^{-1} leucine and 0.05 mg·mL^{-1} rhodamine B. The membrane was dried and interconnection was repeated by the second side of the membrane. After complete drying, the membranes were wiped clean with a wet tissue and stored for several hours at 30°C. Membranes were dissolved in dichloromethane and released rods were purified by three times centrifugation (6,500 x g; 10 min) and redispersion in dichloromethane. Subsequently the pellet was centrifuged at lower forces to remove free nanoparticles (2,000 x g; 10 min) and redispersed in ethylacetate three more times. For NGI analysis the microrod dispersion was dried in an Eppendorf tube at ambient temperature before the powder was stored in a desiccator till further use.

8.2.3. Preparation of spherical microparticles

For each spray drying run 900 mg mannitol, 50 mg leucine and 2.5 mg rhodamine B were dissolved in a nanosuspension aliquot containing 50 mg GNP and diluted by water to reach a final solids concentration of 1%, 10%, or 20%, respectively. The dispersions were spray dried using a B-290 spray dryer (Büchi) at an inlet temperature of 100°C. The atomizing air flow rate was approx. 742 L·h^{-1}, the feed pump rate 5.5 mL·min^{-1}, and the aspirator was set to 100% (approx. 35 m^3·h^{-1}). Each powder was prepared in triplicate and further dried in a desiccator.

8.2.4. SEM imaging and size analysis

Microrod dispersions in ethylacetate were dropped onto silica wafers and air dried. Spray-dried particles were applied directly onto conductive carbon discs. Both were sputter coated with gold (Quorum Q150R ES). Imaging was performed with an EVO HD15 scanning electron microscope (Zeiss) at an accelerating voltage of 5.0 kV for microrods and 3.5 kV for spray-dried particles. Geometric particle sizes were analyzed by ZEN 2012 (blue edition) software. For spray-dried particles 600 particle diameters and for microrods 600 lengths and 300 diameters were measured manually. For size analysis, each three different batches of microparticles were analyzed.

8.2.5. CLSM imaging

Powders were dispersed in immersion oil on a microscope glass slide and covered by a cover slip. The microparticles were imaged using a LSM 710 AxioObserver confocal microscope with an EC Plan-Neofluar 100x objective (Zeiss). Excitation wavelengths of 488 and 561 nm were used and detection was performed at 493-556 nm and 566-685 nm, respectively.

8.2.6. Determination of nanoparticle content

A calibration curve was created for a nanosuspension of known GNP concentration by fluorescence spectroscopy (infinite 200, Tecan; λ_{ex} = 488 nm and λ_{em} = 525 nm). Microparticle powders were accurately weighed, dispersed in water, and subsequently the fluorescence was measured to quantify contained GNP.

8.2.7. Evaluation of aerodynamic properties

The aerodynamic properties of the powders were assessed by Next Generation Impactor (Copley Scientific) experiments. Experiments were performed as described in subchapter 7.2.4. For cylindrical particles 1.5 mg and for spray-dried powders around 20 mg powder per capsule were used. Quantification by fluorescence spectroscopy was performed at an excitation wavelength of 565 nm and an emission wavelength of 625 nm.

8.2.8. Redispersibility behavior

Powder was applied onto a silica wafer and covered with a droplet of water. After 5 minutes of incubation, the droplet was removed by a tissue and the wafer was washed with water. Imaging was performed after sputter coating with gold (Quorum Q150R ES) with an EVO HD15 SEM at an accelerating voltage of 5.0 kV.

8.3. Results and discussion

8.3.1. Nanoparticle characterization

Gelatin is a denaturated protein that is prepared from animal collagen by partial hydrolysis. Due to its biodegradability and biocompatibility, gelatin is already well-established for parenteral and oral use [116, 117]. It is even approved by the FDA (U.S. Food and Drug Administration) for pulmonary route in concentrations up to 10% for powders for inhalation [116]. Gelatin nanoparticles (GNP) are of special interest for a delivery of hydrophilic macromolecules. Macromolecules are usually challenging to deliver, due to their low ability to overcome biological barriers and due to incompatibilities with hydrophobic polymers. GNP are promising candidates for a delivery system to tackle these challenges [49].

As model drug, the fluorescent macromolecule FITC dextran (Mw = 70 kDa) was used in this project for a loading of the nanoparticles. Gelatin nanoparticles were prepared with a size of about 300 nm with a rather narrow size distribution (PDI < 0.2). At a slightly acidic pH value, the particles have a negative zeta potential due to deprotonated carboxylic groups at the particle surface (Table 8.1).

Size [nm]	PDI	Zeta potential [mV]	pH
301.2 ± 12.0	0.125 ± 0.024	- 14.8 ± 3.4	5.5 ± 0.4

Table 8.1. Physicochemical characterization of gelatin nanoparticles (GNP). Values are expressed as mean ± SD (*n* = 5).

8.3.2. Microparticle morphology

GNP were embedded into either cylindrical microparticles by template technique or spherical microparticles by spray drying. Mannitol and leucine were used as excipients. Mannitol was chosen due to its aqueous solubility and because of its advantages for a potential use in cystic fibrosis such as the mucolytic effect and the increased antibiotic efficacy against persister bacteria [95, 96].

Leucine was used because of its ability to reduce the surface cohesiveness of microparticles. Due to its surface-active properties, leucine accumulates at the surface of the droplets. By preventing particle agglomeration, the fine particle fraction of a powder can be increased [118].

The template technique yielded cylindrical microparticles of relatively homogeneous size and a diameter depending on the used membrane pore size (Fig. 8.1). The thickness of

the membrane (10 μm) defines the maximal length of the rods, which was reached for none of the rod sizes (Tab. 8.2). The resulting diameter was as well below the theoretical diameter, which is determined by the pore size of the used membrane. Both can be explained by the reversible swelling behavior of GNP in aqueous solution [49, 119]. The nanoparticles inside the pores shrink upon drying due to loss of water and thus the resulting cylindrical microparticles show sizes smaller than the template pores. Also the excipient solution used for interconnection of the nanoparticles has a higher volume than the dried excipients. The swelling of GNP is furthermore the reason for the need of multiple filling steps to reach a sufficient rod length. In CLSM images it can be seen that the cylindrical microparticles are not completely filled inside (Fig. 8.2). 1 μm rods already show several voids, while 5 μm rods are mostly hollow. For most particles, the nanoparticles (green fluorescence) and the matrix (red fluorescence) are co-localized. However, there are also particles showing only red fluorescence (Fig. 8.2, 3 μm). Probably some pores were not filled by GNP and thus only filled by mannitol and leucine in the interconnection step. With an aspect ratio over 3, only the 1 μm cylindrical particles are fibers per definition.
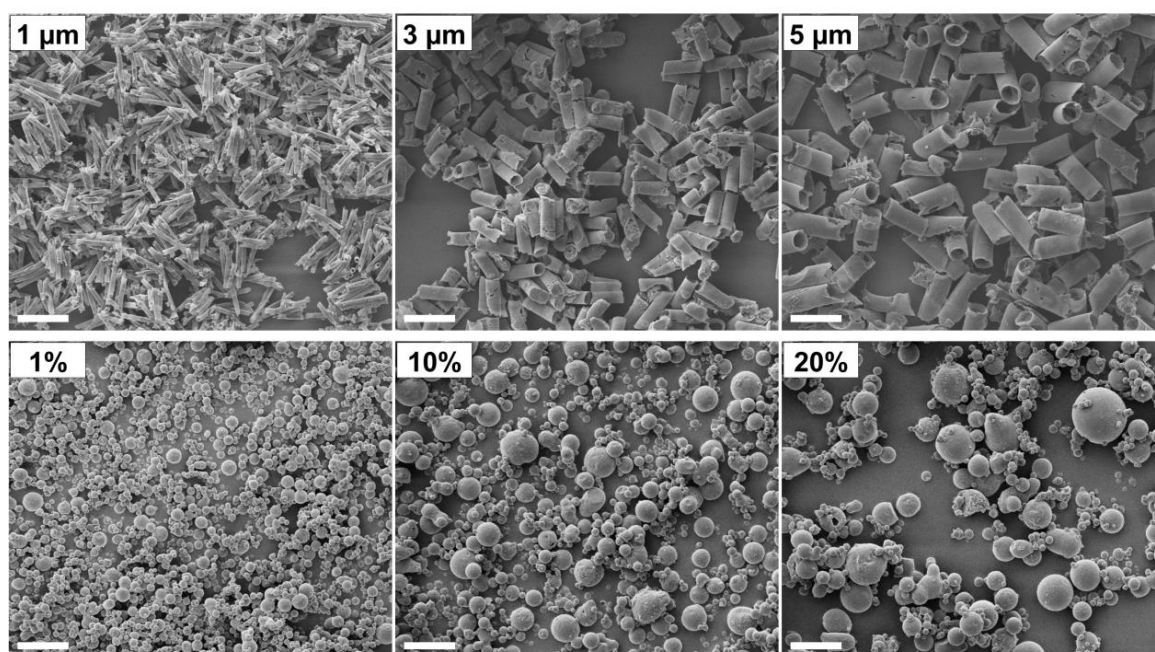
Fig. 8.1. Cylindrical and spherical microparticles imaged by scanning electron microscopy. Cylindrical microparticles show sizes depending on the used template membrane, while an increasing concentration of the feed liquid in spray drying resulted in increased particle sizes. Scale bars represent 10 μm.

		Length [µm]	Diameter [µm]
Cylindrical particles	**1 µm**	6.84 ± 2.12	0.95 ± 0.12
	3 µm	7.20 ± 1.30	2.68 ± 0.31
	5 µm	9.08 ± 1.76	4.32 ± 0.44
Spherical particles	**1%**	-	1.42 ± 0.62
	10%	-	2.03 ± 1.36
	20%	-	2.44 ± 1.86

Table 8.2. Geometric dimensions of microparticles determined from SEM images.
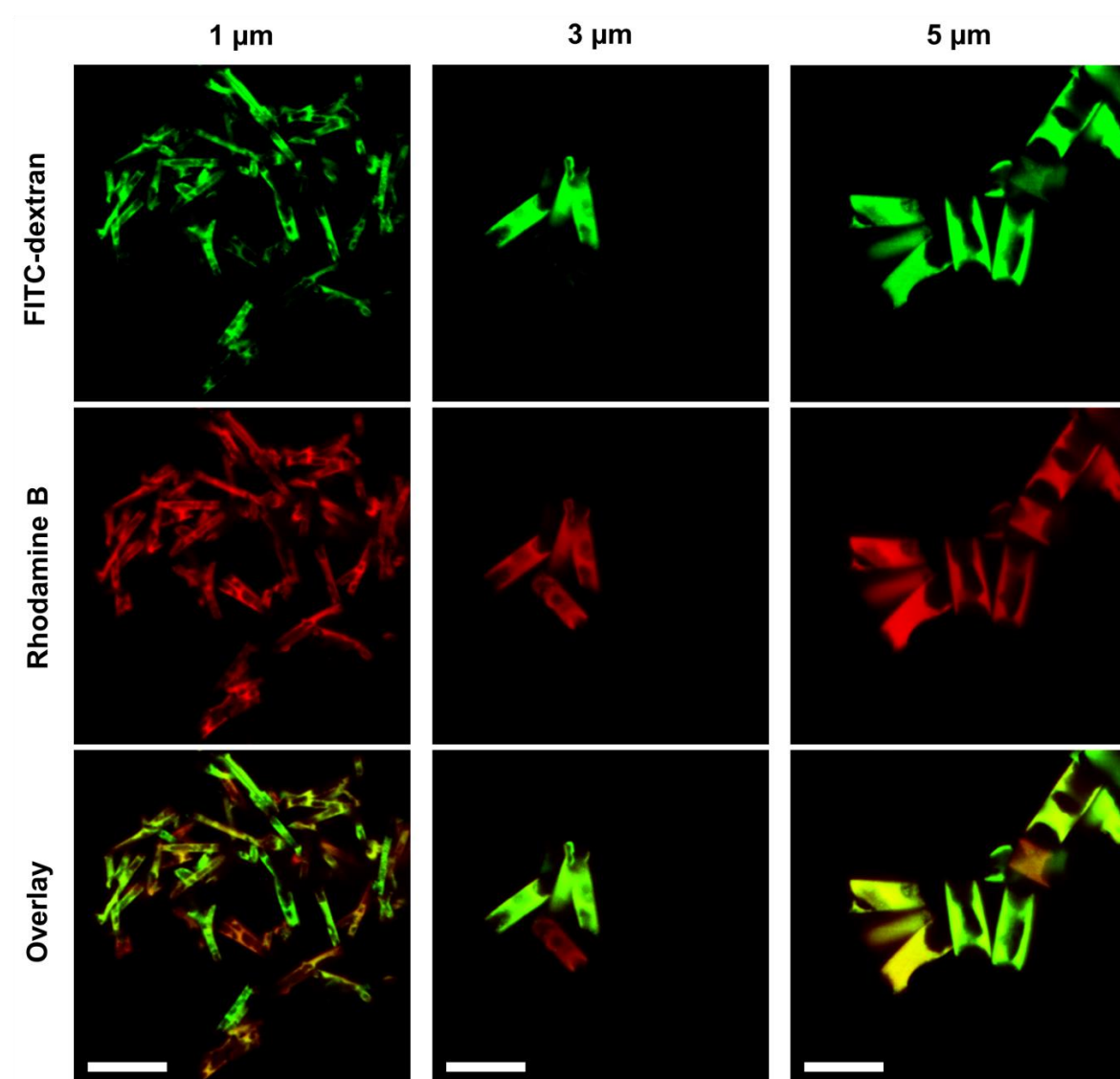
Fig. 8.2. CLSM images for cylindrical particles. The particles are partially hollow and mannitol and GNP are not always co-localized. Scale bars represent 10 µm.

As a second technique to prepare microparticles, spray drying was performed. It is known that the feed concentration used for spray drying influences the resulting particle size [55]. Hence, gelatin nanosuspension was spray dried together with mannitol and leucine in three concentrations to yield powders with different particle sizes. With increasing feed concentration, larger spherical particles were formed. Mean sizes between 1.42 and 2.44 µm could be reached. However, a broad size distribution was indicated by the high standard deviations (Tab. 8.2). CLSM imaging revealed that most particles were solid, with few hollow particles for higher feed concentrations (Fig. 8.3). Fluorescence of GNP and the excipient matrix was co-localized, indicating that GNP were embedded into the matrix.
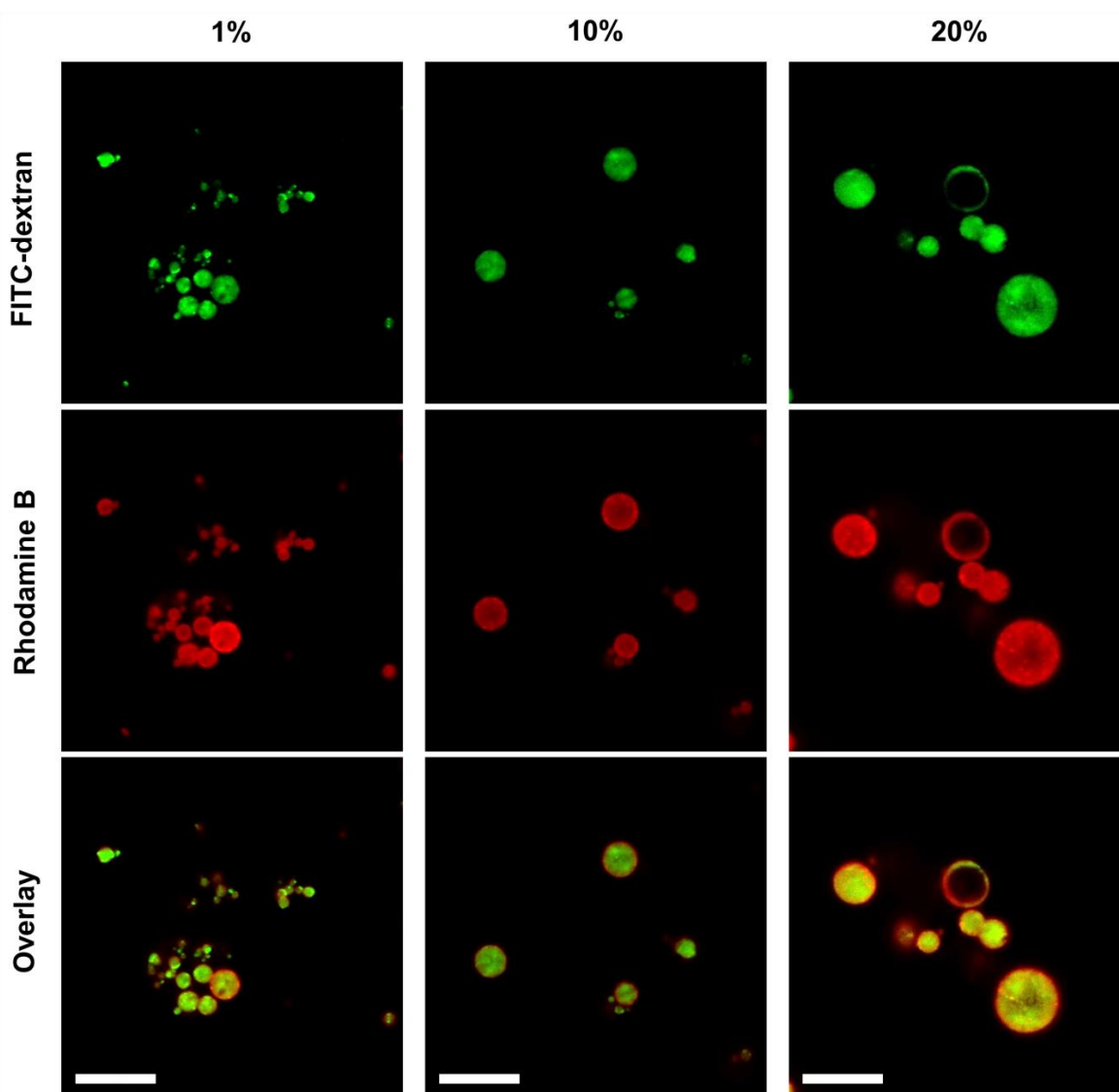
Fig. 8.3. Spherical particles imaged by CLSM. Spray drying resulted in mostly dense particles, for the highest concentration also hollow particles were obtained. GNP and matrix were co-localized. Scale bars represent 10 µm.

The distribution of GNP and matrix excipients was revealed to be homogeneous for spherical microparticles. In comparison, cylindrical microparticles lacking the green fluorescence signal of the GNP were detected. Hence, the template-assisted technique produces particles that are more homogeneous in size, but less homogeneous in terms of the nanoparticle content.

The size of cylindrical microparticles can be easily tuned by using a suitable template. The size distribution is narrow with relative standard deviations of around 10% for the diameter and around 20-30% for the length. For spray drying in comparison several parameters have an influence on the resulting particle size and morphology. The particle size cannot be predicted, so several experiments need to be conducted to reach a certain target size. In this work the parameter with the most pronounced influence on the particle size was changed, the feed concentration. The concentrations that could be used were limited on the one side by the solubility of mannitol, on the other side by the risk of low yields due to product loss for low feed concentrations [56]. By varying the concentration in a reasonable range, the mean particle size could only be influenced in a small span (1.4-2.4 µm). At the same time, the particles showed a broad distribution with relative standard deviations of 44-76%.

The template-assisted technique shows advantages in terms of the tunability of the size in a relatively broad range and allows the preparation of particles with narrow size distribution.
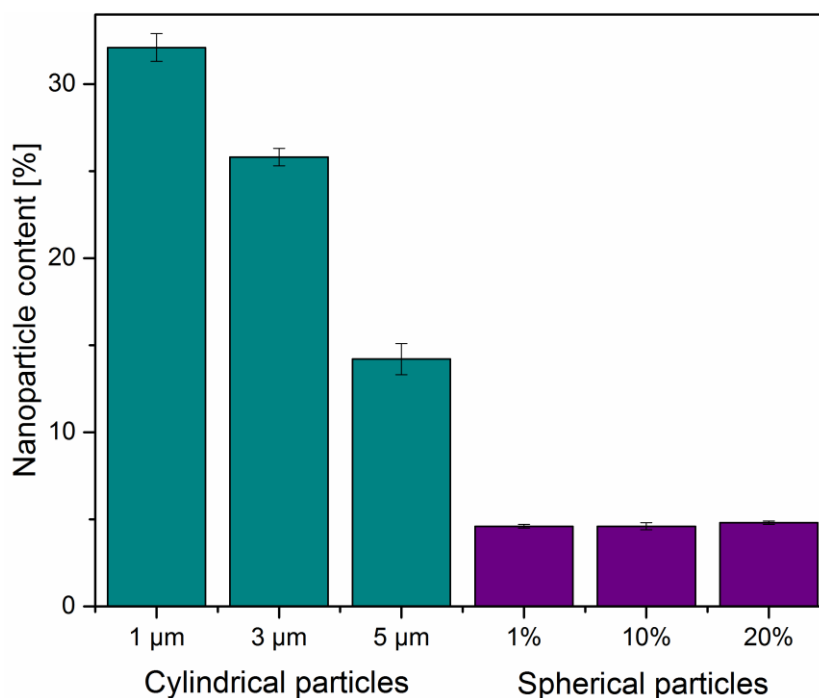

8.3.3. Nanoparticle content

The amount of nanoparticles transported per microparticle is of interest, as higher nanoparticle contents would also allow higher drug amounts to be delivered to the lungs. Especially for an inhalation as dry powder, low excipient content is favored, as only low amounts of powder can be applied with one inhalation. For the spray-dried particles the initially used ratio of nanoparticles to excipients in the spraying feed should also represent the ratio present in the particles. In the template-assisted technique in comparison, an excess of both nanoparticles and excipients is used, so that the final ratio is unknown. To determine the nanoparticle content in both types of particles, GNP were quantified by fluorescence spectrophotometry. The content determined for spherical particles was around 5% (Fig. 8.4) and thus correlated with the initially used nanoparticle concentration. No higher nanoparticle concentration was possible for the sample spray-dried from a 20% feed liquid, as a minimum amount of water was necessary to properly redisperse the nanoparticles upon purification. For the lower spraying feed concentrations, higher nanoparticle contents would have been possible; however it was

kept constant for better comparability. As described in chapter 7, a maximum nanoparticle content of 20% is recommended for spray-dried nano-embedded microparticles. Low nanoparticle contents are furthermore advisable for GNP as proteins have been described to tend to accumulation at the air-liquid interface that is suddenly expanding upon droplet generation in the spray dryer [44]. With the influence of the heat, irreversible aggregation might occur. By using sufficient amounts of excipients, aggregation of nanoparticles can be prevented and redispersibility is facilitated.

For cylindrical microparticles higher nanoparticle contents with values between 14 and 32% could be reached (Fig. 8.4). The amount of nanoparticles was highest for the lowest pore diameter. This might be related to the fact, that 1 μm rods were more completely filled whereas larger diameter rods were mostly hollow. Hence, there are more voids that can be filled by the excipients during the interconnection for larger cylindrical particles. As no heat is involved and lower forces act on the nanoparticles, the template-assisted technique might require lower excipient amounts to prevent irreversible nanoparticle aggregation in comparison to spray drying.

To summarize, higher nanoparticle contents could be reached for cylindrical microparticles. In consequence, higher drug loadings might also be achieved in comparison to spherical particles.

Fig. 8.4. Nanoparticle content of the microparticles. Higher nanoparticle contents were reached for cylindrical particles (n = 3).
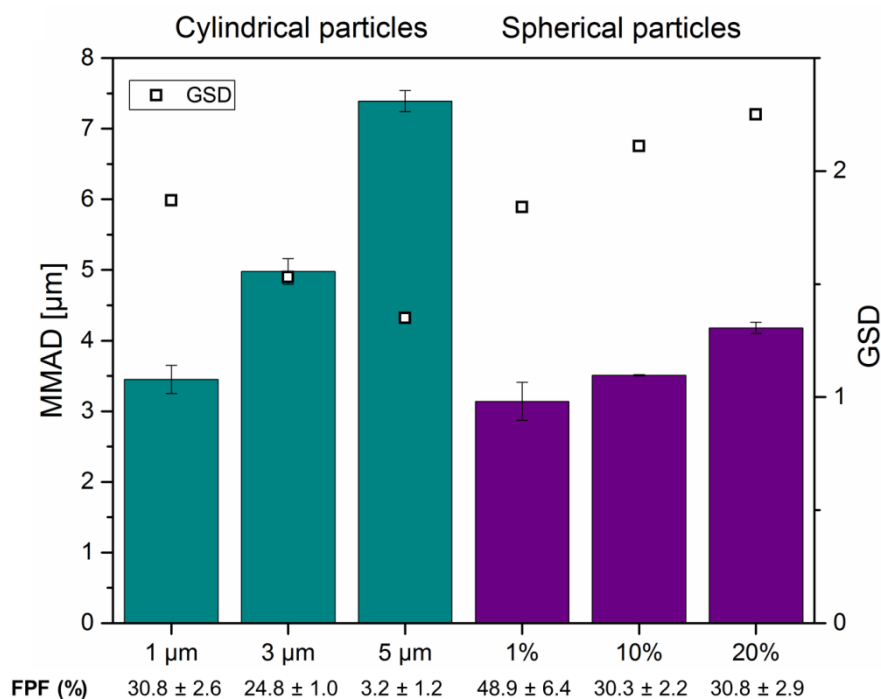
8.3.4. Aerodynamic properties

The aerodynamic properties were determined by next generation impactor (NGI) experiments. By using pores with different diameters, the aerodynamic diameter of the cylindrical particles could be influenced in a range from 3.5 to 7.4 μm (Fig. 8.5). As particles with a MMAD of 5-10 μm are associated with a deposition in the oropharyngeal region and large conducting airways [106], the 5 μm rods with a MMAD of 7.4 μm might be useful for a targeting of the upper airways. Though, with a very low fine particle fraction of 3% a pronounced product loss in the oropharynx is expected and thus they are not considered as well-suited for pulmonary application. Particles with a MMAD of 1-5 μm are reported to deposit in small airways and alveoli. Among these particles, especially particles with a MMAD below 3 μm land mainly in the alveolar region [106]. 1 μm and 3 μm rods can be thus both considered as appropriate for a targeting of the conducting airways. The 1 μm rods would most probably reach relatively small airways close to the alveolar region, while 3 μm rods might deposit mostly in larger conducting airways. By preparing cylindrical particles with a diameter < 1 μm or with a shorter length, an alveolar targeting might be possible as well.

The MMAD of the spherical particles could only be tuned in a range from 3.1 to 4.2 μm. Hence, the powders are all appropriate for a deposition in the conducting airways. However, a targeting of other lung regions would not be feasible without changing further parameters or the spray dryer device, as the geometric size could not be further influenced by the used method.

The geometric standard deviation (GSD) indicates the distribution width of the aerodynamic diameter. The GSD decreased with increasing diameter for cylindrical particles and increased with the sphere diameter (Fig. 8.5). Cylindrical particles showed a tendency to more narrow aerodynamic size distributions in comparison to spherical particles. For the 5 μm rods a monodisperse distribution was achieved. Usually, pharmaceutical aerosols are polydisperse (GSD > 1.5) [29]. If the template-assisted technique would be further improved in terms of the homogeneity of the particle sizes, a further decrease of the GSD would be expected. A powder with a low GSD might be used for a targeting of a certain lung region without exposing the rest of the lungs to the drug. This might be of interest for an inhalative treatment of lung cancer. For the treatment of bacterial infections in comparison, it is often favorable to distribute the drug throughout the lungs to reach all the pathogens [106].

Fig. 8.5. Aerodynamic properties of cylindrical and spherical microparticles. The MMAD (mass median aerodynamic diameter), GSD (geometric standard deviation) and FPF (fine particle fraction) are displayed (*n* = 3).

Comparable fine particle fractions of around 30% were obtained for 1 µm rods and spherical particles spray-dried from 10% and 20% feed liquids. A higher FPF was achieved for the 1% spherical particles. With increasing diameter of the cylindrical particles, the FPF decreased. The fine particle fraction of cylindrical particles might still be improved. The air drying of the rod dispersions resulted in densely packed pellets. Due to the low amount of powder, conventional disaggregation methods could not be applied. The pellet was disintegrated and homogenized with a spatula. By appropriate techniques, a more homogenized powder showing fewer aggregates might be produced and the fine particle fraction would be increased.

The next generation impactor is a well-established state-of-the-art device and perfectly suited for testing of most pharmaceutical aerosols. Nevertheless, it is possible that it is not the best option to simulate the *in vivo* deposition of cylindrical particles. An important deposition mechanism for cylindrical particles is the interception, which is mainly occurring at bifurcations having a diameter comparable to the fiber length, when the particles are propelled out of the airstream [110]. In the NGI the particles are following the airflow in a zig-zag-pattern, which is characterized by smaller angles in comparison to the bends present in bifurcations. It might be that cylindrical particles are deposited in cups with a cut-off diameter larger than their actual aerodynamic diameter,

as they are propelled out of the strongly bending flow streamlines and cannot follow the airflow. Hence, the actual aerodynamic diameters might be below the values obtained from NGI experiments. Airway replica or human tracheobronchiolar casts as presented by Su et al. [110] and Sussman et al. [120], modelling the airways in anatomically correct dimensions, might be options to test the aerodynamic behavior of cylindrical particles under *in vivo* relevant conditions. A study comparing the results from *in vitro* deposition experiments with *in vivo* data would be needed to properly validate available deposition models for the evaluation of aerodynamic properties of cylindrical particles.

8.3.5. Disintegration behavior

To benefit from the advantages of nanoparticles after deposition in the lungs and to prevent toxicological effects, it is essential that the microparticles disintegrate easily. The disintegration behavior was tested by incubating the powder with a droplet of water and subsequent imaging by SEM.

A better disintegration was observed for spherical microparticles. Only free nanoparticles were found (Fig. 8.6). The good redispersibility can be explained by the high content of water soluble mannitol. In comparison, remnants of the cylindrical microparticles were found as they were not completely disintegrated. The incomplete disintegration of the cylindrical microparticles might be attributed to the lower excipient content and to nanoparticles partially touching each other without being separated by mannitol bridges. A higher nanoparticle loading needs hence to be weighed against a better disintegration behavior for lower nanoparticle content.
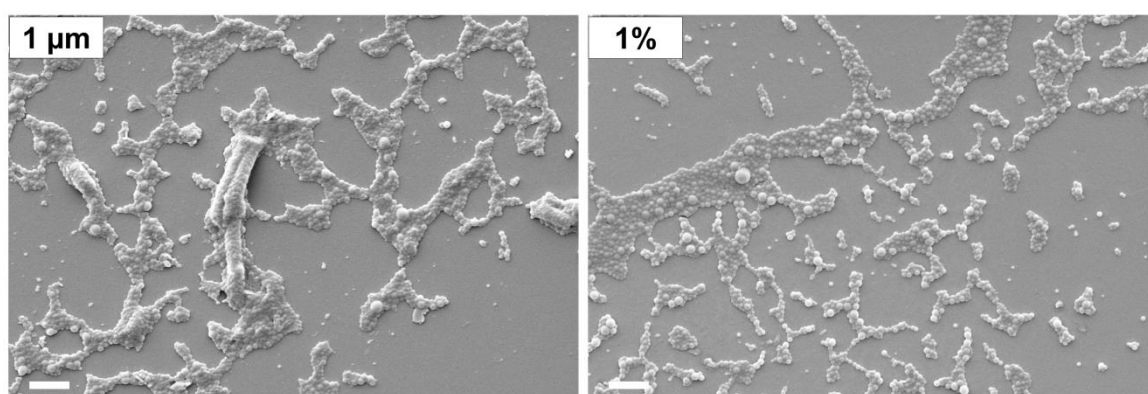
Fig. 8.6. Released nanoparticles after incubation of the microparticles with water. Only free nanoparticles were found for spherical particles (right image), while remnants of cylindrical particles were observed (left image). Scale bars represent 2 µm.

8.3.6. Comparison of the preparation methods

As cylindrical microparticles composed of nanoparticles represent a novel drug delivery system, the expenditure of time for preparation and the feasibility of a scale-up are of high interest. By spray drying with a bench top device, several grams of powder can be prepared in less than one hour. A scale-up to production scale is possible, as spray dryer are available in different dimensions. However, it needs to be considered that with a change of the device, spray-dried particles usually display different sizes and morphologies [121]. For the preparation by template-assisted technique, several days are necessary due to overnight drying steps. In this work membranes of 2.5 cm diameter were used, which had to be treated each individually. The yield per membrane is very low, ranging from 0.29 mg for 5 µm rods to 0.55 mg for 1 µm rods. Hence, for a possible scale-up, the method to prepare cylindrical microparticles would need to be fundamentally adapted. In theory, a preparation in a continuous process with large membranes moving through different filling and drying stations might be possible. A lot of progress still needs to be done to render possible, that cylindrical microparticles might be established one day in pharmaceutical industry.

8.4. Conclusion

Aspherical microparticles represent a novel approach for a delivery of nanoparticles to the lungs. Spray drying of spherical particles in comparison is already well-established and the preparation of particles in a larger scale is feasible. The preparation of cylindrical microparticles by using track-etch membranes as templates in comparison is still far away from a potential industrial application. Nevertheless, particles prepared by template-assisted technique display promising features. The dimensions of the resulting particles can be easily tuned in a relatively broad range by using appropriate templates. Hence, influencing the MMAD is also facilitated. The narrow size distribution might enable to focus therapy on a narrow range of airway generations. Furthermore, higher drug loadings per microparticle can be achieved due to higher nanoparticle contents in comparison to spherical nano-embedded microparticles. A disintegration of the microparticles and release of nanoparticles is possible, however further improvement of the redispersibility is required.

To summarize, cylindrical microparticles composed of nanoparticles represent a promising drug delivery system for the pulmonary application. Further progress is required to enable a future application.

9. CONCLUSION AND OUTLOOK

Immense progress has been made in the therapy of cystic fibrosis in the last decades. Nevertheless, bacterial infections of the respiratory tract are still limiting quality of life and survival of cystic fibrosis patients. Despite the availability of a broad range of antibiotics, biological barriers such as bronchiolar mucus and bacterial biofilm impede an efficient eradication of pathogens. Mucus represents a strong barrier for antibiotics, as deactivation of the drugs can occur and diffusion is limited.

In this thesis valuable information about the structure of respiratory mucus was obtained. Antibiotic-loaded nanocapsules were developed and their ability to transport the drug across the mucus barrier was shown. Finally, nano-embedded microparticles were prepared in different geometries. The microparticulate carrier systems were optimized for a delivery of nanoparticles to the lungs and disintegration and nanoparticle release in the airways.

The first aim of the thesis was the characterization of mucus, as the structure of this biological barrier is not yet fully explored on a microscopic level. Limited availability of fresh human mucus necessitates appropriate preservation methods or use of alternative mucus models. By cryogenic scanning electron microscopy (CSEM) different mucus types were compared. As preservation method, freezing was considered as appropriate technique based on the comparability of the structure. In comparison, structure changes were observed after freeze-drying and rehydration. Further comparison regarding the interactions of nanoparticles with fresh mucus and mucus after freezing is however necessary for full validation of freezing as preservation method.

Strong divergences were observed for pore sizes in porcine and human tracheal mucus. Hence, porcine mucus is not recommended to investigate retention of nanoparticles. In comparison, horse mucus showed only slightly larger pore sizes compared to human mucus and was thus considered as better suited to test nanoparticle-mucus interactions. Human mucus shows a pronounced intraindividual variability. It contains different regions with inhomogeneous pore sizes and potentially different capabilities of interaction with nanoparticles. In consequence, the determination of a precise cut-off size for human mucus, below which nanoparticle permeation is enabled, was not possible. The ability of nanoparticles to permeate through mucus should be evaluated on an individual basis, in best case with human mucus.

As nanoparticles are reported to enable the transport and protection of drugs inside mucus, the second aim was to develop antibiotic mucus-penetrating nanoparticles. Lipid-core nanocapsules were successfully loaded with ciprofloxacin. The apparent solubility of the drug could be considerably increased by encapsulation. It was shown, that drugs with low aqueous solubility benefit strongly from encapsulation into appropriate nanocarriers in terms of transport through mucus. The permeation rate in mucus was increased by 50% in comparison to a drug suspension. The lack of strong interactions of the nanocapsules with mucus can be explained by their size and surface properties. Furthermore, a sustained release over 24 hours was shown. As the release study was conducted in sink-conditions, an even slower release is expected *in vivo* due to the limited fluid volume in mucus. A sustained release enables a reduction of the dosing frequency. Finally, the unimpaired antibacterial efficacy against *P. aeruginosa* and *S. aureus* was shown. The antibiotic effect of the nanoparticles was only tested with planktonic bacteria. As in cystic fibrosis most recurrent lung infections are caused by biofilm-forming bacteria, the next step would be to test the antibacterial efficacy in biofilms. In planktonic bacteria treated with the free drug a formation of biofilm-like *S. aureus* aggregates was observed. By treatment with ciprofloxacin-loaded nanocapsules, biofilm formation could be prevented. Further investigation of this phenomenon is of interest, as the biofilm prevention might be due to a component of the nanocapsules or to the presence of the nanocapsules themselves. Antibacterial therapy might benefit from an extended knowledge about the mechanism of biofilm prevention. Furthermore, an evaluation of the safety of the nanocapsules in cell models is required to exclude toxic effects of the particles on human cells.

The ciprofloxacin-loaded nanocapsules show several benefits over the free drug. However, regarding a potential application, the drug loading might represent a challenge. For antibiotic drugs several milligrams are usually required per dose. Even if the overall dose may be reduced due to the advantages of the nanoencapsulation, nanoparticle amounts necessary for one application might not be feasible to apply. Highly active drugs with doses in the microgram range would be more appropriate for a loading of polymeric nanoparticles. For antibiotics a high drug loading would be required or even the use of nanocrystals consisting of pure drug.

Nanoparticles need to be converted into microparticles to enable an inhalation as dry powder formulation. The third aim was hence to prepare nano-embedded microparticles from PLGA-nanoparticles and mannitol with appropriate aerodynamic properties and disintegration behavior. Further knowledge about the influence of mannitol on the

resulting microparticles was desired to determine an optimal ratio of nanoparticles to excipient. Mannitol was revealed to have a strong influence on the morphology of nano-embedded microparticles. The different morphologies can be explained by processes occurring in the droplets upon spray drying such as the different diffusion behaviors of mannitol and nanoparticles. As the addition of nanoparticles led to hollow raisin-shaped particles, while spray drying of pure mannitol resulted in dense, solid spheres, a different aerodynamic behavior may be expected due to different densities and shapes. However, it was observed that the morphology itself has no influence on the aerodynamic properties. Only by omitting the excipient and thus creating a different surface texture, aggregation tendency was reduced and a lower aerodynamic diameter was achieved. All spray-dried samples were suitable for pulmonary application with respect to their aerodynamic sizes. An *in vitro* model to test the disintegration under conditions similar to the lungs was developed. By exposing the powders to high relative humidity, the conditions present in the lungs can be simulated. The redispersion in high amounts of fluid in comparison is only recommended as preliminary experiment. It was observed, that powders containing mannitol can already disintegrate if only exposed to high relative humidity. If nanoparticles were spray dried without excipient, no nanoparticles could be released. Mannitol was revealed as necessary and appropriate excipient for the embedding of nanoparticles into microparticles. With increasing excipient content, disintegration was observed to occur faster and to a higher degree. As mucociliary clearance might lead to a rapid elimination of the inhaled microparticles, a fast disintegration is favored. In consequence, a maximum nanoparticle content of 20% is recommended. By encapsulating an antimicrobial drug into the PLGA-nanoparticles, the nano-embedded microparticles would represent a promising drug delivery system for the treatment of bacterial infections in cystic fibrosis. It would further be of interest to investigate the influence of mannitol on the permeation rate of the nanoparticles and on the efficacy of the drug on biofilm bacteria.

Besides the preparation of spherical or raisin-shaped nano-embedded microparticles by spray drying, the template-assisted technique can be applied to prepare cylindrical microparticles. Efficient deposition of fiber-shaped particles in the lungs is expected due to an alignment in the airflow. The fourth aim was the comparison of spherical and cylindrical particles and their preparation methods. The template-assisted technique was applied for the first time to prepare microparticles from biodegradable nanoparticles by using gelatin nanoparticles.

Cylindrical microparticles were prepared with dimensions defined by the template and with narrow size distributions. The size of spherical microparticles could be influenced by the concentration of the spraying feed, but only in a relatively small range and yielding a broad size distribution. Similarly, the aerodynamic diameters of cylindrical particles covered a wider range than those of spherical particles. With further improvements of the template-assisted technique, the microparticles might be prepared with even more homogeneous size. In consequence, a targeting of a special lung region, with a reduced exposure of the rest of the lungs, might be possible. As the suitability of available deposition models for a prediction of fiber deposition is questionable, a correlation with *in vivo* deposition data would be needed to validate the impactor devices for evaluation of aspherical particles.

For cylindrical particles, higher nanoparticle contents were achieved, which would also enable higher drug loadings. However, low excipient content is also associated with a less pronounced disintegration upon contact with water. Further evaluation of the redispersibility, also under conditions similar to the lungs, is required.

Due to the easy tunability of the particle size and narrow size distribution, cylindrical particles represent a promising drug delivery system. However, the current preparation method allows only production of small batches and a scale-up is not easily feasible. Spray drying in comparison is well established also for industrial production. By advancing the template-assisted technique a scale-up might be possible one day. Of special interest would be non-destructive approaches for the microparticle release. If the template membranes do not need to be dissolved, they might be reused and a high consumption of organic solvents can be avoided. This might be achieved for example by pushing the particles out of the template by applying pressure or by pulling them out with the help of an adhesive material. Furthermore, the method would need to be adapted to enable a continuous process using large membranes running through different stations for the filling, drying, interconnection and microparticle release steps.

In this thesis, innovative nano- and microparticulate drug delivery systems for the treatment of bacterial infections in cystic fibrosis were presented. As the eradication of bacteria is often unsuccessful, more innovative therapy approaches are needed. This includes new antibiotic drugs to circumvent resistances, as well as new delivery systems to improve the drug transport across biological barriers. Nano-embedded microparticles bear the potential for an improved drug delivery and enable at the same time a fast and easy application by dry powder inhaler. In this work, the basis for such a drug delivery system was provided. The main question to be followed up is the limited drug loading of

polymeric nanoparticles. An approach would be the use of highly efficient drugs, for which low doses are sufficient. Cylindrical microparticles composed of nanoparticles would be promising in terms of increased drug content, as higher nanoparticle loadings can be achieved in the microparticles. Furthermore, high drug loading can be achieved by using nanocrystals consisting from the pure drug, prepared for example by nanomilling. As for nanocrystals stabilizers containing polyethylene glycol chains can be used [80], they might show good mucus-permeating properties. By spray drying antibiotic nanocrystals with an appropriate excipient, nano-embedded microparticles with a high drug loading would be prepared. As the required processes are well established in the pharmaceutical industry, this system is considered to have the potential to find its way to production and finally to the market.

Cystic fibrosis therapy would benefit from the combination of nano- and microparticles in one system, tackling the challenges of pulmonary drug delivery and biological barriers in the lungs and improving the outcome of cystic fibrosis patients.

10. ANNEX

10.1. List of abbreviations

AFM	atomic force microscopy
CF	cystic fibrosis
CFTR	cystic fibrosis transmembrane conductance regulator
CLSM	confocal laser scanning microscopy
Cryo-TEM	cryogenic transmission electron microscopy
CSEM	cryogenic scanning electron microscopy
EE%	encapsulation efficiency
FPF	fine particle fraction
GSD	geometric standard deviation
HPLC	high-performance liquid chromatography
LNC	lipid-core nanocapsules
LNC-blank	blank lipid-core nanocapsules
LNC-CIP	ciprofloxacin-loaded lipid-core nanocapsules
LoD	limit of detection
LoQ	limit of quantification
MMAD	mass median aerodynamic diameter
NE-CIP	ciprofloxacin-loaded nanoemulsion
NGI	next generation impactor
NP	nanoparticles
OD600	optical density (absorbance) measured at a wavelength of 600 nm
PCL	poly(ε-caprolactone)
PCS	photon correlation spectroscopy
PEG	polyethylene glycol / polyoxyethylene
PLGA	poly(lactic-*co*-glycolic acid)
PVA	poly(vinyl alcohol)
SEM	scanning electron microscopy
SLF	simulated lung fluid
TEM	transmission electron microscopy
λ_{em}	emission wavelength
λ_{ex}	excitation wavelength

10.2. List of materials

Substances

Substance		Supplier
Acetone	analytical reagent grade	Fisher Scientific, Loughborough, UK
Agarose	for electrophoresis	Sigma-Aldrich, Steinheim, Germany
Brij® 35		Atlas Chemie, Essen, Germany
Ciprofloxacin		Sigma-Aldrich, São Paulo, Brazil
Coumarin 6	98%	Sigma-Aldrich, Steinheim, Germany
Dichloromethane	for HPLC, > 99,8%	Fisher Scientific, Loughborough, UK
D-Mannitol	≥ 98%	Sigma-Aldrich, Steinheim, Germany
Ethylacetate	analytical reagent grade	Fisher Scientific, Loughborough, UK
FITC–dextran 70	Mw 70 kDa	TdB Consultancy, Uppsala, Sweden
Gelatin	from bovine skin (Type B)	Sigma-Aldrich, Steinheim, Germany
Glutaraldehyde sol.	grade II (25% in H_2O)	Sigma-Aldrich, Steinheim, Germany
Glycerol		Sigma-Aldrich, Steinheim, Germany
LB medium	Luria/Miller	Carl Roth, Karlsruhe, Germany
L-Leucine	reagent grade > 98%	Sigma-Aldrich, Steinheim, Germany
MEM medium		kind gift from Helmholtz Institute for Pharmaceutical Research Saarland
Mucus, equine respiratory		horse clinic Altforweiler, Überherrn, Germany
Mucus, human tracheal		kind gift from Helmholtz Institute for Pharmaceutical Research Saarland
Mucus, porcine tracheal		kind gift from Helmholtz Institute for Pharmaceutical Research Saarland
Oleic acid		Dinâmica, Diadema, Brazil
P. aeruginosa **PAO1**	DSM-19880	DSMZ, Braunschweig, Germany
PLGA	Resomer RG 503H	Evonik, Darmstadt, Germany
Poloxamer 188	Pluronic® F68	PanReac AppliChem, Darmstadt, Germany
Poly(ε-caprolactone)	MW = 80,000 g·mol^{-1}	Sigma-Aldrich, São Paulo, Brazil
Polysorbate 80		Vetec, Rio de Janeiro, Brazil
PVA	Mowiol® 4-88, MW = 31,000	Sigma-Aldrich, Steinheim, Germany
Rhodamine B	for fluorescence	Sigma-Aldrich, Steinheim, Germany
S. aureus **Newman**		kind gift from Prof. Rolf Müller, Saarbrücken, Germany
Sorbitan monostearate		Sigma-Aldrich, São Paulo, Brazil

Consumables

Consumable		Supplier
8-well microscope slides	8-well on glass, detachable	Sarstedt, Nümbrecht, Germany
96-well-plate	CELLSTAR® 655180	GreinerBioOne, Frickenhausen, Germany
Acrodisc filter	Acrodisc® 25 mm syringe filter with 1 µm glass fiber membrane	Pall Life Sciences, Port Washington, USA
AFM tips	OMCL-AC160TS	Olympus, Shinjuku, Japan
CSEM metal freezing tubes		Gatan, Pleasanton, USA
Dialysis tubing cellulose membrane bags	molecular weight cut-off 14.000	Sigma Aldrich, São Paulo, Brazil
Filter holder for 25 mm membranes	Swinnex 25 mm filter holder PP	EMD Millipore Corporation; Billerica, USA
Hard gelatin capsules	Transparent, Size 3	WEPA Apothekenbedarf GmbH, Hillscheid, Germany
Holey carbon TEM grid	S147-4	Plano GmbH, Wetzlar, Germany
Mica	for AFM analysis	Plano GmbH, Wetzlar, Germany
Polycarbonate membranes	Nuclepore Track-Etch Membranes (Diameter 0.05, 1, 3 and 5 µm)	Whatman, Maidstone, UK
Redispersibility membranes	NC 05 membrane filters; 0,05 µm	Schleicher & Schuell, Dassel, Germany
Transwell® inserts	polyester membrane; 12 mm diameter; pore size 3.0 µm	Corning Incorporated, Corning, USA)
Ultrafiltration-centrifugation tubes	Amicon® Ultra Centrifugal Filters, 10k	Merck Millipore, Billerica, USA

10.3. List of devices

Technique/Device	Model	Manufacturer
AFM	BioScope BS3-Z2 AFM + Nanoscope IV controller	Bruker Corporation, Billerica, USA
CLSM	LSM 710 AxioObserver	Zeiss, Oberkochen, Germany
Critical flow controller (NGI)	Critical flow controller	Erweka, Heusenstamm, Germany
Cryoplunger	CP3 Cryoplunger	Gatan, Pleasanton, USA
Cryo-TEM	JEM-2100 (HR pole piece) with LaB6 cathode and Gatan Orius SC1000 camera	JEOL, Tokyo, Japan
Cryo-TEM holder	914 Cryo-TEM holder	Gatan, Pleasanton, USA
CSEM	JSM-7500F	JEOL, Tokyo, Japan
CSEM transfer system with sputter coater	Alto 2500 Cryo transfer system	Gatan, Pleasanton, USA
Dry powder inhaler	HandiHaler®	Boehringer Ingelheim, Ingelheim, Germany
Flow meter	M1A Flow meter	Copley Scientific, Nottingham, UK
Fluorescence spectrophotometer (bacterial growth assays)	FLUOstar Omega microplate reader	BMG Labtech, Ortenberg, Germany
Fluorescence spectrophotometer (NGI)	infinite 200	Tecan, Männedorf, Switzerland
Freeze dryer	Alpha 2-4 LSC	Christ, Osterode am Harz, Germany
HPLC column (determination EE% and release studies)	Nova-Pak® C18 (60Å pore diameter, 4 µm, 3.9x150 mm)	Waters, Milford, USA
HPLC column (mucus permeation)	LiChrospher®100 RP-18 (LiChroCART® 125-4, 5 µm)	Merck, Darmstadt, Germany
HPLC system (determination EE% and release studies)	LC-20AT Pump, SIL-20A auto-sampler, SPD-20AV detector (UV-VIS), Class-VP Software	Shimadzu, Tokyo, Japan
HPLC system (mucus permeation)	Dionex UltiMate 3000 HPLC system: RS Pump, ASI-100 Automated Sample Injector, RS Variable Wavelength Detector and Chromeleon Client 6.80 SR12 Software	Dionex, Sunnyvale, USA

Impactor	Next Generation Impactor	Copley Scientific, Nottingham, UK
Laser diffraction analysis	Mastersizer® 2000	Malvern Instruments, Worcestershire, UK
PCS and laser Doppler electrophoresis (LNC)	Zetasizer® Nanoseries ZS ZEN3601	Malvern Instruments, Worcestershire, UK
PCS and laser Doppler electrophoresis (PLGA-NP and GNP)	Zetasizer® Nanoseries Nano-ZS	Malvern Instruments, Worcestershire, UK
pH meter (LNC)	DM-22	Digimed, Campo Grande, Brazil
pH meter (PLGA-NP, GNP)	Seven compact	Mettler Toledo, Columbus, USA
Rotary evaporator	Rotavapor	Büchi, Flawil, Switzerland
SEM	EVO HD15	Zeiss, Oberkochen, Germany
SEM (*S. aureus* imaging)	JSM-7000F	JEOL, Tokyo, Japan
Sonicator	Sonopuls UW 3100 with MS73 sonotrode	Bandelin electronic, Berlin, Germany
Spray dryer (GNP)	Mini Spray Dryer B-290	Büchi, Flawil, Switzerland
Spray dryer (PLGA-NP)	Nano Spray Dryer B-90	Büchi, Flawil, Switzerland
Sputter coater	Quorum Q150R ES	Quorum Technologies Ltd., East Grinstead, UK
Syringe pump	Legato 210	KD Scientific, Holliston, USA
TEM	JEM 1200-ExII	JEOL, Tokyo, Japan
Vacuum pump (NGI)	Vacuum pump	Erweka, Heusenstamm, Germany
White light interferometer	NewView™ 7300 3D Optical Surface Profiler	Zygo Corporation, Middlefield, USA

10.4. List of used software

Type of analysis	Software	Manufacturer
AFM	NanoScope Analysis 1.40	Bruker Corporation, Billerica, USA
Release analysis	Scientist®	MicroMath®, Saint Louis, USA
Size analysis (CSEM)	ImageJ 1.48v	National Institutes of Health, USA
Size analysis (SEM)	ZEN 2012 (blue edition)	Zeiss, Oberkochen, Germany
White light interferometric analysis	MetroPro 8.3.5	Zygo Corporation, Middlefield, USA

10.5. References

[1] B. Sens, M. Stern, Berichtsband Qualitätssicherung Mukoviszidose 2012, Zentrum für Qualität und Management im Gesundheitswesen, Mukoviszidose e.V. und Mukoviszidose Institut gemeinnützige Gesellschaft für Forschung und Therapieentwicklung, (2012).

[2] P.G. Bhat, D.R. Flanagan, M.D. Donovan, The limiting role of mucus in drug absorption: Drug permeation through mucus solution, Int J Pharm, 126 (1995) 179-187.

[3] N. Günday Türeli, A.E. Türeli, M. Schneider, Inhalable Antibiotic Nanoformulations for the Treatment of Pseudomonas Aeruginosa Infection in Cystic Fibrosis – A Review, Drug Deliv Lett, 4 (2014) 193-207.

[4] F.M. Müller, J. Bend, I. Huttegger, A. Möller, C. Schwarz, M. Abele-Horn, M. Ballmann, J. Bargon, I. Baumann, W. Bremer, R. Bruns, F. Brunsmann, R. Fischer, C. Geidel, H. Hebestreit, T.O. Hirche, M. Hogardt, S. Illing, A. Koitschev, M. Kohlhäufl, R. Mahlberg, J.G. Mainz, S. Pfeiffer-Auler, M. Puderbach, J. Riedler, B. Schulte-Hubbert, L. Sedlacek, H. Sitter, C. Smaczny, D. Staab, B. Tümmler, R.P. Vonberg, T.O.F. Wagner, J. Zerlik, E. Rietschel, S3-Leitlinie „Lungenerkrankung bei Mukoviszidose", Monatsschr Kinderheilkd, 163 (2015) 590-599.

[5] M. Cohen-Cymberknoh, D. Shoseyov, E. Kerem, Managing cystic fibrosis: strategies that increase life expectancy and improve quality of life, Am J Respir Crit Care Med, 183 (2011) 1463-1471.

[6] U. Griesenbach, K.M. Pytel, E.W. Alton, Cystic Fibrosis Gene Therapy in the UK and Elsewhere, Hum Gene Ther, 26 (2015) 266-275.

[7] M.L. Aitken, G. Bellon, K. De Boeck, P.A. Flume, H.G. Fox, D.E. Geller, E.G. Haarman, H.U. Hebestreit, A. Lapey, I.M. Schou, J.B. Zuckerman, B. Charlton, C.F. Investigators, Long-term inhaled dry powder mannitol in cystic fibrosis: an international randomized study, Am J Respir Crit Care Med, 185 (2012) 645-652.

[8] E. Fröhlich, E. Roblegg, Mucus as Barrier for Drug Delivery by Nanoparticles, J Nanosci Nanotechno, 14 (2014) 126-136.

[9] R.A. Cone, Barrier properties of mucus, Adv Drug Deliv Rev, 61 (2009) 75-85.

[10] J. Kirch, A. Schneider, B. Abou, A. Hopf, U.F. Schaefer, M. Schneider, C. Schall, C. Wagner, C.M. Lehr, Optical tweezers reveal relationship between microstructure and nanoparticle penetration of pulmonary mucus, Proc Natl Acad Sci USA, 109 (2012) 18355-18360.

[11] P.G. Bhat, D.R. Flanagan, M.D. Donovan, Drug diffusion through cystic fibrotic mucus: Steady-state permeation, rheologic properties, and glycoprotein morphology, J Pharm Sci, 85 (1996) 624-630.

[12] J. Levy, Antibiotic Activity in Sputum, J Pediatr, 108 (1986) 841-846.

[13] J.W. Costerton, Z. Lewandowski, D.E. Caldwell, D.R. Korber, H.M. Lappinscott, Microbial Biofilms, Annu Rev Microbiol, 49 (1995) 711-745.

[14] K. Forier, K. Raemdonck, S.C. De Smedt, J. Demeester, T. Coenye, K. Braeckmans, Lipid and polymer nanoparticles for drug delivery to bacterial biofilms, J Control Release, 190 (2014) 607-623.

[15] H.G. Ahlgren, A. Benedetti, J.S. Landry, J. Bernier, E. Matouk, D. Radzioch, L.C. Lands, S. Rousseau, D. Nguyen, Clinical outcomes associated with Staphylococcus aureus and

Pseudomonas aeruginosa airway infections in adult cystic fibrosis patients, Bmc Pulm Med, 15 (2015).

[16] M.I. Marks, Clinical Significance of Staphylococcus Aureus in Cystic Fibrosis, Infection, 18 (1990) 53-56.

[17] K. Hadinoto, W.S. Cheow, Nano-antibiotics in chronic lung infection therapy against Pseudomonas aeruginosa, Colloids Surf B Biointerfaces, 116 (2014) 772-785.

[18] V. Bourganis, T. Karamanidou, E. Samaridou, K. Karidi, O. Kammona, C. Kiparissides, On the synthesis of mucus permeating nanocarriers, Eur J Pharm Biopharm, 97 (2015) 239-249.

[19] S.K. Lai, Y.Y. Wang, J. Hanes, Mucus-penetrating nanoparticles for drug and gene delivery to mucosal tissues, Adv Drug Deliv Rev, 61 (2009) 158-171.

[20] M. Yang, S.K. Lai, Y.Y. Wang, W.X. Zhong, C. Happe, M. Zhang, J. Fu, J. Hanes, Biodegradable Nanoparticles Composed Entirely of Safe Materials that Rapidly Penetrate Human Mucus, Angew Chem Int Edit, 50 (2011) 2597-2600.

[21] S. Dunnhaupt, O. Kammona, C. Waldner, C. Kiparissides, A. Bernkop-Schnurch, Nano-carrier systems: Strategies to overcome the mucus gel barrier, Eur J Pharm Biopharm, 96 (2015) 447-453.

[22] O. Lieleg, K. Ribbeck, Biological hydrogels as selective diffusion barriers, Trends Cell Biol, 21 (2011) 543-551.

[23] G. Aljayyoussi, M. Abdulkarim, P. Griffiths, M. Gumbleton, Pharmaceutical nanoparticles and the mucin biopolymer barrier, BioImpacts : BI, 2 (2012) 173-174.

[24] N.N. Sanders, S.C. De Smedt, E. Van Rompaey, P. Simoens, F. De Baets, J. Demeester, Cystic fibrosis sputum - A barrier to the transport of nanospheres, Am J Resp Crit Care, 162 (2000) 1905-1911.

[25] J.S. Suk, Q. Xu, N. Kim, J. Hanes, L.M. Ensign, PEGylation as a strategy for improving nanoparticle-based drug and gene delivery, Adv Drug Deliv Rev, 99 (2016) 28-51.

[26] L.M. Ensign, B.C. Tang, Y.Y. Wang, T.A. Tse, T. Hoen, R. Cone, J. Hanes, Mucus-Penetrating Nanoparticles for Vaginal Drug Delivery Protect Against Herpes Simplex Virus, Sci Transl Med, 4 (2012) 1-10.

[27] B.C. Tang, M. Dawson, S.K. Lai, Y.Y. Wang, J.S. Suk, M. Yang, P. Zeitlin, M.P. Boyle, J. Fu, J. Hanes, Biodegradable polymer nanoparticles that rapidly penetrate the human mucus barrier, Proc Natl Acad Sci USA, 106 (2009) 19268-19273.

[28] K. Hara, H. Tsujimoto, Y. Tsukada, C.C. Huang, Y. Kawashima, M. Tsutsumi, Histological examination of PLGA nanospheres for intratracheal drug administration, Int J Pharm, 356 (2008) 267-273.

[29] S. Newman, P. Anderson, P. Byron, R. Dalby, J. Peart, Respiratory Drug Delivery: Essential Theory and Practice, Respiratory Drug Delivery Online, Richmond, Virginia, 2009.

[30] M. Hussain, P. Madl, A. Khan, Lung deposition predictions of airborne particles and the emergence of contemporary diseases Part-I, theHealth, 2 (2011) 51-59.

[31] X.M. Zeng, G.P. Martin, C. Marriott, Particulate Interactions in Dry Powder Formulations for Inhalation in: T. Francis (Ed.), London, New York, 2000.

[32] T.C. Carvalho, J.I. Peters, R.O. Williams, 3rd, Influence of particle size on regional lung deposition - What evidence is there?, Int J Pharm, 406 (2011) 1-10.

[33] R. Sturm, W. Hofmann, A theoretical approach to the deposition and clearance of fibers with variable size in the human respiratory tract, J Hazard Mater, 170 (2009) 210-218.

[34] E. Frohlich, S. Salar-Behzadi, Toxicological Assessment of Inhaled Nanoparticles: Role of in Vivo, ex Vivo, in Vitro, and in Silico Studies, Int J Mol Sci, 15 (2014) 4795-4822.

[35] H. Heijerman, E. Westerman, S. Conway, D. Touw, G. Doring, g. consensus working, Inhaled medication and inhalation devices for lung disease in patients with cystic fibrosis: A European consensus, J Cyst Fibros, 8 (2009) 295-315.

[36] M.T. Newhouse, P.H. Hirst, S.P. Duddu, Y.H. Walter, T.E. Tarara, A.R. Clark, J.G. Weers, Inhalation of a dry powder tobramycin PulmoSphere formulation in healthy volunteers, Chest, 124 (2003) 360-366.

[37] C.A. Ruge, A. Bohr, M. Beck-Broichsitter, V. Nicolas, N. Tsapis, E. Fattal, Disintegration of nano-embedded microparticles after deposition on mucus: A mechanistic study, Colloids Surf B Biointerfaces, 139 (2016) 219-227.

[38] N. Tsapis, D. Bennett, B. Jackson, D.A. Weitz, D.A. Edwards, Trojan particles: Large porous carriers of nanoparticles for drug delivery, P Natl Acad Sci USA, 99 (2002) 12001-12005.

[39] F. Ungaro, I. d'Angelo, A. Miro, M.I. La Rotonda, F. Quaglia, Engineered PLGA nano- and micro-carriers for pulmonary delivery: challenges and promises, J Pharm Pharmacol, 64 (2012) 1217-1235.

[40] T. Lebhardt, S. Roesler, H.P. Uusitalo, T. Kissel, Surfactant-free redispersible nanoparticles in fast-dissolving composite microcarriers for dry-powder inhalation, Eur J Pharm Biopharm, 78 (2011) 90-96.

[41] K. Hadinoto, P. Phanapavudhikul, Z. Kewu, R.B. Tan, Dry powder aerosol delivery of large hollow nanoparticulate aggregates as prospective carriers of nanoparticulate drugs: effects of phospholipids, Int J Pharm, 333 (2007) 187-198.

[42] K. Kho, W.S. Cheow, R.H. Lie, K. Hadinoto, Aqueous re-dispersibility of spray-dried antibiotic-loaded polycaprolactone nanoparticle aggregates for inhaled anti-biofilm therapy, Powder Technol, 203 (2010) 432-439.

[43] K. Kho, K. Hadinoto, Aqueous re-dispersibility characterization of spray-dried hollow spherical silica nano-aggregates, Powder Technol, 198 (2010) 354-363.

[44] J.O.H. Sham, Y. Zhang, W.H. Finlay, W.H. Roa, R. Löbenberg, Formulation and characterization of spray-dried powders containing nanoparticles for aerosol delivery to the lung, Int J Pharm, 269 (2004) 457-467.

[45] K. Tomoda, T. Ohkoshi, Y. Kawai, M. Nishiwaki, T. Nakajima, K. Makino, Preparation and properties of inhalable nanocomposite particles: effects of the temperature at a spray-dryer inlet upon the properties of particles, Colloids Surf B Biointerfaces, 61 (2008) 138-144.

[46] A. Grenha, B. Seijo, C. Remunan-Lopez, Microencapsulated chitosan nanoparticles for lung protein delivery, Eur J Pharm Sci, 25 (2005) 427-437.

[47] D. Kohler, M. Schneider, M. Kruger, C.M. Lehr, H. Mohwald, D. Wang, Template-assisted polyelectrolyte encapsulation of nanoparticles into dispersible, hierarchically nanostructured microfibers, Adv Mater, 23 (2011) 1376-1379.

[48] C. Tscheka, M. Hittinger, C.M. Lehr, N. Schneider-Daum, M. Schneider, Macrophage uptake of cylindrical microparticles investigated with correlative microscopy, Eur J Pharm Biopharm, 95 (2015) 151-155.

[49] S.A. Khan, M. Schneider, Improvement of Nanoprecipitation Technique for Preparation of Gelatin Nanoparticles and Potential Macromolecular Drug Loading, Macromol Biosci, 13 (2013) 455-463.

[50] S.A. Galindo-Rodriguez, F. Puel, S. Briancon, E. Allemann, E. Doelker, H. Fessi, Comparative scale-up of three methods for producing ibuprofen-loaded nanoparticles, Eur J Pharm Sci, 25 (2005) 357-367.

[51] C.E. Mora-Huertas, H. Fessi, A. Elaissari, Polymer-based nanocapsules for drug delivery, Int J Pharm, 385 (2010) 113-142.

[52] D.S. Jornada, L.A. Fiel, K. Bueno, J.F. Gerent, C.L. Petzhold, R.C.R. Beck, S.S. Guterres, A.R. Pohlmann, Lipid-core nanocapsules: mechanism of self-assembly, control of size and loading capacity, Soft Matter, 8 (2012) 6646.

[53] R. Dinarvand, N. Sepehri, S. Manoochehri, H. Rouhani, F. Atyabi, Polylactide-co-glycolide nanoparticles for controlled delivery of anticancer agents, Int J Nanomed, 6 (2011) 877-895.

[54] G. Pilcer, K. Amighi, Formulation strategy and use of excipients in pulmonary drug delivery, Int J Pharm, 392 (2010) 1-19.

[55] A. Bohr, C.A. Ruge, M. Beck-Broichsitter, Preparation of nanoscale pulmonary drug delivery formulations by spray drying, Adv Exp Med Biol, 811 (2014) 183-206.

[56] R. Högger, Schulungsunterlagen Sprühtrocknung, in, Büchi Labortechnik AG, Flawil, Switzerland.

[57] X.A. Li, N. Anton, C. Arpagaus, F. Belleteix, T.F. Vandamme, Nanoparticles by spray drying using innovative new technology: The Buchi Nano Spray Dryer B-90, J Control Release, 147 (2010) 304-310.

[58] K. Kho, K. Hadinoto, Effects of excipient formulation on the morphology and aqueous re-dispersibility of dry-powder silica nano-aggregates, Colloids Surf., A, 359 (2010) 71-81.

[59] N. Daum, C. Tscheka, A. Neumeyer, M. Schneider, Novel approaches for drug delivery systems in nanomedicine: effects of particle design and shape, Wires Nanomed Nanobi, 4 (2012) 52-65.

[60] L.A. Dailey, Inhalative Verabreichung von Proteinen und Peptiden, in: K. Mäder, U. Weidenauer (Eds.) Innovative Arzneiformen - Ein Lehrbuch für Studium und Praxis, Wissenschaftliche Verlagsgesellschaft Stuttgart, Stuttgart, 2010.

[61] V.A. Marple, D.L. Roberts, F.J. Romay, N.C. Miller, K.G. Truman, M.J. Holroyd, J.P. Mitchell, D. Hochrainer, Next generation pharmaceutical impactor (A new impactor for pharmaceutical inhaler testing). Part I: Design, J Aerosol Med, 16 (2003) 283-299.

[62] Ph. Eur. 2.9.18 Preparations for Inhalation: Assessment of fine particles, in: Ph.Eur. Suppl. 5.1, Council of Europe, Strasbourg, France, 2005.

[63] B.S. Schuster, J.S. Suk, G.F. Woodworth, J. Hanes, Nanoparticle diffusion in respiratory mucus from humans without lung disease, Biomaterials, 34 (2013) 3439-3446.

[64] J.S. Suk, S.K. Lai, N.J. Boylan, M.R. Dawson, M.P. Boyle, J. Hanes, Rapid transport of muco-inert nanoparticles in cystic fibrosis sputum treated with N-acetyl cysteine, Nanomedicine, 6 (2011) 365-375.

[65] A. Gross, A. Torge, U.F. Schaefer, M. Schneider, C.-M. Lehr, C. Wagner, A foam model highlights the differences of the macro- and microrheology of respiratory horse mucus, 71 (2017) 216-222.

[66] M. Boegh, S.G. Baldursdottir, A. Mullertz, H.M. Nielsen, Property profiling of biosimilar mucus in a novel mucus-containing in vitro model for assessment of intestinal drug absorption, Eur J Pharm Biopharm, 87 (2014) 227-235.

[67] M. Carey, Optimisation of Cryo-SEM and How to Minimize Artefacts, Microsc Microanal, 15 (2009) 928-929.

[68] N. Principi, S. Esposito, Appropriate use of fluoroquinolones in children, Int J Antimicrob Ag, 45 (2015) 341-346.

[69] S.A. Antoniu, Inhaled ciprofloxacin for chronic airways infections caused by Pseudomonas aeruginosa, Expert Rev Anti Infect Ther, 10 (2012) 1439–1446.

[70] N. Nafee, A. Husari, C.K. Maurer, C. Lu, C. de Rossi, A. Steinbach, R.W. Hartmann, C.M. Lehr, M. Schneider, Antibiotic-free nanotherapeutics: Ultra-small, mucus-penetrating solid lipid nanoparticles enhance the pulmonary delivery and anti-virulence efficacy of novel quorum sensing inhibitors, J Control Release, 192 (2014) 131-140.

[71] A.R. Pohlmann, F.N. Fonseca, K. Paese, C.B. Detoni, K. Coradini, R.C.R. Beck, S.S. Guterres, Poly(epsilon-caprolactone) microcapsules and nanocapsules in drug delivery, Expert Opin Drug Del, 10 (2013) 623-638.

[72] F.S. Poletto, C.P. de Oliveira, H. Wender, D. Regent, B. Donida, S.R. Teixeira, S.S. Guterres, B. Rossi-Bergmann, A.R. Pohlmann, How Sorbitan Monostearate Can Increase Drug-Loading Capacity of Lipid-Core Polymeric Nanocapsules, J Nanosci Nanotechno, 15 (2015) 827-837.

[73] M.D. Bianchin, I.C. Kulkamp-Gurreiro, C.P. de Oliveira, R.V. Contri, S.S. Guterres, A.R. Pohlmann, Radar charts based on particle sizing as an approach to establish the fingerprints of polymeric nanoparticles in aqueous formulations, J Drug Deliv Sci Tec, 30 (2015) 180-189.

[74] A.R. Pohlmann, G. Mezzalira, C.D. Venturini, L. Cruza, A. Bernardi, E. Jager, A.M.O. Battastini, N.P. da Silveira, S.S. Guterres, Determining the simultaneous presence of drug nanocrystals in drug-loaded polymeric nanocapsule aqueous suspensions: A relation between light scattering and drug content, Int J Pharmaceut, 359 (2008) 288-293.

[75] M.R.C. Marques, R. Loebenberg, M. Almukainzi, Simulated Biological Fluids with Possible Application in Dissolution Testing, Dissolut Technol, (2011) 15-28.

[76] M.M. Bakshi, S.C., G. Bhandara, Formulation design and evaluation of self micro emulsifying drug delivery system of ciprofloxacin, IJPRBS, 2 (2013) 29-53.

[77] S.S. Guterres, V. Weiss, L.D. Freitas, A.R. Pohlmann, Influence of benzyl benzoate as oil core on the physicochemical properties of spray-dried powders from polymeric nanocapsules containing indomethacin, Drug Deliv, 7 (2000) 195-199.

[78] L.A. Fiel, L.M. Rebêlo, T. de Melo Santiago, M.D. Adorne, S.S. Guterres, J. Soares de Sousa, A.R. Pohlmann, Diverse deformation properties of polymeric nanocapsules and lipid-core nanocapsules, Soft Matter, 7 (2011) 7240.

[79] S.A. Breda, A.F. Jimenez-Kairuz, R.H. Manzo, M.E. Olivera, Solubility behavior and biopharmaceutical classification of novel high-solubility ciprofloxacin and norfloxacin pharmaceutical derivatives, Int J Pharm, 371 (2009) 106-113.

[80] X.Q. Yu, G.L. Zipp, G.W.R. Davidson, The Effect of Temperature and Ph on the Solubility of Quinolone Compounds - Estimation of Heat of Fusion, Pharmaceut Res, 11 (1994) 522-527.

[81] N. Günday Türeli, A.E. Türeli, M. Schneider, Counter-ion complexes for enhanced drug loading in nanocarriers: Proof-of-concept and beyond, Int J Pharm, 511 (2016) 994-1001.

[82] M. Schneider, M. Brinkmann, H. Möhwald, Adsorption of Polyethylenimine on Graphite: An Atomic Force Microscopy Study, Macromolecules, 36 (2003) 9510-9518.

[83] S. Höfl, L. Zitzler, T. Hellweg, S. Herminghaus, F. Mugele, Volume phase transition of "smart" microgels in bulk solution and adsorbed at an interface: A combined AFM, dynamic light, and small angle neutron scattering study, Polymer, 48 (2007) 245-254.

[84] H. Friedl, S. Dunnhaupt, F. Hintzen, C. Waldner, S. Parikh, J.P. Pearson, M.D. Wilcox, A. Bernkop-Schnurch, Development and evaluation of a novel mucus diffusion test system approved by self-nanoemulsifying drug delivery systems, J Pharm Sci, 102 (2013) 4406-4413.

[85] A.C. Groo, K. Mircheva, J. Bejaud, C. Ailhas, I. Panaiotov, P. Saulnier, T. Ivanova, F. Lagarce, Development of 2D and 3D Mucus Models and Their Interactions with Mucus-Penetrating Paclitaxel-Loaded Lipid Nanocapsules, Pharm Res, 31 (2014) 1753-1765.

[86] N. Nafee, M. Schneider, Towards a versatile technique for tracking nanoparticle-mucus interaction: a step on the road, Proc SPIE, 8954 (2014) 89540J.

[87] X.Y. Li, S.Y. Guo, C.L. Zhu, Q.L. Zhu, Y. Gan, J. Rantanen, U.L. Rahbek, L. Hovgaard, M.S. Yang, Intestinal mucosa permeability following oral insulin delivery using core shell corona nanolipoparticles, Biomaterials, 34 (2013) 9678-9687.

[88] D. Chen, D.N. Xia, X.Y. Li, Q.L. Zhu, H.Z. Yu, C.L. Zhu, Y. Gan, Comparative study of Pluronic (R) F127-modified liposomes and chitosan-modified liposomes for mucus penetration and oral absorption of cyclosporine A in rats, Int J Pharmaceut, 449 (2013) 1-9.

[89] O. Mert, S.K. Lai, L. Ensign, M. Yang, Y.Y. Wang, J. Wood, J. Hanes, A poly(ethylene glycol)-based surfactant for formulation of drug-loaded mucus penetrating particles, J Control Release, 157 (2012) 455-460.

[90] G. Lafitte, K. Thuresson, P. Jarwoll, M. Nyden, Transport properties and aggregation phenomena of polyoxyethylene sorbitane monooleate (polysorbate 80) in pig gastrointestinal mucin and mucus, Langmuir, 23 (2007) 10933-10939.

[91] P.L. Ritger, N.A. Peppas, A simple equation for description of solute release I. Fickian and non-fickian release from non-swellable devices in the form of slabs, spheres, cylinders or discs, J Control Release, 5 (1987) 23-36.

[92] N.H. Georgopapadakou, B.A. Dix, P. Angehrn, A. Wick, G.A. Olson, Monocyclic and Tricyclic Analogs of Quinolones: Mechanism of Action, Antimicrob Agents Ch, 31 (1987) 614-616.

[93] J. Haaber, M.T. Cohn, D. Frees, T.J. Andersen, H. Ingmer, Planktonic aggregates of Staphylococcus aureus protect against common antibiotics, PloS one, 7 (2012) e41075.

[94] E. Rytting, J. Nguyen, X.Y. Wang, T. Kissel, Biodegradable polymeric nanocarriers for pulmonary drug delivery, Expert Opin Drug Del, 5 (2008) 629-639.

[95] C.B. Burness, G.M. Keating, Mannitol Dry Powder for Inhalation In Patients with Cystic Fibrosis, Drugs, 72 (2012) 1411-1421.

[96] N. Barraud, A. Buson, W. Jarolimek, S.A. Rice, Mannitol enhances antibiotic sensitivity of persister bacteria in Pseudomonas aeruginosa biofilms, PloS one, 8 (2013) e84220.

[97] J.S. Patton, Mechanisms of macromolecule absorption by the lungs, Adv Drug Deliver Rev, 19 (1996) 3-36.

[98] U. Nobbmann, Polydispersity – what does it mean for DLS and chromatography?, in: Malvern (Ed.), http://www.materials-talks.com/blog/2014/10/23/polydispersity-what-does-it-mean-for-dls-and-chromatography/, 2014.

[99] V. Naini, P.R. Byron, E.M. Phillips, Physicochemical stability of crystalline sugars and their spray-dried forms: Dependence upon relative humidity and suitability for use in powder inhalers, Drug Dev Ind Pharm, 24 (1998) 895-909.

[100] E. Lintingre, F. Lequeux, L. Talini, N. Tsapis, Control of particle morphology in the spray drying of colloidal suspensions, Soft Matter, 12 (2016) 7435-7444.

[101] R. Vehring, Pharmaceutical particle engineering via spray drying, Pharm Res, 25 (2008) 999-1022.

[102] S. Zellmer, G. Garnweitner, T. Breinlinger, T. Kraft, C. Schilde, Hierarchical Structure Formation of Nanoparticulate Spray-Dried Composite Aggregates, Acs Nano, 9 (2015) 10749-10757.

[103] P.J. Dunlop, Diffusion and Frictional Coefficients for 2 Concentrated Compositions of System Water-Mannitol-Sodium Chloride at 25 Degrees Tests of Onsager Reciprocal Relation, J Phys Chem-Us, 69 (1965) 4276-&.

[104] N. Tsapis, E.R. Dufresne, S.S. Sinha, C.S. Riera, J.W. Hutchinson, L. Mahadevan, D.A. Weitz, Onset of buckling in drying droplets of colloidal suspensions, Phys Rev Lett, 94 (2005) 018302.

[105] E. Lintingre, G. Ducouret, F. Lequeux, L. Olanier, T. Perie, L. Talini, Controlling the buckling instability of drying droplets of suspensions through colloidal interactions, Soft Matter, 11 (2015) 3660-3665.

[106] N.R. Labiris, M.B. Dolovich, Pulmonary drug delivery. Part I: Physiological factors affecting therapeutic effectiveness of aerosolized medications, Br J Clin Pharmacol, 56 (2003) 588-599.

[107] R. Williams, N. Rankin, T. Smith, D. Galler, P. Seakins, Relationship between the humidity and temperature of inspired gas and the function of the airway mucosa, Crit Care Med, 24 (1996) 1920-1929.

[108] C. O'Mahony, M. Hill, M. Brunet, R. Duane, A. Mathewson, Characterization of micromechanical structures using white-light interferometry, Meas Sci Technol, 14 (2003) 1807-1814.

[109] E. Houtmeyers, R. Gosselink, G. Gayan-Ramirez, M. Decramer, Regulation of mucociliary clearance in health and disease, Eur Respir J, 13 (1999) 1177-1188.

[110] W.C. Su, Y.S. Cheng, Deposition of fiber in a human airway replica, J Aerosol Sci, 37 (2006) 1429-1441.

[111] M. Lippmann, Effects of Fiber Characteristics on Lung Deposition, Retention, and Disease, Environ Health Persp, 88 (1990) 311-317.

[112] F. Pott, Problems in Defining Carcinogenic Fibers, Ann Occup Hyg, 31 (1987) 799-802.

[113] J.A. Champion, S. Mitragotri, Role of target geometry in phagocytosis, Proc Natl Acad Sci USA, 103 (2006) 4930-4934.

[114] M.S. Hassan, R.W.M. Lau, Effect of Particle Shape on Dry Particle Inhalation: Study of Flowability, Aerosolization, and Deposition Properties, AAPS PharmSciTech, 10 (2009) 1252-1262.

[115] A. Garcia, P. Mack, S. Williams, C. Fromen, T. Shen, J. Tully, J. Pillai, P. Kuehl, M. Napier, J.M. Desimone, B.W. Maynor, Microfabricated engineered particle systems for respiratory drug delivery and other pharmaceutical applications, J Drug Deliv, 2012 (2012) 941243.

[116] Inactive Ingredient Search for Approved Drug Products, in, FDA/Center for Drug Evaluation and Research, http://www.accessdata.fda.gov/scripts/cder/iig/index.cfm, 2017.

[117] A.O. Elzoghby, Gelatin-based nanoparticles as drug and gene delivery systems: reviewing three decades of research, J Control Release, 172 (2013) 1075-1091.

[118] P.H. Moghaddam, V. Ramezani, E. Esfandi, A. Vatanara, M. Nabi-Meibodi, M. Darabi, K. Gilani, A.R. Najafabadi, Development of a nano–micro carrier system for sustained pulmonary delivery of clarithromycin, Powder Technol, 239 (2013) 478-483.

[119] N. Sahoo, R.K. Sahoo, N. Biswas, A. Guha, K. Kuotsu, Recent advancement of gelatin nanoparticles in drug and vaccine delivery, Int J Biol Macromol, 81 (2015) 317-331.

[120] R.G. Sussman, B.S. Cohen, M. Lippmann, Asbestos Fiber Deposition in a Human Tracheobronchial Cast. I. Experimental, Inhal Toxicol, 3 (2008) 145-160.

[121] E.M. Littringer, R. Paus, A. Mescher, H. Schroettner, P. Walzel, N.A. Urbanetz, The morphology of spray dried mannitol particles - The vital importance of droplet size, Powder Technol, 239 (2013) 162-174.

10.6. Curriculum vitae

Afra Torge

* May 20, 1987 in Schrobenhausen

May 2013 – Jan. 2017	**PhD project** *Microparticles composed of nanoparticles for the pulmonary application of antibiotics in Cystic Fibrosis* Saarland University, Biopharmaceutics and Pharmaceutical Technology (July 2015 – Jan. 2017) Philipps University Marburg, Department of Pharmaceutics and Biopharmacy (May 2013 – Jan. 2015)
Feb. – June 2015	**DAAD research fellowship** Pharmaceutical Nanotechnology Group, Universidade Federal do Rio Grande do Sul (Porto Alegre, Brazil)
Sept. 2012 – May 2013	**Pharmacist** in public pharmacy Apotheke am Perlacher Forst, Munich
July 2012	**Pharmacist licensure (Approbation)**
Nov. 2011 – April 2012	**Practical training** in public pharmacy Kloster-Apotheke, Munich
May – Oct. 2011	**Practical training** in pharmaceutical industry Department of Medical Communications – Oncology, Amgen, Munich
Nov. 2011	**Award** of the foundation *"Dr. August und Dr. Anni Lesmüller Stiftung"* for excellent academic performance
Oct. 2006 – April 2011	**Studies in Pharmacy**, Ludwig Maximilian University (Munich)
June 2006	General qualification for university entrance (**Abitur**) Gymnasium Schrobenhausen

10.7. Scientific output

Articles

A. Torge und M. Schneider, *Nano-in-Mikro-Partikel zur pulmonalen Applikation*, *journal 10^{-9}*, Deutscher Verband Nanotechnologie, 2016 (1), 26-29.

D.B. Nguyen, T.B. Thuy Ly, M.C. Wesseling, M. Hittinger, **A. Torge**, A. Devitt, Y. Perrie, I. Bernhardt, *Characterization of Microvesicles Released from Human Red Blood Cells*, *Cell Physiol Biochem*, 2016 (38), 1085-1099.

A. Gross, **A. Torge**, U. F. Schäfer, M. Schneider, CM. Lehr, C. Wagner, *A foam model highlights the differences of the macro- and microrheology of respiratory horse mucus*, *J Mech Behav Biomed Mater,* 2017 (71) 216-222.

A. Torge, S. Wagner, P. S. Chaves, E. G. Oliveira, S. S. Guterres, A. R. Pohlmann, A. Titz, R.C.R. Beck, M. Schneider, *Ciprofloxacin-loaded lipid-core nanocapsules as mucus penetrating drug delivery system intended for the treatment of bacterial infections in cystic fibrosis*
(submitted)

A. Torge, P. Grützmacher, F. Mücklich, M. Schneider, *The influence of mannitol on morphology and disintegration of spray-dried nano-embedded microparticles*
(submitted)

N. Günday Türeli, **A. Torge**, J. Juntke, B. C. Schwarz, N. Schneider-Daum, A. E. Türeli, CM. Lehr, M. Schneider, *Ciprofloxacin-loaded PLGA nanoparticles against Cystic Fibrosis P. aeruginosa Lung Infections*
(submitted)

Oral presentations

Cylindrical particles made from biodegradable nanoparticles
A. Torge, C. Tscheka, M. Schneider
CRS Local chapter meeting, Kiel, 2014

Knocking on Cystic Fibrosis Lung`s Door: Microformulations of Antibiotic loaded Muco-Inert Nanoparticles
N. Günday Türeli*, **A. Torge***, A. E. Türeli, M. Schneider
Crossing Biological Barriers, Dresden, 2015

Poster presentations

Microspheres embedding biodegradable nanoparticles
A. Torge, M. Schneider
Sino-German Workshop "Functional (Nano-)Biomaterials", Marburg, 2014

Redispersible microspheres composed of nanoparticles for pulmonary application
A. Torge, J. Rinas, M. Schneider
GPEN, Helsinki, Finland, 2014

Redispersible microparticles composed of nanoparticles by spray drying with mannitol
A. Torge, M. Schneider
CRS Annual Meeting 2015, Edinburgh, UK

Battle against Cystic Fibrosis Lung Infections: Ciprofloxacin Complex-Loaded Mucus-Inert PLGA Nanoparticles
N. Günday Türeli, **A. Torge**, J. Juntke, A. E. Türeli, N. Schneider-Daum, CM. Lehr and M. Schneider
AAPS Annual Meeting and Exposition 2015, Orlando, USA

Ciprofloxacin loaded lipid-core nanocapsules as drug delivery system for the treatment of bacterial infections in Cystic Fibrosis
A. Torge, P. S. Chaves, E. G. Oliveira, S. Wagner, A. Titz, R.C.R. Beck, M. Schneider
BioBarriers 2016, Saarbrücken

Staphylococcus aureus biofilm prevention by antibiotic mucus-penetrating nanocapsules
A. Torge, S. Wagner, P. S. Chaves, E. G. Oliveira, A. Titz, R.C.R. Beck, M. Schneider
6th HIPS Symposium, Saarbrücken, 2016

Overcoming the mucus barrier – Antibiotic nanocapsules as drug delivery system for the treatment of pulmonary infections in Cystic Fibrosis
A. Torge, S. Wagner, P. S. Chaves, E. G. Oliveira, A. Titz, R.C.R. Beck, M. Schneider
DPhG Annual Meeting, Munich, 2016

Influence of different excipients on morphology and disintegration behavior of nano-embedded microparticles
A. Könneke*, **A. Torge***, P. Grützmacher, M. Schneider
Zsgimondy Colloquium, Saarbrücken, 2017

Further conference contributions

A Novel Strategy to Enhance Antibiotic Load for Pulmonary Treatment of Cystic Fibrosis Infections: Ciprofloxacin Lipid Complex Loaded PLGA Nanoparticles
N. Günday Türeli, J. Juntke, **A. Torge**, A. E. Türeli, EM. Prinz, C. de Souza Carvalho, CM. Lehr and M. Schneider
CRS Annual Meeting, Chicago, USA, 2014 – selected for oral presentation

* both authors contributed equally

10.8. Acknowledgements